REPORT NO.
UC SESM 74-13

STRUCTURES AND MATERIALS RESEARCH
DEPARTMENT OF CIVIL ENGINEERING

A STUDY OF THE ONE-DIMENSIONAL THEORY OF ARTERIAL PULSE PROPAGATION

by

THOMAS J.R. HUGHES

DECEMBER 1974

STRUCTURAL ENGINEERING LABORATORY
UNIVERSITY OF CALIFORNIA
BERKELEY CALIFORNIA

Structures and Materials Research
Department of Civil Engineering
Division of Structural Engineering
and Structural Mechanics

Report Number 74-13

A STUDY OF THE ONE-DIMENSIONAL THEORY OF ARTERIAL PULSE PROPAGATION

by

Thomas J.R. Hughes

Structural Engineering Laboratory
University of California
Berkeley, California

December 1974

TABLE OF CONTENTS

ACKNOWLEDGEMENT v

I. INTRODUCTION. 1

II. DERIVATION OF THE ONE-DIMENSIONAL EQUATIONS . . 8

2.1 Introduction. 8

2.2 Geometry and Kinematics 8

2.3 One-Dimensional Equations of Blood Flow .11

2.4 Constitutive Theory 21

III. FLAT-PROFILE THEORY 28

3.1 Introduction. 28

3.2 Cauchy Problem. 28

3.3 Mixed Initial-Boundary Value Problem. . .50

3.4 Consequences of the Discontinuity Conditions. 68

3.5 Shock Wave Velocities 73

3.6 Acceleration Wave Velocity. 74

3.7 Weak Shock Wave Velocity. 76

3.8 Shock Stability 77

3.9 Shock Admissibility Criterion 85

3.10 Local Qualitative Behavior of Shock Waves 87

3.10a Preliminaries. 87

3.10b Evolution of the Shock 92

3.11 Comparison with Experimental Work 99

3.12 Identification. 103

3.12a Identification of an Elastic Constitutive Model via Acceleration or Shock Wave Data. . . . 103

3.12b A Simple Nonlinear Viscoelastic Constitutive Model 106

3.12c Identification of the Viscoelastic Model via Shock Data. . . . 108

3.13 Smooth Pulses and the Shock Relations . 115

IV. NO-SLIP THEORY. 119

4.1 Introduction. 119

4.2 Consequences of the Discontinuity Conditions. 125

4.3 Shock and Acceleration Wave Velocities. 127

4.4 Previous Shock Relations Appearing in the Literature. 131

4.5 Shock Stability 135

4.6 Local Qualitative Behavior of Shocks. . 139

4.7 Identification. 142

4.8 Growth and Decay of Acceleration Waves. 145

4.8a Preliminaries 145

4.8b Evolution of the Amplitude. . . . 149

4.8c Resume of Previous Work 156

4.8d Asymptotic Formulas 158

4.8e The Dicrotic Notch. 160

4.8f Appendix. 161

V. NUMERICAL SIMULATION OF THE ONE-DIMENSIONAL THEORIES. 165

5.1 Introduction. 165

5.2 Lax-Wendroff and Abarbanel-Goldberg Algorithms. 165

5.3 Consistency with Weak Forms and Shock Stability 171

5.4 Boundary Condition Study. 175

5.5 Comparison of One-Step and Two-Step Lax-Wendroff Algorithms 179

5.6 Rockwell's Model of the Canine Aorta. . 186

5.7 Aortic Phenomena and Shock Waves. . . . 190

REFERENCES. 200

ACKNOWLEDGEMENT

This work was supported in part by the National Science Foundation and the University of California, Berkeley.

The author wishes to express his gratitude to the members of his thesis committee, R.L. Taylor and A. Chorin, for the help they provided in the course of this work and particularly to J. Lubliner, committee chairman, for his patience and encouragement.

I. INTRODUCTION

The nonlinear one-dimensional theory of arterial flow, presented by Lambert [1,2], has attracted considerable attention by researchers [3-27]. The theory is concise and, due to the inclusion of nonlinear effects, is capable of more faithfully representing many phenomena in the major arteries than previous theories [3,17,22-25]. The method of characteristics has been employed in conjunction with the theory to generate numerical solutions to simulated arterial flow problems [1,2,4,5,7-12,14,16,17,23,24] and wave front analysis has been used to derive exact relations governing the growth and decay of wave fronts [8,18-20]. In addition, asymptotic solutions have been developed to exhibit the first and second-order predictions of the theory for pulsatile flow problems [15,18]. Results of these studies have indicated that qualitative features of the evolution of the natural pulse, which are anomolous within the scope of the classical linear blood-flow theories, can be accounted for within the nonlinear theory [15,17,18,23,24]. Accordingly, much insight into the physics of arterial flow can be gained from the theory.

Since Lambert's initial work, attempts have been made to attain a deeper understanding of the basic theory. In this regard the work of Barnard et al. [7] is noteworthy. They endeavored to derive

rationally a one-dimensional theory based upon the Navier-Stokes equations for incompressible, axisymmetric flow employing approximations for pulsatile flow based on physiological data. In their derivation they included effects due to a curved flow profile satisfying a no-slip boundary condition. The resulting theory, being more refined, helps to identify the approximations inherent in Lambert's theory.

A further generalization, of considerable physiological significance, is the inclusion of an outflow term in the equation of mass conservation to simulate blood loss due to branching. This term first appeared in Rudinger's review article [9] but no derivation was given. Hughes and Lubliner [27], in their derivation of the one-dimensioanl theory, have shown that an outflow term may appear in the momentum balance equation as well as the equation of mass conservation. The experimental data for the aorta employed in the extensive numerical study of Rockwell [17,23,24] indicate the necessity of accounting for outflow in real physiological circumstances.

An interesting development in the application of the theory appeared in Rockwell's thesis [17], in which the theory was used to identify the consitutive equation (pressure-luminal area relation) for an assumed elastic artery from experimentally determined pulse wave data. This procedure illustrates the

potential usefulness of employing the theory, in conjunction with wave propagation data, for identifying the nonlinear mechanical properties of arteries - a problem of considerable physiological importance. However, it is well known that arteries behave in a nonlinear viscoelastic fashion and the identification of a constitutive equation representing this behavior is considerably more difficult. The importance of including such effects in arterial flow problems has apparently not yet been assessed.

Despite the many references that have already appeared on the one-dimensional theory, certain fundamental aspects of the theory are still poorly understood. An example of this concerns shock waves for which at least four mutually contradictory expressions have already been published governing the shock structure. It is to basic analytical issues such as this one that the present work is addressed.

In Chapter II the derivation of the theory is considered in detail. The results in [27] are extended to explicitly include second-derivative viscosity terms and it is shown later on how the inclusion of these terms points to a clarification of the shock structure problem. In addition, a constitutive theory is presented for the mean pressure-luminal area relation which accounts for nonlinear elastic and viscoelastic phenomena.

The simplest form of the one-dimensional theory arises when the fluid velocity profile is assumed flat over the lumen. The resulting theory, termed the flat-profile theory herein, is the subject of Chapter III. In most applications to problems of arterial flow the second-derivative viscosity term can be eliminated in the one-dimensional theory and the resulting differential equations are of the quasi-linear hyperbolic type. Basic concepts about these systems, such as weak solutions, are discussed in Chapter III and the well-posedness of various initial-boundary value problems arising in arterial flow is considered. It is shown how two distinct shock structures can be associated with the quasi-linear hyperbolic form of this theory, but if one insists that shock solutions arise as limits of viscous ones, then a unique shock structure is singled out. The velocities of various wave motions are derived and the stability of shock profiles is determined in terms of qualitative properties of the mean pressure-luminal area relation. The local qualitative growth and decay characteristics of shocks are established and shown to compare favorably with the experiments of Landowne [51,52] involving induced impact waves. Simple identification procedures for the mean pressure-luminal area relation are discussed and it is exhibited how wave propagation data can, in principle, be used

to determine certain model constitutive relations. Finally, the way in which the shock relations may be considered approximations for smooth pulses is established.

When the fluid velocity profile is assumed to satisfy the no-slip boundary condition on the luminal surface, a refined one-dimensional theory arises. This theory is termed the no-slip theory and is studied and compared with the flat-profile theory in Chapter IV. Many qualitative aspects of the two theories are shown to be in substantial agreement. Terms present in the no-slip theory but absent in the flat-profile theory (e.g., a term measuring the deviation from a flat profile in the momentum equation) are studied numerically using Rockwell's model of the canine aorta [17]. The shock relations for the no-slip theory are determined and found to be inconsistent with those for the flat-profile theory. This is not so surprising in light of the well known fact that as viscosity tends towards zero, solutions of the Navier-Stokes equations do not converge to solutions of the Euler equations when boundaries are present. Since the no-slip boundary condition is viewed as physically more realistic than the flat-profile boundary condition, one is lead to view the no-slip shock conditions as correct. In addition, it is shown that the no-slip shock relations imply that momentum is conserved,

whereas the flat-profile relations do not. These results enable the ambiguous situation in the literature to be cleared up.

In the weak-shock limit both theories agree through first-order measures of the shock amplitude. However, an analysis of some data calculated by Rockwell [17] indicates that for stronger shocks differences may be substantial.

Finally, the growth and decay characteristics of acceleration waves are considered in the context of the no-slip theory. This enables interpretations of the formation mechanism of the dicrotic notch and, as has been pointed out previously [18,20], the front of the cardiac pulse.

In Chapter V, some problems associated with numerically analyzing the theory are considered. The Lax-Wendroff and Abarbanel-Goldberg algorithms are studied to determine their applicability to blood-flow problems. Numerical results indicate that one can capture the appropriate class of shock relations, but instabilities, which ostensibly emanate from the boundary conditions, either make solutions impossible or can only be made to go away by treating the boundary conditions in such a way as to detrimentally affect the accuracy of the methods.

It is argued that realistic natural pulse data is shock-like within the context of the one-dimensional

theories. The opposite has been concluded by some authors because of the smooth fronts produced in numerical simulations, but this smoothing is due to the dissipation and dispersion inherent in the algorithms. This feature of the one-dimensional simulation of the natural pulse is contrary to experimental data. An explanation of this phenomenon has not been given, although it may be attributable to features of the physical system not yet included in the model (e.g., the curvature of the aortic arch).

II. DERIVATION OF THE ONE-DIMENSIONAL EQUATIONS

2.1 Introduction

This section overlaps considerably the paper "On the One-Dimensional Theory of Blood Flow in the Larger Vessels" by the author and J. Lubliner [27]. The main points of that paper were to show that an outflow term may appear in the momentum balance and that assumptions of axisymmetry were unnecessary for deriving the theory. However, here the approach is slightly more general and this additional generality is necessary for an understanding of some of the work to follow.

As was shown in [27], the starting point for the development of a rational one-dimensional theory of flow through a distensible, permeable tube (e.g., an artery) is a corollary of the Reynolds Transport Theorem. In what follows in this section it is assumed that all functions are smooth enough so that all operations make sense.

2.2 Geometry and Kinematics

Assume the tube is aligned with the z-axis of a rectangular cartesian coordinate system whose canonical coordinate functions are denoted x_1, x_2 and x_3. Points in this system are denoted by (x,y,z). The luminal area is denoted by S (not necessarily assumed circular) and C is the luminal boundary (Fig. 2.1). The symbols S and C will also denote functions:

$$\mathbb{R}^2 \longrightarrow \mathbb{R}, \text{ e.g., } S : (z,t) \longrightarrow S(z,t)$$

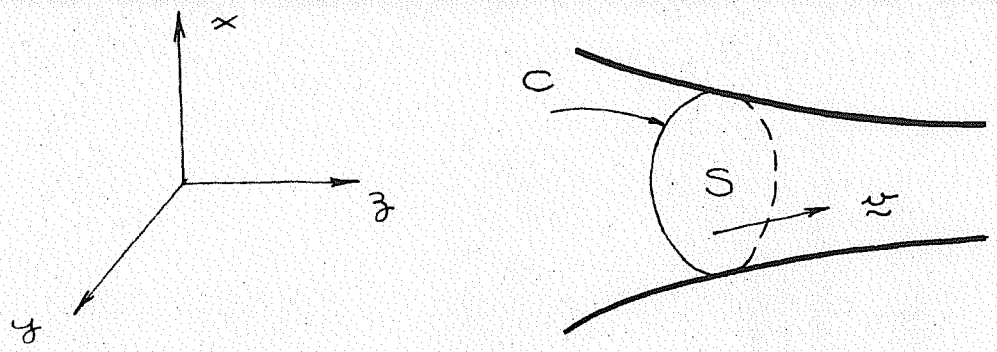

Figure 2.1

the luminal area at the point z at time t . Let

$$\xi : \mathbb{R}^4 \longrightarrow \mathbb{R}\,,\ (x,y,z,t) \longmapsto \xi(x,y,z,t)$$

be a smooth function, and define its <u>area mean</u> to be

$$\bar{\xi} = \Big(\int_S \xi\, da\Big)/S \ : \ \mathbb{R}^2 \longrightarrow \mathbb{R}$$

where da is the (Lebesgue) measure corresponding to S . This always makes sense since by assumption $S>0$. Denote by $d\ell$ the measure associated with C . Let $\underset{\sim}{v}$ be the <u>fluid velocity vector</u>. The z-component of $\underset{\sim}{v}$ is denoted by $v_3 = x_3 \circ \underset{\sim}{v}$. Let $\underset{\sim}{n} : C \times \mathbb{R}^2 \longrightarrow \mathbb{R}^3$ be the <u>unit outward normal vector</u> to the tube. The tube in general will have an arbitrary degree of time dependent taper, thus $\underset{\sim}{n}$ does not necessarily lie in the plane defined by S . No assumption is made about $\underset{\sim}{v}$ on C , thus fluid is free to pass through the luminal boundary. Let v_n represent the component of $\underset{\sim}{v}$ in the direction $\underset{\sim}{n}$, i.e. $v_n = \underset{\sim}{v} \cdot \underset{\sim}{n}$. If u_n denotes the <u>normal velocity of the luminal surface</u>, then w_n , the <u>relative normal velocity of the lumen</u>, is defined by $u_n = v_n + w_n$. Thus the amount of fluid leaving the tube through the luminal surface is measured by $-w_n$. The <u>material time derivative</u> (derivative following the motion) is denoted by a superposed dot, i.e., $\dot{\xi} = \partial\xi/\partial t + \underset{\sim}{v} \cdot \operatorname{grad} \xi$. With these definitions one can obtain the following identity:

$$\frac{\partial}{\partial t}(S\overline{\xi}) + \frac{\partial}{\partial z}[S(\overline{\xi v_3})] = \int_S (\dot{\xi} + \xi \operatorname{div} \underset{\sim}{v})\, da + \oint_C \xi w_n\, dl \qquad (2.2.1)$$

The derivation is given essentially in [27], although there it was assumed $\operatorname{div}\underset{\sim}{v}=0$ from the start and thus the term $\int_S \xi \operatorname{div}\underset{\sim}{v}\, da$ was absent. The generalization makes (2.2.1) applicable to compressible as well as incompressible flows.

The significance of (2.2.1) is as follows. Every balance law in mechanics involves terms of the form $\dot{\xi} + \xi \operatorname{div}\underset{\sim}{v}$. Two examples, which will be used here, are conservation of mass ($\xi=\rho=$ mass density) and balance of momentum ($\xi = \rho v_3 =$ momentum density). Most of the difficulties of deriving one-dimensional theories is computing the correct one-dimensional counterpart of $\dot{\xi} + \xi \operatorname{div}\underset{\sim}{v}$. Equation (2.2.1) is the device by which this computation can be carried out.

2.3 One-Dimensional Equations of Blood Flow

The basic assumptions are:

(A) The flow is incompressible, which may be stated in the alternative forms $\dot{\rho}=0$ or $\operatorname{div}\underset{\sim}{v}=0$. This assumption can be justified on the basis of the distensibility of the vessel compared with the bulk

compressibility of blood [18].

(B) The fluid is homogeneous $\partial\rho/\partial x_i = 0$. Together with (A) this implies ρ = constant. These two assumptions and (2.2.1) imply the <u>one-dimensional equation of mass conservation for an incompressible, homogeneous fluid</u>:

$$\frac{\partial S}{\partial t} + \frac{\partial}{\partial z} S\bar{v} + \psi = 0 \quad , \tag{2.3.1}$$

where $\bar{v} = \overline{v_3}$ is the <u>mean axial velocity</u> and $\psi = -\oint_C w_n \, dl$ is the <u>outflow function</u>. The derivation of (2.3.1) involves simply substituting ρ into (2.2.1), noting that $\overline{\rho} = \rho$, $\overline{\rho v_3} = \rho\bar{v}$ and dividing through by ρ. This equation, without the outflow term, has been traced back to Euler [18]. Its modern discovery is due to Lambert [1]. The formal addition of the outflow term is due to Rudinger [9]. Note that (2.3.1) holds even if the fluid is not homogeneous, i.e., substitute $\bar{\rho}$ = any constant function in (2.2.1), [27]. However, in this case the term $-\oint_C w_n \, dl$ can only be identified as proportional to the mass outflow if $\rho|_C$ is constant. It is further assumed that:

(C) Blood in the major vessels behaves like a Newtonian viscous fluid,

$$\underset{\sim}{T} = -p\underset{\sim}{I} + 2\mu\underset{\sim}{D} \quad , \tag{2.3.2}$$

where $\underset{\sim}{T}$ is the stress tensor, p is the pressure, $\underset{\sim}{I}$ is the identity tensor, μ = constant is the viscosity and $\underset{\sim}{D}$ is the rate of deformation tensor, which is the symmetric part of the velocity gradients.

Assumptions (A), (B), and (C) imply that blood flow in the major vessels obeys the Navier-Stokes equations: $\rho \dot{\underset{\sim}{v}} + \text{grad } p = \rho \underset{\sim}{f} + \mu \Delta \underset{\sim}{v}$, where $\underset{\sim}{f}$ is the extrinsic body force vector and Δ is the Laplace operator. The second equation of the one-dimensional theory is the one-dimensional counterpart of the NS equation for the z-direction:

$$\rho \dot{v}_3 + \frac{\partial p}{\partial z} = \rho f_3 + \mu \Delta v_3 \quad . \tag{2.3.3}$$

The first term can be computed from (2.2.1). Set $\xi = \rho v_3$, then $\dot{\xi} = \dot{\rho} v_3 + \rho \dot{v}_3$ and thus

$$\begin{aligned} \dot{\xi} + \xi \, \text{div} \, \underset{\sim}{v} &= \rho \dot{v}_3 + v_3 (\dot{\rho} + \rho \, \text{div} \, \underset{\sim}{v}) \\ &= \rho \dot{v}_3 + v_3 (0) \\ &= \rho \dot{v}_3 \, , \end{aligned}$$

by mass conservation. Using this in (2.2.1) and eliminating ρ yields

$$\int_S \dot{v}_3 \, da = \frac{\partial}{\partial t} (Sv) + \frac{\partial}{\partial z} [S \overline{v_3^2}] - \oint_C v_3 w_n \, dl, \tag{2.3.4}$$

The last term (modulo the constant ρ) is the momentum flux through the luminal surface. Define $f = \overline{f}_3$. The viscous term splits into

$$\Delta v_3 = \Delta_{(2)} v_3 + \frac{\partial^2 v_3}{\partial z^2} \qquad (2.3.5)$$

where $\Delta_{(2)} = \frac{\partial^2}{\partial x^2} + \frac{\partial^2}{\partial y^2}$ is the two-dimensional Laplace operator. Integrating (2.3.5) over S yields

$$\int_S \Delta v_3 \, da = \oint_C \frac{\partial v_3}{\partial m} \, dl + \int_S \frac{\partial^2 v_3}{\partial z^2} \, da \quad , \qquad (2.3.6)$$

where use has been made of the divergence theorem, and $\partial v_3 / \partial m$ denotes the directional derivative of v_3 with respect to $\underset{\sim}{m} = (m_1, m_2, 0)$, the unit outward normal vector to C in the plane defined by S. Putting (2.3.3), (2.3.4) and (2.3.6) together results in

$$\frac{\partial}{\partial t}(Sv) + \frac{\partial}{\partial z}\left[S\overline{v_3^2}\right] + \frac{1}{\rho}\int_S \frac{\partial p}{\partial z} \, da = f + \oint_C \left[\nu \frac{\partial v_3}{\partial m} + v_3 w_n\right] dl + \nu \int_S \frac{\partial^2 v_3}{\partial z^2} \, da \quad , \qquad (2.3.7)$$

where $\nu = \mu/\rho$ is the kinematic viscosity. In the context of a one-dimensional theory, this equation is not very useful without additional assumptions on p and v_3. Assume that:

(D) $p(x,y,z,t) = p(z,t)$, i.e.,

the pressure profile is flat. Thus $\bar{p} = p$ and therefore

$$\int_S \frac{\partial p}{\partial z}\, da = S \frac{\partial p}{\partial z} .$$

(E) The velocity profile is expressible as

$$v_3(x,y,z,t) = \phi(x,y,z,t)\, v(z,t) ,$$

where ϕ, called the profile function, satisfies the consistency condition $\bar{\phi} = 1$. With (D) and (E), Eq. (2.3.7) becomes

$$\frac{\partial}{\partial t}(Sv) + \frac{\partial}{\partial z}\left[(1+\delta)(Sv^2)\right] + \frac{S}{\rho}\frac{\partial p}{\partial z} = f + v \oint_C \left[\nu \frac{\partial \phi}{\partial m} + \phi w_n\right] dl + \nu \int_S \frac{\partial^2}{\partial z^2}(\phi v)\, da , \tag{2.3.8}$$

where $\delta = \frac{1}{S}\int_S (\phi^2 - 1)\, da \geq 0$ by the Schwartz inequality.

Consider two cases for ϕ:

(E_1) The velocity profile is flat, i.e., $\phi \equiv 1 \Leftrightarrow v_3 = v$. This is the simplest assumption, but is clearly in violation of the boundary conditions on C. Equation (2.3.8) then simplifies to

$$\frac{\partial}{\partial t}(S v) + \frac{\partial}{\partial z}(S v^2) + \frac{S}{\rho}\frac{\partial p}{\partial z} + v\psi =$$

$$f + \nu S \frac{\partial^2 v}{\partial z^2} \quad , \qquad (2.3.9)$$

which when combined with (2.3.1) yields

$$\frac{\partial v}{\partial t} + \frac{\partial}{\partial z}\left(\frac{v^2}{2} + \frac{p}{\rho}\right) = f + \nu \frac{\partial^2 v}{\partial z^2} \quad . \qquad (2.3.10)$$

Eqs. (2.3.9) and (2.3.10) are the flat-profile momentum and velocity forms, respectively, of the momentum equation.

The second case is logically preceded by the assumption:

(F) Longitudinal motion of the vessel wall is negligible. Then assume:

(E_2) ϕ satisfies the no-slip boundary condition, i.e., by (F) $\phi|_C = 0$. The consequences of (E_2) in (2.3.8) are:

$$\frac{\partial}{\partial t}(S v) + \frac{\partial}{\partial z}(1+\delta)(S v^2) + \frac{S}{\rho}\frac{\partial p}{\partial z} = \qquad (2.3.11)$$

$$Sf + vN + \nu \frac{\partial^2}{\partial z^2}(Sv) \quad ,$$

where $N = \nu \oint_C \frac{\partial \phi}{\partial m} d\ell$. The derivation of the last term is not completely obvious so the details of

the computation are presented here.

The result to be shown is that if $v_3 = 0$ on C for all z then $\int_S \frac{\partial^2 v_3}{\partial z^2}\, da = \frac{\partial^2}{\partial z^2}(Sv)$. Suppose $v_3(x,y,\cdot,t): \mathbb{R} \to \mathbb{R}$ is C^2 , express everything in polar coordinates,

$$da = dx\,dy = r\,dr\,d\theta$$

$$v_3(x,y,z,t) = \tilde{v}_3(r,\theta,z,t)$$

and compute:

$$\frac{\partial}{\partial z}\int_S v_3\, da = \frac{\partial}{\partial z}\int_0^{2\pi}\int_0^{R(\theta,z,t)} \tilde{v}_3(r,\theta,z,t)\, r\,dr\,d\theta$$

$$= \int_0^{2\pi}\frac{\partial}{\partial z}\int_0^{R} \tilde{v}_3\, r\,dr\,d\theta$$

$$= \int_0^{2\pi}\int_0^{R}\left(\frac{\partial}{\partial z}\tilde{v}_3\right) r\,dr\,d\theta$$

$$+ \int_0^{2\pi} \tilde{v}_3(R,\theta,z,t)\, R(\theta,z,t)\frac{\partial R}{\partial z}(\theta,z,t)\,d\theta$$

$$= \int_0^{2\pi}\int_0^{R(\theta,z,t)} \frac{\partial \tilde{v}_3}{\partial z}(r,\theta,z,t)\, r\,dr\,d\theta\ .$$

Line 3 follows from Leibniz' theorem and line 4 from $\tilde{v}_3\big|_R = 0$. Differentiate again

$$\frac{\partial^2}{\partial z^2}\int_S v_3\,da = \int_0^{2\pi}\int_0^{R(\theta,z,t)} \frac{\partial^2 \tilde{v}_3}{\partial z^2}(r,\theta,z,t)\,r\,dr\,d\theta$$

$$+ \int_0^{2\pi} \frac{\partial \tilde{v}_3}{\partial z}(R,\theta,z,t)\,R(\theta,z,t)\frac{\partial R}{\partial z}(\theta,z,t)\,d\theta$$

$$= \int_0^{2\pi}\int_0^{R(\theta,z,t)} \frac{\partial^2 \tilde{v}_3}{\partial z^2}(r,\theta,z,t)\,r\,dr\,d\theta .$$

Here again use has been made of Leibniz' theorem and the fact that $\frac{\partial}{\partial z}\left(\tilde{v}_3\big|_R\right) = D_3\left(\tilde{v}_3\big|_R\right) = 0$, follows from $\tilde{v}_3(R,\theta,z,t) = 0$. Changing coordinates back and noting $Sv = \int_S v_3\,da$ yields the result.

Eq. (2.3.11) is the <u>no-slip momentum form of the momentum equation</u>.

<u>Remarks</u>: (A) It is clear from the derivation that vessel deformations in the present theory are accounted for only in the form of luminal area changes which corresponds to so-called pressure waves.

(B) $\delta \to 0$ as the profile function ϕ approaches the unit constant function in the $L^2(S)$ sense, as can be seen from the definition of δ . Thus δ may be considered a measure of the deviation of the assumed profile from a flat profile. As an example of the range of δ and the values taken by N for specific flow profiles, take the case of a circular lumen

($C^2 = 4\pi S$) and an axisymmetric flow profile, in which

$$\phi = \frac{k+2}{k}\left(1 - \left(\frac{r}{R}\right)^k\right) \quad , \tag{2.3.12}$$

where k is a positive integer and R is the luminal radius. Substituting (2.3.12) in the definitions of δ and N yields

$$\begin{aligned} \delta &= 1/(1+k) \quad , \\ N &= -2(k+2)\pi\nu \quad . \end{aligned} \tag{2.3.13}$$

For a Poiseuille profile ($k=2$), $\delta = 1/3$ and $N = -8\pi\nu$. The viscosity (μ) of blood for normal hematocrit of 45 to 50% is between 3 and 4 times that of water at the same temperature, while the relative viscosity of plasma is about 1.8 [28]. Taking ρ equal to 1.06 gm/cm for blood, the kinematic viscosity ($\nu = \mu/\rho$) ranges between .012 and .026 cm /sec at body temperature (37°C). The former value corresponds to plasma and the latter to normal hematocrit (relative viscosity 4). The corresponding range of N is .31 to .66 cm^2/sec. As the profile flattens (i.e., k increases), δ decreases while N increases in magnitude. Experimental results indicate that actual flow profiles may deviate considerably from a Poiseuille profile, (e.g., see [29]).

(C) In the construction of one-dimensional momentum balances for blood flow, one can, under the appropriate circumstances, avail oneself of the long-wave approximation [18], or the approximation of [15], to deduce assumption (D) and eliminate the contribution of the second-derivative viscous terms. This was done in [27] and thus the second-derivative viscous terms do not appear. The contributions of these terms should be small in many instances. However, in the present formulation of shocks they play an interesting role.

(D) The one-dimensional equations of blood flow are similar to the one-dimensional equations of gas dynamics. In blood flow the variable S plays a role akin to ρ in compressible flow. Thus many of the ideas of this more well developed subject are applicable here (see for example, any of the standard treatises [30, 31]), and supply a background for understanding the one-dimensional blood-flow theory.

(E) f, ψ and p are assumed to be assigned functions. Although this is more generality than is envisioned in application, it is assumed that f and ψ are at most functions of S, v, p, z and t, and that the dependence is smooth. The properties of p are taken up in the next section.

2.4 Constitutive Theory

The treatment of constitutive theory here is patterned after the theory of materials with memory, as developed by Coleman and his associates in many publications (see for example [32]). Some basic notions of Banach calculus are helpful to understand the theory (see for example [33]). The theory is general enough so that most of the results to follow do not depend upon a particular model. However, in subsequent sections it is sometimes convenient to abandon this general description in favor of more specific forms.

Let $\mathcal{C}$ denote the space of continuous functions from $(-\infty, t]$ into $\mathbb{R}$. Points in $\mathcal{C}$ are called <u>histories</u>. To each history $\chi \in \mathcal{C}$ corresponds the unique decomposition

$$\chi = \chi^t + \chi^r \tag{2.4.1}$$

where

$$\chi^t(s) = \begin{cases} \chi(s) & s = t \\ 0 & s \neq t \end{cases}$$

$$\chi^r(s) = \begin{cases} 0 & s = t \\ \chi(s) & s \neq t \end{cases} \tag{2.4.2}$$

χ^t is the <u>instantaneous part</u> of χ and χ^r the <u>past history</u> of χ.

Let $\tilde{\mathcal{C}}$ be the space of pairs (χ^t, χ^r) contructed from members χ of $\mathcal{C}$. Clearly $\tilde{\mathcal{C}}$ and

C are isomorphic. To each functional F on C (maps from C to $\mathbb{R}$) there corresponds a functional $\tilde{F}$ on $\tilde{C}$ defined by

$$\tilde{F}(x^t, x^r) = F(x) . \tag{2.4.3}$$

Let $\|\cdot\|_t$ be a norm on C which depends only upon the instantaneous part of each member of C and let $\|\cdot\|_r$ be a norm on C which depends only on the past history of members of C . The sum

$$\|\cdot\| = \|\cdot\|_t + \|\cdot\|_r \tag{2.4.4}$$

defines a norm on C and on $\tilde{C}$. The completions of C , $\tilde{C}$ with respect to $\|\cdot\|$ define isomorphic Banach spaces which are denoted by $B, \tilde{B}$ respectively.

A functional $\tilde{F}$ on $\tilde{B}$ is (Fréchet) differentiable at $x \in (x^t, x^r) \in \tilde{B}$ if there exists a linear map λ such that

$$\begin{aligned} \tilde{F}(x^t + h^t, x^r + h^r) = \tilde{F}(x^t, x^r) + \\ \lambda \cdot (h^t, h^r) + o(\|h\|) , \end{aligned} \tag{2.4.5}$$

for each $h \in \tilde{B}$, as $\|h\| \to 0$. The map λ is the derivative of $\tilde{F}$ at x and is denoted by $D\tilde{F}(x)$. In components,

$$D\tilde{F}(x) = (D_1\tilde{F}(x), D_2\tilde{F}(x)) , \tag{2.4.6}$$

and $D_1\tilde{F}$ is called the instantaneous derivative of $\tilde{F}$, and $D_2\tilde{F}$ the past history derivative of $\tilde{F}$. $\tilde{F}$ is

said to be differentiable if it is differentiable at each $(x^t, x^r) \in \tilde{B}$. If $\tilde{F}$ is differentiable at x , the partial derivatives may be computed (via the Gateaux definition) from the formulas:

$$D_1\tilde{F}(x)\cdot h^t = \frac{d}{d\epsilon}\,\tilde{F}(x^t+\epsilon h^t, x^r)\Big|_{\epsilon=0}$$
$$D_2\tilde{F}(x)\cdot h^r = \frac{d}{d\epsilon}\,\tilde{F}(x^t, x^r+\epsilon h^r)\Big|_{\epsilon=0} \quad . \tag{2.4.7}$$

A mechanical model with memory is one whose constitutive functional $\tilde{F}:\tilde{B}\longrightarrow\mathbb{R}$ is differentiable and $\|\cdot\|_r$ is finite for "reasonable" past histories. An example illustrates what might be considered reasonable. Certainly x^r = constant should be among the class of reasonable past histories. Define $\|\cdot\|_r$ by

$$\|x\|_r = \left(\int_{(-\infty,\,t]} |x|^2\, d\nu\right)^{1/2} , \tag{2.4.8}$$

where ν is absolutely continuous with respect to Lebesgue measure such that $\|x\|_r < \infty$ for all constant $x \in \tilde{B}$. A candidate for ν can be constructed as follows: let μ be Lebesgue measure on the μ- measurable subsets of $(-\infty, t]$. Fix $T \in (-\infty, t]$ and define ν by

$$\nu(A) = \mu(A \cap [T, t]) , \tag{2.4.9}$$

where A is any μ -measurable subset of $(-\infty, t]$. In this case $\tilde{F}$ would characterize a material with finite memory extending back to T . Note that if

$$\tilde{\tilde{F}}(x^t, x_1^r) = \tilde{\tilde{F}}(x^t, x_2^r) \qquad (2.4.10)$$

for all x^t and past histories x_1^r, x_2^r then $\tilde{\tilde{F}}$ can be represented as a function on the first component

$$\tilde{\tilde{F}}(x^t) = \tilde{\tilde{F}}(x^t, x^r) . \qquad (2.4.11)$$

Such functionals characterize elastic behavior, their memory being restricted to the present instant.

On the other hand, if

$$\tilde{\tilde{F}}(x_1^t, x^r) = \tilde{\tilde{F}}(x_2^t, x^r) \qquad (2.4.12)$$

for all x^r and instantaneous values x_1^t and x_2^t, then $\tilde{\tilde{F}}$ can be expressed as a functional on the second component

$$\tilde{\tilde{F}}(x^r) = \tilde{\tilde{F}}(x^t, x^r). \qquad (2.4.13)$$

Such materials represent the absence of instantaneous elastic behavior, e.g., the Kelvin model of linear viscoelasticity.

In the present work, materials are considered in which $\tilde{\tilde{F}}$ depends non-trivially upon both components.

The (wall) constitutive equation is the case of interest here. It is assumed to take the form:

$$p(\zeta, t) = \rho \tilde{\tilde{p}}(S^t, S^r; \zeta, t) \qquad (2.4.14)$$

where $p(\cdot, \cdot; \zeta, t) : \tilde{\tilde{B}} \longrightarrow \mathbb{R}$ represents a material with memory, in which S^t and S^r are notations

for $S^t(\zeta,\cdot)$ and $S^r(\zeta,\cdot)$ where

$$S(\zeta,\cdot) = S^t(\zeta,\cdot) + S^r(\zeta,\cdot) \tag{2.4.15}$$

is an element of $\tilde{B}$.

It is necessary to compute $\partial p/\partial \zeta$, since it appears in the momentum equation. By the chain rule

$$\begin{aligned}\frac{1}{\rho}\frac{\partial p}{\partial \zeta}(\zeta,t) = {} & D_1\tilde{p}(S^t,S^r;\zeta,t)\cdot\frac{\partial S^t}{\partial \zeta}(\zeta,t) \\ & + D_2\tilde{p}(S^t,S^r;\zeta,t)\cdot\frac{\partial S^r}{\partial \zeta}(\zeta,\cdot) \\ & + D_3\tilde{p}(S^t,S^r;\zeta,t)\,.\end{aligned} \tag{2.4.16}$$

By the above

$$\frac{\partial S^t}{\partial \zeta}(\zeta,t) = \frac{\partial S}{\partial \zeta}(\zeta,t)\,. \tag{2.4.17}$$

Thus in the first term of Eq. (2.4.16) the dot just represents multiplication, whereas in the second it represents the action of the linear map $D_2\tilde{p}$ upon $\frac{\partial S^r}{\partial \zeta}$. The first term is a measure of instantaneous elastic response, the second, dissipative effects, and the third, axial inhomogeneity.

From physical considerations it is assumed that

$$D_1\tilde{p} > 0\,. \tag{2.4.18}$$

For typical arterial behavior (see Fig. 2.2)

$$D_1^2\tilde{p} = D_1D_1\tilde{p} > 0\,, \tag{2.4.19}$$

however, any assumptions made upon $D_1^2\tilde{p}$ will be

stated as they are used. $D_1\tilde{P}$ and $D_1^2\tilde{P}$ are called the first and second instantaneous tangent moduli, respectively. In the sequel they will often be denoted simply by $\tilde{P}_s$ and $\tilde{P}_{ss}$, respectively.

For a fixed history S^r, the function $\tilde{P}(\cdot, S^r; \zeta, t)$ represents the instantaneous response function at (ζ, t); it is assumed to be a diffeomorphism over a preassigned domain of S, i.e., it and its inverse are smooth and one-to-one. It is also assumed that $\tilde{P}$ is smooth with respect to slots 2 to 4.

Note that $\tilde{P}$ is assumed to depend explicitly upon t (4th slot) to simulate physiomechanical changes produced, for example, by the administering of a drug.

If $P_A \geq 0$ is the constant ambient pressure, it is assumed that

$$P \geq P_A \ , \tag{2.4.20}$$

since otherwise an artery would tend to collapse.

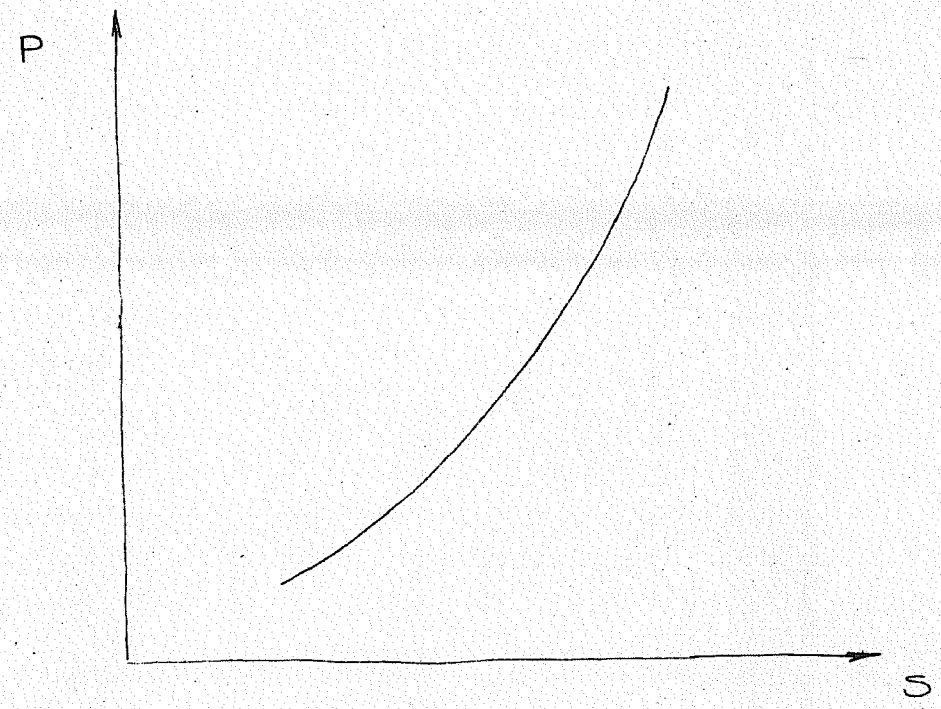

Figure 2.2.

Schematic of typical instantaneous pressure (p) vs. area (S) curve for an artery.

III. FLAT-PROFILE THEORY

3.1 Introduction

The continuity equation

$$\frac{\partial S}{\partial t} + \frac{\partial}{\partial z} Sv + \psi = 0 \quad , \tag{3.1.1}$$

when combined with the flat-profile velocity form of the momentum equation,

$$\frac{\partial v}{\partial t} + \frac{\partial}{\partial z}\left(\frac{v^2}{2} + \frac{p}{\rho} \right) = f + \nu \frac{\partial^2 v}{\partial z^2} \quad , \tag{3.1.2}$$

and the constitutive equation

$$p = \rho \tilde{p} \quad , \tag{3.1.3}$$

comprise the simplest model for simulating arterial flow. This system of equations, with $\nu = 0$, a specific form given to $\tilde{p}$ (usually $\tilde{p}$ is assumed to represent only elastic behavior), and ψ often ignored, has attracted considerable interest in the engineering blood-flow literature. It is the purpose of the present chapter to establish some of the basic properties of this system.

3.2 Cauchy Problem

In most problems of arterial blood flow, the effect of the second-order viscous term in Eq. (3.1.2) is quite small and thus this term is omitted (see Remark (C), p.20). In this case, Eqs. (3.1.1) - (3.1.3) constitute a pair of quasi-linear, hyperbolic, functional-partial differential equations. A system of

this sort can always be put in balance law form*

$$\frac{\partial}{\partial t}\underset{\sim}{U} + \frac{\partial}{\partial z}\underset{\sim}{F}(\underset{\sim}{U}) + \underset{\sim}{G}(\underset{\sim}{U}) = \underset{\sim}{0} , \qquad (3.2.1)$$

though not necessarily uniquely. When $\underset{\sim}{G}=\underset{\sim}{0}$, Eq. (3.2.1) is said to be a system of conservation laws. In the present case, Eqs. (3.1.1) - (3.1.3),

$$\underset{\sim}{U} = (S, v) , \quad \underset{\sim}{F}(\underset{\sim}{U}) = (Sv, \tfrac{v^2}{2} + \tilde{p})$$

$$\text{and} \quad \underset{\sim}{G}(\underset{\sim}{U}) = (\psi, -f) .$$

If the potentials

$$\Phi(z,t) = \int_{-\infty}^{z} \psi(z',t)\,dz' ,$$

$$\mathcal{F}(z,t) = \int_{-\infty}^{z} f(z',t)\,dz' ,$$

are defined, Eqs. (3.1.1) - (3.1.3) can be put into conservation law form, i.e., set $\underset{\sim}{U} = (S, v)$, $\underset{\sim}{F}(\underset{\sim}{U}) = (Sv + \Phi, \tfrac{v^2}{2} + \tilde{p} - \mathcal{F})$, $\underset{\sim}{G}(\underset{\sim}{U}) = \underset{\sim}{0}$. Systems such as Eq. (3.2.1) possess discontinuous solutions, even for C^∞ initial data, the form of which depends upon the way the system is written. An example, due to Gelfand[34], is illustrative of what is meant by this:

Consider the single conservation law

$$\frac{\partial v}{\partial t} + \frac{\partial}{\partial z}\left(\frac{v^2}{2}\right) = 0 . \qquad (3.2.2)$$

---

* When there are more than two equations this is in general not true; see [35].

It can be shown that if v is discontinuous across a curve $z = y_1(t)$, then the jump $[v] = v^- - v^+$ must satisfy

$$u_1 [v] = \left[\frac{v^2}{2}\right] , \tag{3.2.3}$$

where $u_1 = y_1'$. Note however that Eq. (3.2.2) can be written as

$$\frac{\partial}{\partial t}\left(\frac{v^2}{2}\right) + \frac{\partial}{\partial z}\left(\frac{v^3}{3}\right) = 0 , \tag{3.2.4}$$

which is also a conservation law. The associated jump condition across a curve $z = y_2(t)$ is

$$u_2 \left[\frac{v^2}{2}\right] = \left[\frac{v^3}{3}\right] \tag{3.2.5}$$

where $u_2 = y_2'$. The u's are seen to be the propagation velocities of the discontinuities. In general $u_1 \neq u_2$ and thus Eqs. (3.2.3) and (3.2.5) define two different classes of discontinuous solutions for the conservation law, Eq. (3.2.2). In fact, by multiplying Eq. (3.2.2) by higher powers of v, an infinite number of conservation forms can be obtained, each one with a different class of discontinuous solutions. The question naturally arises, which one is physically relevant?

This question is not an abstract one, since Eqs. (3.1.1) - (3.1.3) can be written as a system of balance laws in more than one way. The alternative

forms involve Eq. (3.1.2) and are illustrated by the following example:

Assume for simplicity that $\tilde{p}$ depends only upon the instantaneous value of S, i.e., $\tilde{p}: \mathbb{R} \to \mathbb{R}$. Multiply Eq. (3.1.2) by S, denote $D\tilde{p}$ by $\tilde{p}_s$, and employ Eq. (3.1.1) to get

$$\frac{\partial S v}{\partial t} + \frac{\partial}{\partial z}\left(S v^2 + \int_{\text{const.}}^{S} S' \tilde{p}_s(S')\, dS'\right) + v\psi = Sf , \tag{3.2.6}$$

which is in balance law form. Thus when $\tilde{p} = \tilde{p}(S)$ and $\nu = 0$, Eq. (3.2.6) is equivalent to the flat profile momentum form, Eq. (2.3.9). The jump condition associated with the velocity form is

$$u[v] = \left[\frac{v^2}{2} + \tilde{p}\right] , \tag{3.2.7}$$

whereas the jump condition associated with the momentum form is

$$u[Sv] = [Sv^2] + \int_{S^+}^{S^-} S\tilde{p}_s . \tag{3.2.8}$$

These are clearly different. This example is in fact general, i.e., it does not depend on the simplifying assumption made for $\tilde{p}$. Note that Eqs. (3.2.7) and (3.2.8) can be put in the alternative forms

$$0 = \left[\frac{w^2}{2} + \tilde{p}\right] , \tag{3.2.9}$$

$$0 = [Sw^2] + \int_{S^+}^{S^-} S\tilde{p}_s , \tag{3.2.10}$$

where $w^{\pm} = u - v^{\pm}$ is the relative velocity with respect to a fluid particle.

In continuum mechanics this question is easily disposed of since the balance laws are postulated in integral form, thus implying differential equations where the fields are smooth enough, and also a unique set of jump conditions where the fields experience discontinuities [36]. Thus it may seem natural to attempt to use the integral forms of mass conservation and balance of momentum to resolve the issue. However, such an approach is not workable for the following reasons:

First of all, the three-dimensional balance laws imply that for a homogeneous, incompressible, Newtonian fluid no discontinuities in particle velocity or pressure can exist. Even in the limiting case $\nu = 0$ the same conslusions hold. Thus discontinuities as envisioned here do not exist in the three-dimensional theory. Nevertheless they do arise in the one-dimensional theory and as such are a product of the approximations employed in its construction. A classical example in elasticity theory, of considerable similarity to the situation here, can be cited. In simple bar theory the so-called bar wave exists and can propagate as a discontinuity. Although it does not exist in the three-dimensional theory, under the appropriate circumstances it represents a close approximation to the bulk of the solution. For instance consider the example of a semi-infinite elastic bar

subjected to a step velocity input. The schematic, Fig. 3.1, is indicative of the nature of the approximation (see [37]).

Simple bar theory can be obtained as the long-wave approximation of the three-dimensional theory. Analogously, in the case of the one-dimensional theory here, the long-wave approximation eliminates, in particular, the $\nu \partial^2 v / \partial z^2$ term, rendering the system hyperbolic and capable of propagating discontinuities that the enlarged theory does not. With this view, a discontinuous solution is simply an approximation to a continuous one.

A criterion for selecting the appropriate form for a system of balance laws is not intrinsic. In the present, however, there is a natural criterion available for selecting the appropriate form of the momentum balance. Recall that ν is positive, and require that discontinuous solutions of Eq. (3.2.1) be obtained from smooth solutions of Eqs. (3.1.1) - (3.1.3) in the limit $\nu \to 0$.*

An example, also due to Gelfand [34], shows how a discontinuity may be formed by this process. Consider the case where ψ and f are zero. Let $z = y(t)$ be a curve in $\mathbb{R}^2$ across which a solution of Eq. (3.2.1) experiences a discontinuity. Let

* This raises the question, are all solutions of the system of Eqs. (3.1.1) - (3.1.3) smooth when $\nu > 0$? In gas dynamics where similar systems are studied this seems to be commonly believed. This matter is investigated in Section 3.4.

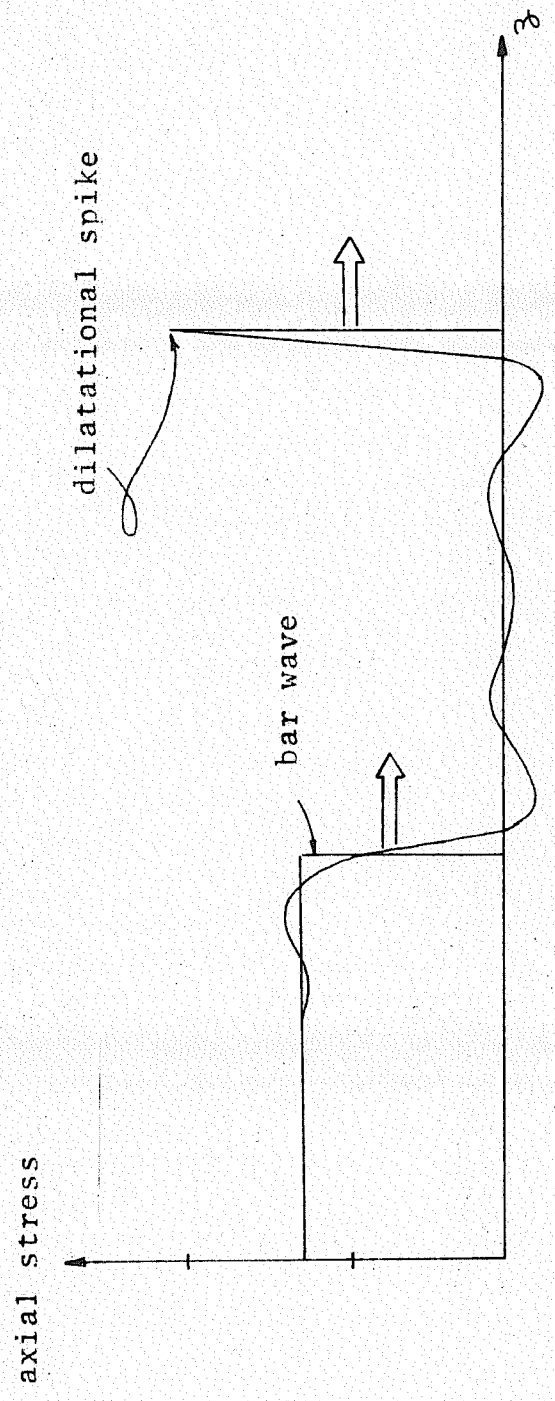

Figure 3.1

$(\bar{z},\bar{t})$ be a fixed point in $\mathbb{R}^2$ along this curve, and let $\bar{u} = y'(\bar{t})$. To study solutions of Eqs. (3.1.3) - (3.1.3) when $\nu > 0$ in a neighborhood of $(\bar{z},\bar{t})$, define the coordinate $\xi = z - \bar{u}t$ which runs perpendicular to the tangent of $y(t)$ at $(\bar{z},\bar{t})$, Fig. 3.2. Assume that the solution of Eqs. (3.1.1) - (3.1.3), to a sufficient degree of accuracy, is of the form $(S,v) = (S(\xi),v(\xi))$ in some neighborhood of $(\bar{z},\bar{t})$. Eqs. (3.1.1) and (3.1.2) become

$$
\begin{aligned}
-\bar{u}\,\frac{\partial S}{\partial \xi} + \frac{\partial Sv}{\partial \xi} &= 0 , \\
-\bar{u}\,\frac{\partial v}{\partial \xi} + \frac{\partial}{\partial \xi}\left(\frac{v^2}{2} + \bar{P}\right) &= \nu\,\frac{\partial^2 v}{\partial \xi^2} .
\end{aligned}
\tag{3.2.11}
$$

The solution of this system satisfies the relationship

$$
(S(\xi,\nu),v(\xi,\nu)) = (S(\xi/\nu,1),v(\xi/\nu,1)) . \tag{3.2.12}
$$

Suppose , as $\xi \longrightarrow \pm\infty$,

$$
(S(\xi,\nu),v(\xi,\nu)) \longrightarrow (S^{\pm},v^{\pm}), \text{ constants.} \tag{3.2.13}
$$

Then, by Eq. (3.2.12), as $\nu \longrightarrow 0$ this will converge to the discontinuous solution

$$
(S(\xi),v(\xi)) = \begin{cases} (S^{+},v^{+}) & \text{for } \xi > 0 \\ (S^{-},v^{-}) & \text{for } \xi < 0 \end{cases} . \tag{3.2.14}
$$

The situation is illustrated schematically in Fig. 3.3

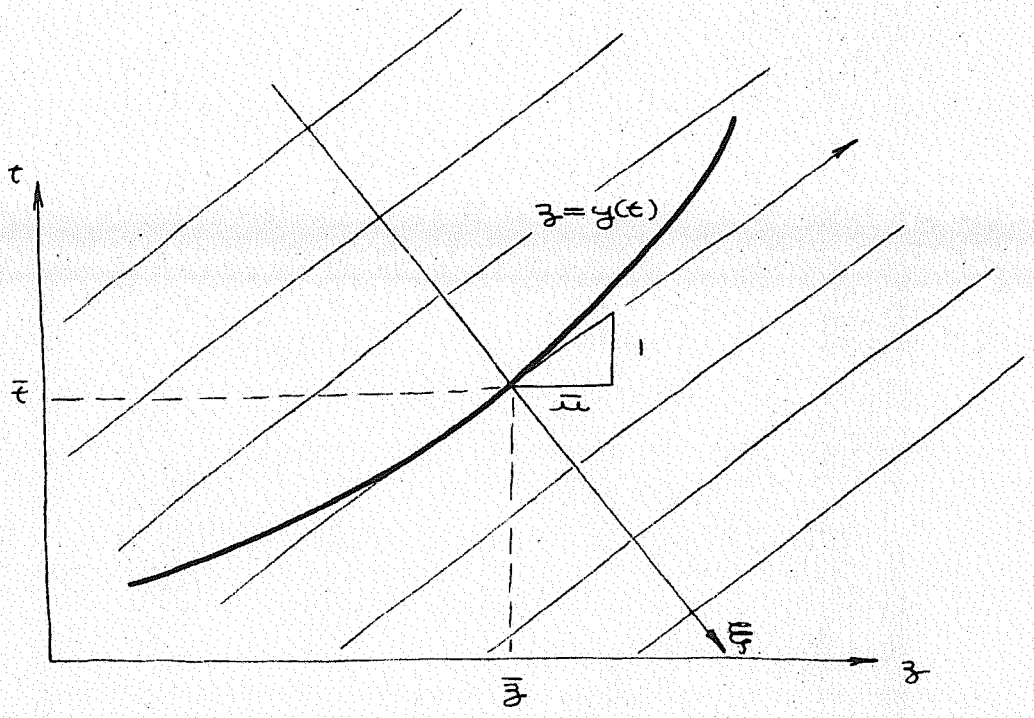

Figure 3.2

where $\bar{\xi}$ denotes $\bar{x} - \bar{u}\bar{t}$.

Integrating Eqs. (3.2.11) results in

$$
\begin{aligned}
&-\bar{u}(S^+ - S^-) + (S^+ v^+ - S^- v^-) = 0 \,, \\
&-\bar{u}(v^+ - v^-) + \left(\frac{v^{+2}}{2} + \bar{p}^+ - \frac{v^{-2}}{2} - \bar{p}^-\right) = \nu \left.\frac{\partial v}{\partial \bar{\xi}}\right|_{-\infty}^{+\infty} \,,
\end{aligned}
\tag{3.2.15}
$$

which upon using Eq. (3.2.13) and rearranging yields the jump conditions associated with Eqs. (3.1.1) - (3.1.3). This suggests that the velocity form of the momentum equation is the balance law form consistent with the flat-profile assumption.

It should be noted that the criterion of insisting that discontinuous solutions of Eqs. (3.1.1) - (3.1.3) when $\nu = 0$ be obtained from continuous ones in the limit $\nu \to 0$ is not the same as the so-called pseudo-viscosity criterion. In that criterion "viscosity" terms are added to a system of balance laws making it into a second-order parabolic system. The class of jump conditions which results when the "viscous" terms tend to zero, depends entirely on the form of the terms added. Thus this technique is useless to detect which is the physically appropriate class of jump conditions. On the other hand, if the model under study contains such terms ab initio, such as in the case here for the momentum equation, the technique of vanishing viscosity can be used effectively.

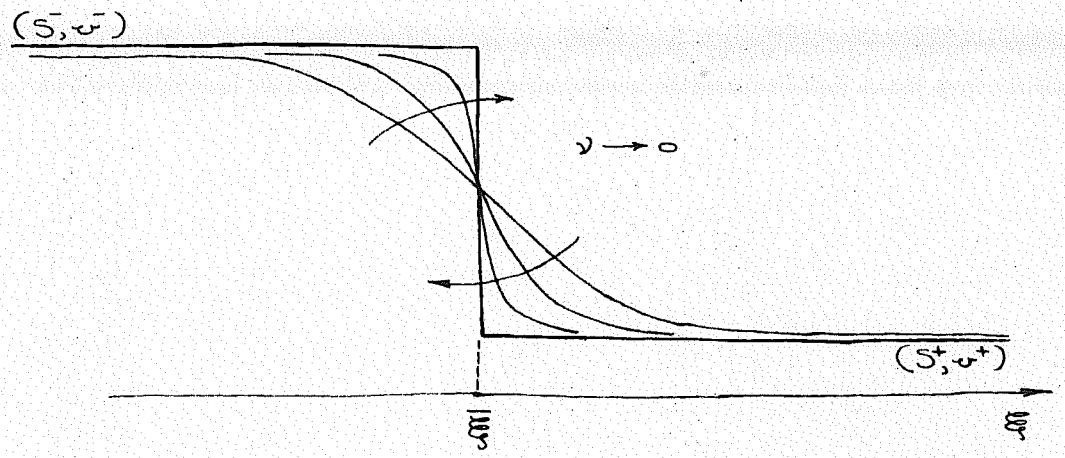

Figure 3.3

With the previous discussion as motivation, a definition of a solution to the Cauchy problem can now be given. A Cauchy problem for Eqs. (3.1.1) - (3.1.3) is one in which (S,v) are specified at $t=0$ for all $z \in \mathbb{R}$. A "solution" to Eqs. (3.1.1) - (3.1.3) is then sought in the interior $\mathcal{S}^\circ$ of the semi-infinite strip

$$\mathcal{S} = \{(z,t) \mid z \in (-\infty,+\infty),\ t \in [0,T)\}$$

which satisfies this initial data in some sense. Often T will be taken to be $+\infty$. In this case $\mathcal{S}$ is the upper half-plane $\mathcal{H}$. Let the initial data be given by measurable functions

$$S_0 : \mathbb{R} \longrightarrow \mathbb{R} ,$$

$$v_0 : \mathbb{R} \longrightarrow \mathbb{R} .$$

Then require that

$$S(z,t) \doteq S_0(z) ,$$

$$v(z,t) \doteq v_0(z) ,$$

where $\doteq$ means equality in a sense which will be made precise in short order.

Some standard notions from distribution theory are employed [38]. A map $\phi : \mathbb{R}^2 \longrightarrow \mathbb{R}$ is a test function if it is infinitely differentiable (of class C^∞) and has compact support. The space of test functions will be denoted by K . Let K_T be the subset of K such that each ϕ in K_T vanishes

identically when the second coordinate is restricted to T, i.e. ϕ is in K_T iff ϕ is in K and $\phi(\zeta,T)=0$ for all ζ.

In the following development the half-plane $\mathcal{H}$ will be used, for which the appropriate space of test functions is K. Everything can be recast for the strip $\mathcal{S}$ by replacing $\mathcal{H}$ by $\mathcal{S}$ and K by K_T.

By a <u>weak solution of Eqs.</u> (3.1.1) - (3.1.3) <u>for the Cauchy problem</u> is meant a pair of maps (S,v) such that

$$0=\int_{\mathcal{H}}\Big\{S\frac{\partial\phi_1}{\partial t}+Sv\frac{\partial\phi_1}{\partial\zeta}-\gamma\phi_1+v\frac{\partial\phi_2}{\partial t}$$

$$+\Big(\frac{v^2}{2}+\tilde{P}\Big)\frac{\partial\phi_2}{\partial\zeta}+f\phi_2+\nu v\frac{\partial^2\phi_2}{\partial\zeta^2}\Big\}d\zeta dt \qquad (3.2.16)$$

$$+\int_{\mathbb{R}}(S_0\phi_1+v_0\phi_2)\Big|_{t=0}d\zeta$$

for all ϕ_α in K, where (S_0,v_0) are given initial data. A <u>strong solution</u> is a weak solution such that S has continuous first derivatives throughout $\mathcal{H}^\circ$ and v has continuous derivatives of order 2 (1, resp.) throughout $\mathcal{H}^\circ$ when $\nu>0$ ($\nu=0$). In this case the equations are satisfied in the classical sense. Note that a history of S up to $t=0$ must always be assumed so that $\tilde{P}$ can be computed for $t>0$.

Integration by parts exhibits the way in which a weak solution satisfies the initial conditions,

namely

$$0 = \lim_{t \to 0} \int_{\mathbb{R}} \{(S_0(z) - S(z,t))\phi_1(z,t) + (v_0(z) - v(z,t))\phi_2(z,t)\}\, dz \qquad (3.2.17)$$

for all ϕ_α in K .

The possibility of Eqs. (3.1.1) - (3.1.3) having weak solutions with finite discontinuities across a curve y with tangent defined by $dy/dt = u$, the propagation velocity of the discontinuity, will now be examined. For the present analysis, it is assumed that $0 \neq u \neq \pm\infty$.

Let $\lambda = \{(t, y(t)) \mid t \in \mathbb{R}\}$, the graph of y . Assume that on the complement of λ , (S,v) comprises a strong solution. Without loss of generality, assume λ splits $\mathcal{H}$ into two regions, $\mathcal{H}^+$ and $\mathcal{H}^-$.

Let ℓ be the arc-length parameter for λ . An orientation of λ is given by requiring that the tangent vector to λ at $t=0$ point in the positive t direction. The unit tangent vector $\dot{\lambda}$ along λ is given by $\dot{\lambda} = (u,1)/(1+u^2)^{1/2}$; the unit outward normal vector with respect to $\mathcal{H}^+$ is given by $n^+ = (-1,u)/(1+u^2)^{1/2}$; and $n = n^- = -n^+$ is the outward unit normal vector to $\mathcal{H}^-$, Fig. 3.4.

The operator $\nabla = \left(\frac{\partial}{\partial z}, \frac{\partial}{\partial t}\right)$ is the gradient operator on $\mathbb{R}^2$. Thus if $x = (x_1, x_2)$ is smooth in $\mathcal{H}^+$ and $\mathcal{H}^-$, but it and its first derivatives experience finite discontinuities across λ , and Φ is in K ,

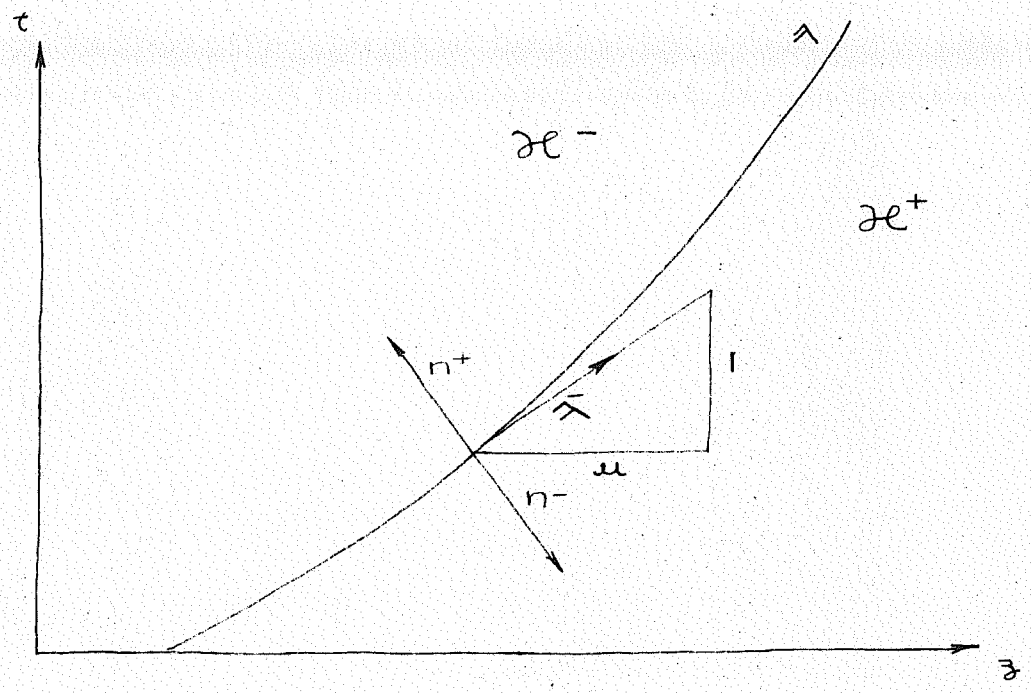

Figure 3.4

then by the divergence theorem

$$\int_{\partial\mathcal{E}} \nabla\cdot(x_1\phi, x_2\phi)\,dz\,dt = \int_{\lambda} n\cdot([x_1]\phi, [x_2]\phi)\,d\ell,$$

where the jump operator $[\,\cdot\,]$ is defined by $[x]=x^- - x^+$ and $x^{\mp}(z,t)$ is the limit of a sequence in $\mathcal{E}^{\mp}$.

If the weak solution (S,v) and its derivatives of order ≤ 2 have finite discontinuities across λ then integrating (3.2.16) by parts yields

$$\begin{aligned} 0 = &-\int_{\mathcal{E}^+\cup\mathcal{E}^-} \{\phi_1\left(\frac{\partial S}{\partial t} + \frac{\partial Sv}{\partial z} + \psi\right) + \\ &\phi_2\left(\frac{\partial v}{\partial t} + \frac{\partial}{\partial z}\left(\frac{v^2}{2}+\tilde{p}\right) - f - \nu\frac{\partial^2 v}{\partial z^2}\right)\}dz\,dt \\ &+\int_{\mathbb{R}} \{\phi_1(z,0)(S_0(z)-S(z,0)) + \\ &\phi_2(z,0)(v_0(z)-v(z,0))\}dz \\ &+\int_{\lambda} \{\phi_1([Sv]-u[S])/(1+u^2)^{1/2} \\ &+\phi_2([\tfrac{v^2}{2}+\tilde{p}-\nu\tfrac{\partial v}{\partial z}]-u[v])/(1+u^2)^{1/2} \\ &+\frac{\partial\phi_2}{\partial z}\nu[v]\}\,d\ell \end{aligned} \tag{3.2.18}$$

By virtue of the fact that (S,v) is a weak solution, the integral involving the initial conditions vanishes, and since (S,v) is a strong solution on the complement of λ, the integral over $\mathcal{E}^+\cup\mathcal{E}^-$ also vanishes. Thus the integral over λ vanishes identically. Since ϕ_1, ϕ_2, $\partial\phi_2/\partial z$ are independent on λ and assuming u is finite, it follows that

$$\begin{aligned} u[S] &= [Sv]\,, \\ u[v] &= [\tfrac{v^2}{2}+\tilde{p}-\nu\tfrac{\partial v}{\partial z}]\,, \\ 0 &= \nu[v]. \end{aligned} \tag{3.2.19}$$

Note that as $\nu \to 0$ in Eqs. (3.2.19) the desired jump conditions are obtained.

The following conjectures* are made about the system when $\nu > 0$. The Cauchy problem $(S^\nu, u^\nu)(x,0) = (S_0, u_0)(x)$ can be solved for all bounded measurable pairs (S_0, u_0). The solution (S^ν, u^ν) is unique, and as $\nu \to 0$, (S^ν, u^ν) converges boundedly, almost everywhere in some interval $0 \le t \le T$ to a limit (S, u).

With these conjectures the form of the definition of a weak solution is motivated. For example, if ϕ_1, ϕ_2, S_0, u_0 are held fixed and $\nu \to 0$ in Eq. (3.2.16) the viscous term approaches zero and

$$
\begin{aligned}
S^\nu u^\nu &\longrightarrow S u \,, \\
\psi^\nu &\longrightarrow \psi \,, \\
\left(\frac{u^\nu}{2}\right)^2 + \tilde{P}^\nu &\longrightarrow \frac{u^2}{2} + \tilde{P} \,, \\
f^\nu &\longrightarrow f \,;
\end{aligned}
$$

in $0 \le t \le T$. Thus the limiting pair (S,u) is by definition a weak solution in $0 \le t \le T$ when $\nu = 0$, and the definition of a weak solution is consistent with the physical idea that the solution for the case $\nu = 0$ should be obtainable as the limit of a family of solutions each of which corresponds to some $\nu > 0$.

The situation will arise when a solution can

---

* These conjectures emanate from the work of P.D.Lax [39].

be constructed directly for the case $\nu = 0$ and it may be impossible to say whether or not it is the limit of a viscous solution. Setting $\nu = 0$ in Eq. (3.2.16) does not give rise to a unique definition of a weak solution. To see this consider the example of Lax [40] for a single conservation law:

Define a Cauchy problem for the conservation law

$$\frac{\partial v}{\partial t} + \frac{\partial}{\partial x}\left(\frac{v^2}{2}\right) = 0, \tag{3.2.20}$$

by requiring

$$v(x,0) = \begin{cases} 0 & x < 0 \\ 1 & x > 0 \end{cases}, \tag{3.2.21}$$

and define the relevant class of discontinuous solutions by the jump condition

$$u\,[v] = \left[\frac{v^2}{2}\right]. \tag{3.2.22}$$

The form of the definition of a weak solution is easily seen to be

$$0 = \int_{\mathcal{R}} \left\{ v \frac{\partial \phi}{\partial t} + \frac{v^2}{2} \frac{\partial \phi}{\partial x} \right\} dx\,dt + \int_0^\infty \phi(x,0)\,dx. \tag{3.2.23}$$

The function (Fig. 3.5)

$$v_1(x,t) = \begin{cases} 0 & x < t/2 \\ 1 & x > t/2 \end{cases}, \tag{3.2.24}$$

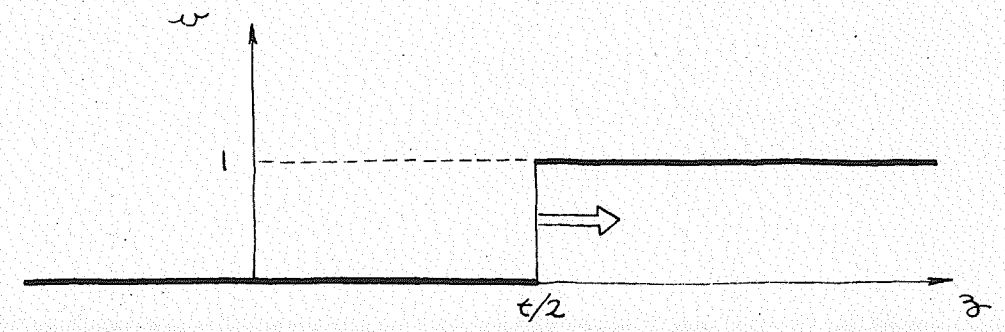

Figure 3.5

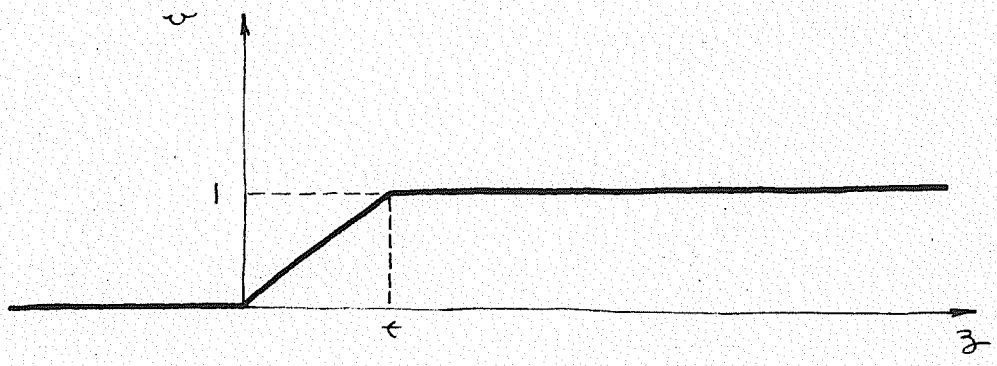

Figure 3.6

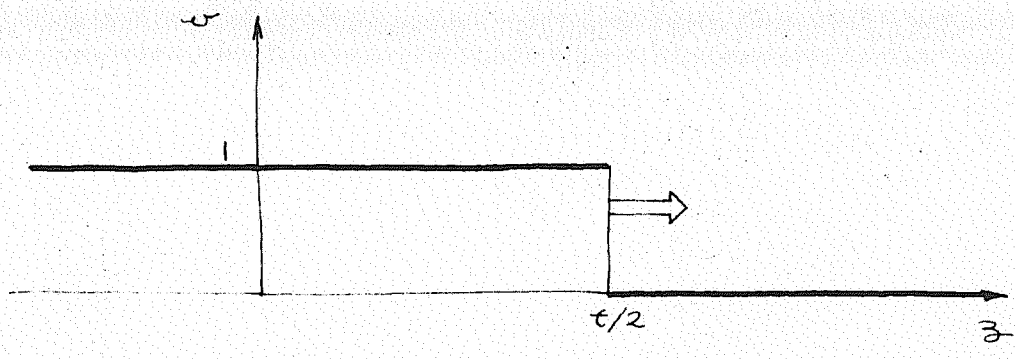

Figure 3.7

satisfies Eq. (3.2.23); or equivalently satisfies Eq. (3.2.20), except on the line $\xi = t/2$ where Eq. (3.2.22) applies and is satisfied, and takes on the initial values, Eq. (3.2.21). However the function (Fig. 3.6)

$$v_2(\xi,t) = \begin{cases} 0 & \xi \le 0 \\ \xi/t & 0 < \xi \le t \\ 1 & t \le \xi \end{cases}$$

which is continuous for all $t>0$, also satisfies Eq. (3.2.23) and thus is a weak solution.

Much effort has been exerted to develop a criterion for selecting the physically relevant solution.* For the above situation all criteria proposed are equivalent to the condition

$$v^- > u > v^+ , \qquad (3.2.25)$$

hold on a line of discontinuity where, as before, v^- and v^+ are the values of v to the left and right, respectively, of the discontinuity line. The function v_2 automatically satisfies this condition since it is continuous for $t>0$. For v_1, $v_1^- = 0$, $v_1^+ = 1$ and $u = 1/2$ which violates (3.2.25). Thus v_2 is the

---

* See Lax [41] which deals with the shock, entropy and viscosity criteria. An entropy-rate criterion is given by Dafermos [42]. Thermodynamic arguments are considered by Bland [43] and Courant-Friedrichs [30], and a shock stability argument is also given by Bland [43].

physically relevant solution.

It is interesting to note that the Cauchy problem defined by Eqs. (3.2.20), (3.2.22) and

$$v(z,0) = \begin{cases} 1 & z<0 \\ 0 & z>0 \end{cases} \qquad (3.2.26)$$

has the discontinuous solution (Fig. 3.7)

$$v(z,t) = \begin{cases} 1 & z< t/2 \\ 0 & z> t/2 \end{cases} \qquad (3.2.27)$$

which satisfies (3.2.25). Note that $dz/dt = v$ defines the characteristic curves for Eq. (3.2.20). Condition (3.2.25) for solutions (3.2.24) and (3.2.27) is depicted in Fig. 3.8.

Consideration of this issue for Eqs. (3.1.1)-(3.1.3) is given in Sections 5.3 and 5.9 via examples and numerical computations.

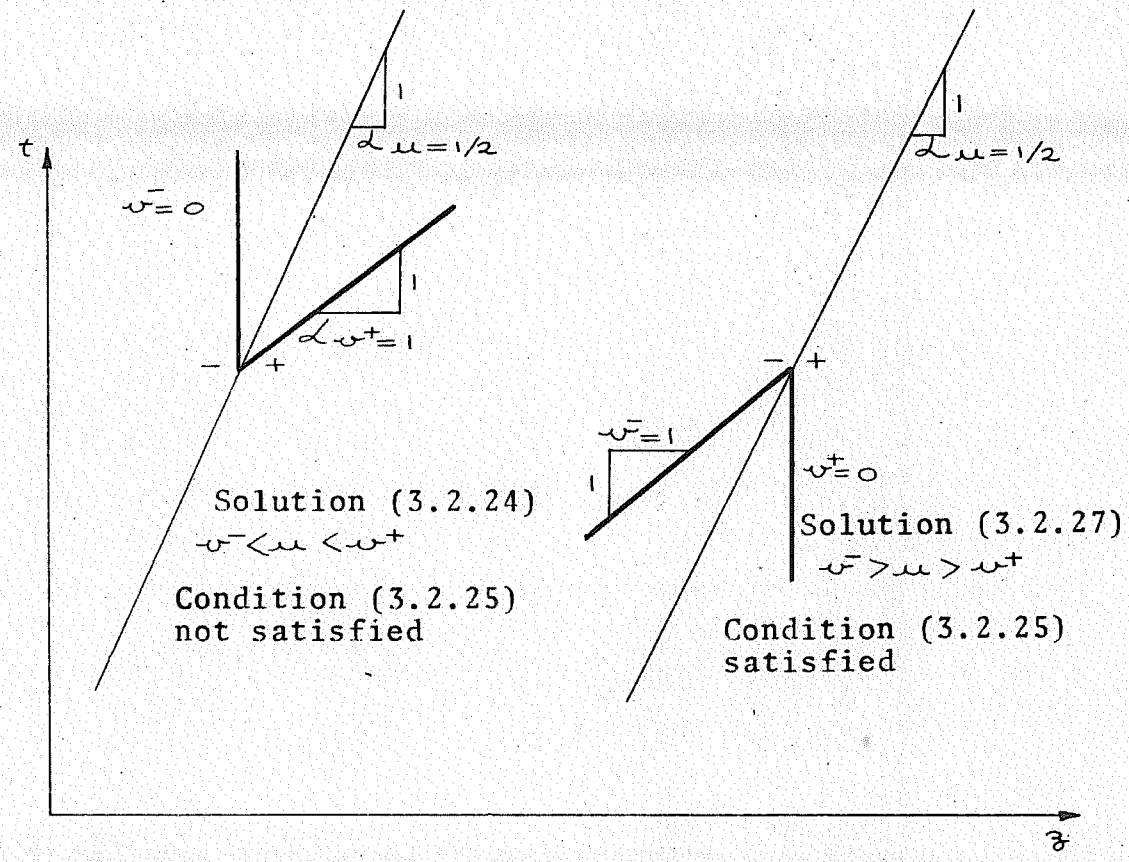
t
x
1
$\alpha_{u=1/2}$
$v^- = 0$
1
$\alpha_{v^+=1}$
−
+
Solution (3.2.24)
$v^- < u < v^+$
Condition (3.2.25)
not satisfied
1
$\alpha_{u=1/2}$
−
+
$v^- = 1$
1
$v^+ = 0$
Solution (3.2.27)
$v^- > u > v^+$
Condition (3.2.25)
satisfied

Figure 3.8

3.3 Mixed Initial-Boundary Value Problem

Most problems of interest involve finite domains. It is the purpose of this section to define what is meant by a weak solution to the general mixed initial-boundary value problem for Eqs. (3.1.3) - (3.1.3).

Let the arterial segment be defined by the interval $[a,b]$, $a<b$. The aim is to compute (S,v) in the interior $\mathcal{R}^\circ$ of the rectangle

$$\mathcal{R} = \{(z,t) \mid z \in [a,b],\ t \in [0,T]\},$$

given the initial data (S_0,v_0) along $t=0$ and some boundary data along $z=a$ and $z=b$. As before, T will often be taken to be $+\infty$ and a,b may equal $-\infty,+\infty$, respectively. When $a=-\infty$ and $b=+\infty$ the definition must be equivalent to the one given for the Cauchy problem. The case $a=0, b=L$ will be considered here. The deduction of the formulation for any other specific case, e.g., $L\to\infty$ will be obvious.

The number of boundary data to be specified is not so obvious, in that different specifications might be expected for the cases $\nu=0$ and $\nu>0$. Consider first the case $\nu=0$, since the classical approach, using characteristics, gives the complete answer, assuming everything is smooth enough for the analysis to be valid.

When $\nu=0$ the equations are hyperbolic and the development of a solution may be studied by way

of the characteristic equations. The first step then is to obtain the characteristic equations corresponding to Eqs. (3.1.1) - (3.1.3). The techniques used for this are standard and are contained in all works on first order systems (e.g., Courant-Friedrichs [30], Aris-Amundson [44], whose notation is employed here) and thus details will be omitted. The characteristic equations are

$$\begin{aligned}
&\frac{\partial z}{\partial \alpha} - \sigma_+ \frac{\partial t}{\partial \alpha} = 0 \ , \\
&\frac{\partial z}{\partial \beta} - \sigma_- \frac{\partial t}{\partial \beta} = 0 \ , \\
&\mathcal{L} \frac{\partial S}{\partial \alpha} + M_+ \frac{\partial v}{\partial \alpha} + N_+ \frac{\partial t}{\partial \alpha} = 0 \ , \\
&\mathcal{L} \frac{\partial S}{\partial \beta} + M_- \frac{\partial v}{\partial \beta} + N_- \frac{\partial t}{\partial \beta} = 0 \ ,
\end{aligned} \tag{3.3.1}$$

where α and β are parameters along the families of curves satisfying at each point of $\mathcal{R}$

$$\lambda_+ : \frac{dz}{dt} = \sigma_+ \quad , \quad \lambda_- : \frac{dz}{dt} = \sigma_- \ .$$

In the present case

$$\begin{aligned}
\sigma_\pm &= v \pm c \ , \\
c &= (S\tilde{p}_S)^{1/2} \ , \\
\mathcal{L} &= \tilde{p}_S \ , \\
M_\pm &= \pm c \ , \\
N_\pm &= (D_2\tilde{p} \cdot \frac{\partial S^r}{\partial z} + D_3\tilde{p} - f)(\sigma_\pm - v) \\
&\quad - \psi \tilde{p}_S \ .
\end{aligned}$$

The condition of hyperbolicity is $S\tilde{p}_S > 0$ which is guaranteed since $S > 0$, $\tilde{p}_S > 0$. This insures that

there exists two families of real characteristics, namely those defined by $\sigma_{\pm}$. It is assumed that

$$S\tilde{P}_S > v^2 \quad ;$$

therefore the characteristic velocities always satisfy

$$\sigma_+ > 0 \quad , \quad \sigma_- < 0 \quad ,$$

as illustrated in Fig. 3.9.

To see how the solution develops, construct finite difference analogs of Eqs. (3.3.1) for the triangle ABC:

$$\begin{aligned} &\mathcal{L}_A (S_C - S_A) + M_{-A}(v_C - v_A) + N_{-A}(t_C - t_A) = 0 \ , \\ &\mathcal{L}_B (S_C - S_B) + M_{+B}(v_C - v_B) + N_{+B}(t_C - t_B) = 0 \ , \\ &z_C = z_A + \sigma_{-A}(t_C - t_A) \ , \\ &z_C = z_B + \sigma_{+B}(t_C - t_B) \ . \end{aligned} \tag{3.3.2}$$

Eqs. $(3.3.2)_{3,4}$ are solved simultaneously to locate the coordinates (z_C, t_C) . Then from the set of initial data, S_o and v_o , which give (S_A, v_A) and (S_B, v_B) Eqs. $(3.3.2)_{1,2}$ can be used to compute (S_C, v_C) . Thus the prescription of S and v along

$$\{(z,t) \mid z \in [0,L], t = 0\}$$

is seen to be necessary to generate the solution in the interior of $\mathcal{R}$.

What data can be specified along $\{(z,t) \mid z = 0, t \in [0,T]\}$? Analogous to the construction of Eq. (3.3.2), difference equations can

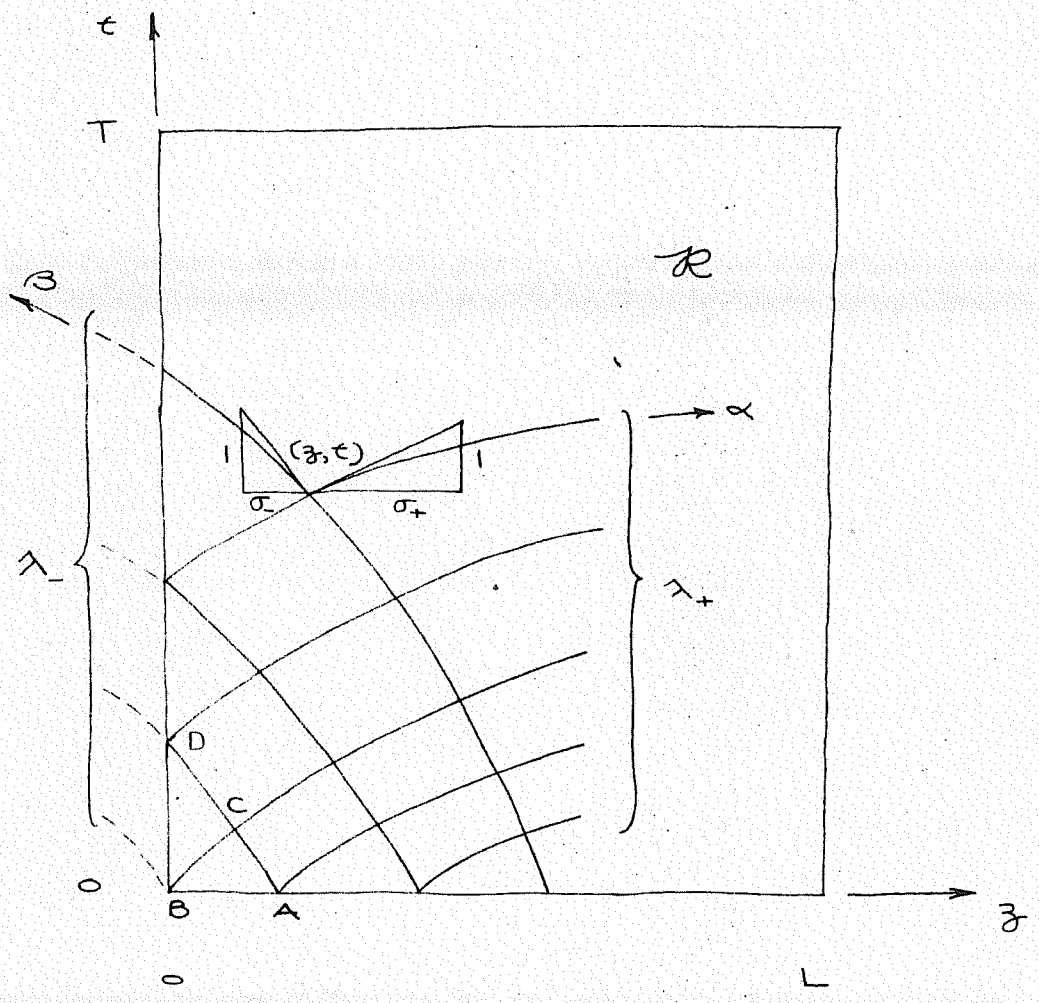

Figure 3.9

be set up along the λ_- characteristic through A and D :

$$z_D = z_A + \sigma_{-A}(t_D - t_A) ,$$
$$\mathcal{L}_A(S_D - S_A) + M_{-A}(v_D - v_A) + N_{-A}(t_D - t_A) = 0. \qquad (3.3.3)$$

Since $z_D = 0$, Eq. $(3.3.3)_1$ determines t_D . Thus Eq. $(3.3.3)_2$ is an equation relating S_D and v_D , and so only one of them (or one condition relating both of them) can be specified at D . Thus along $\{(z,t) \mid z=0, t \in [0,T]\}$ only one datum may be prescribed. The same argument applies along $\{(z,t) \mid z=L, t \in [0,T]\}$. Thus with both data given along $t=0$ and one datum given along each of $z=0$ and $z=L$, a solution throughout $\mathcal{R}$ can unambiguously be constructed. Notice that the condition

$$\sigma_+ > 0 \quad , \quad \sigma_- < 0 ,$$

was essential for this argument to work.

The general case is clear. For example, suppose $\sigma_+, \sigma_- > 0$ (Fig. 3.10); then no characteristic emanating from the $t=0$ or $z=L$ boundary can intersect the boundary $z=0$. In this case two data would be specified along $z=0$ and none on $z=L$. This case and the case when both $\sigma_+, \sigma_- < 0$ are not anticipated in problems of blood flow.

It is expected that under steady flow conditions the same number of boundary data are to be

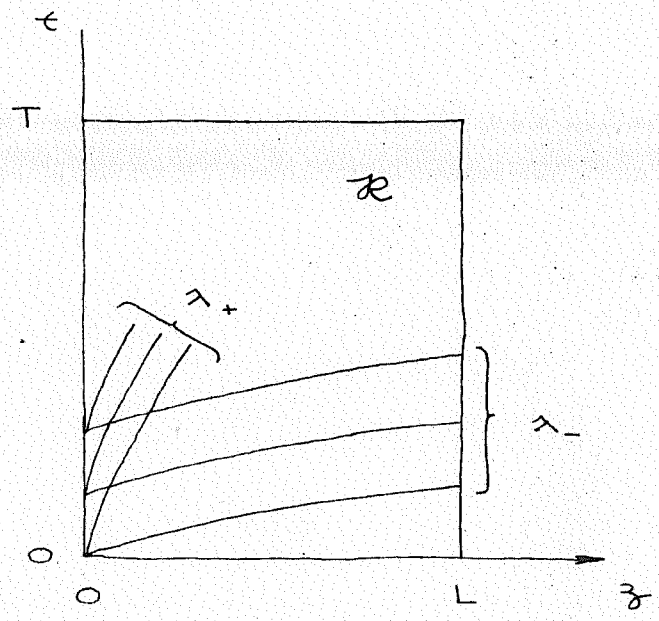

Figure 3.10

specified as for the time dependent case. A short analysis makes this assertion plausible:

Assume ψ and f are zero, a fixed history S^r has been substituted in $\tilde{p}$, and conditions are steady. Then Eqs. (3.1.1) - (3.1.3) can be integrated

$$\begin{aligned} S v &= c_1 , \\ \frac{v^2}{2} + \tilde{p} &= c_2 , \end{aligned} \tag{3.3.4}$$

where c_1, c_2 are constants.

Assuming $\tilde{p}$ is defined for all positive S, Eqs. (3.3.4) can always be solved for S, v in terms of c_1 and c_2, with the obvious consistency condition $c_2 > 0$. To see this write Eqs. (3.3.4) as

$$c_\alpha = \hat{c}_\alpha(S,v) = \hat{c}_\alpha(u_1, u_2) = \hat{c}_\alpha(u_\beta) , \tag{3.3.5}$$

where α, β range over 1 and 2. Then, by the implicit function theorem, a unique solution to Eqs. (3.3.5) exists if the Jacobian, $\det(\partial \hat{c}_\alpha / \partial u_\beta)$, does not vanish. This happens as long as $v^2 \neq c^2$, which has been assumed.

Therefore, whenever c_1 and c_2 can be unambiguously determined from the boundary data, a unique solution exists. For example, if the flow, Sv, were specified at $z=0$, and the apparent stress, $\rho\frac{v^2}{2} + p$, were specified at $z=L$, then c_1, c_2 are immediately defined by evaluating Eqs. (3.3.4) at

$z=0$ and $z=L$, respectively.

Other combinations, involving S and v individually, and the flow and apparent stress, can be studied similarly. The rule of thumb then is one datum at each end enables the computation of the two c_k's. Its application must be tempered with reasonableness however since there are some obvious consistency conditions for steady flow, e.g., one could not specify the flow or the apparent stress independently at both ends. In steady flow things can also be done which cannot be done in the time dependent case, e.g., the flow and apparent stress can be specified at either $z=0$ or $z=L$ and a solution could be obtained.

The characteristic equations were useful in determining the number of boundary data for the case $\nu=0$. It is natural to try to use this technique when $\nu>0$. Defining

$$q = \frac{\partial v}{\partial z} , \tag{3.3.6}$$

Eqs. (3.1.1) - (3.1.3) and (3.3.6) define a first-order system of three equations with S, v and q as unknowns. The eigenvalues of this system, which define the characteristic directions, are

$$\begin{aligned} \frac{dt}{dz} &= 0 , \quad \text{(multiplicity 2)}, \\ \frac{dt}{dz} &= \frac{1}{v} . \end{aligned} \tag{3.3.7}$$

Thus the characteristic grid consists of the lines t = constant, Eq. $(3.3.7)_1$, and the particle paths, Eq. $(3.3.7)_2$, (Fig. 3.11). The next step is to try to write the system as three ordinary differential equations along the characteristics - two along t = constant and one along the particle paths. The appropriate differential operators along these characteristics are $\partial/\partial z$ and $\dot{(\ )} = \partial/\partial t + w\,\partial/\partial z$, respectively. Eq. (3.3.6) is already solely in terms of $\partial/\partial z$ and the first two terms of Eq. (3.1.1) can be grouped to form $\dot{S}$, viz., $\dot{S} + Sq + \psi = 0$. Thus it remains to transform Eq. (3.1.2), using Eqs. (3.1.1) and (3.3.6), to a form solely in terms of the operator $\partial/\partial z$. This does not appear to be possible. It is not surprising, due to the multiplicity of eigenvalues.

If the system were rendered parabolic by adding a term $k\,\partial^2 S/\partial z^2$ to Eq. (3.1.1), where $k>0$ is a constant, it is reasonable to expect that two data should be specified at each end. For the present case, Eqs. (3.1.1) - (3.1.3), one might guess then that two data be specified at one end and one datum be specified at the other. An analysis of the steady flow equations makes this plausible.

Assume ψ and f are zero, a fixed history S^t has been substituted in $\tilde{p}$, and conditions are steady. Integrating Eqs. (3.1.1) - (3.1.3) yields

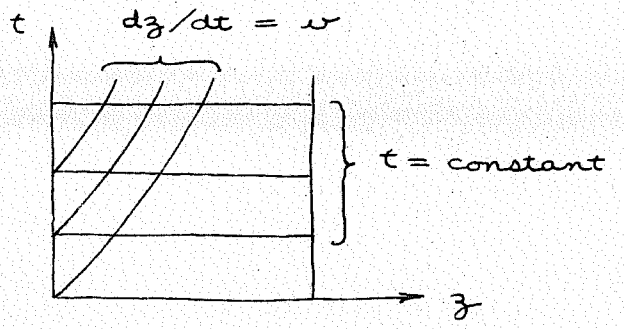

Figure 3.11

$$S\upsilon = c_1 \,,$$
$$\frac{\upsilon^2}{2} + \tilde{P} - \nu \frac{d\upsilon}{dz} = c_2 \,, \qquad (3.3.8)$$

where c_1, c_2 are constants. Solving Eq. $(3.3.8)_1$ for υ and substituting into Eq. $(3.3.8)_2$, results in an ordinary differential equation for S,

$$\frac{dS}{dz} = g(z,S) = \frac{S^2}{\nu c_1}\left(c_2 - \frac{c_1^2}{2S^2} + \tilde{P}\right). \qquad (3.3.9)$$

Since g is continuous in $\mathcal{O} = [0,L] \times (0,\infty)$ and satisfies a Lipschitz condition in S locally in $\mathcal{O}$, then through every $(\bar{z}, \bar{S}) \in \mathcal{O}$ there exists a unique continuous integral curve $S(z)$ which extends to the boundary of $\mathcal{O}$ or becomes unbounded ([45], pp. 15-17). Assume the former case holds for all physically relevant data. This result can be written as

$$S = \hat{S}(c_1, c_2, c_3) \,, \qquad (3.3.10)$$

where c_3 is the constant of integration, and the z dependence is implicit; υ can then be obtained from Eq. $(3.3.8)_1$. Thus if the three c_i's can be computed from the prescribed boundary data, S and υ can be determined from Eqs. (3.3.10) and (3.3.8). It is thus reasonable to assume that three boundary data are required to determine the c_i's. Henceforth it is assumed this is also true for the time dependent case.

It goes without saying that better methods are needed to study this problem.

Some new spaces of test functions will be needed. Let $K(a) = \{\phi \mid \phi \in K, \phi(a,t) = 0 \ \forall t\}$ and define $K(a,b) = K(a) \cap K(b)$. Similarly define the spaces

$$K_T(a) = K(a) \cap K_T \ ,$$

$$K_T(a,b) = K(a,b) \cap K_T \ , \text{ etc.}$$

Let $K'(a) = \{\phi \mid \phi \in K, D_1\phi(a,t) = 0 \ \forall t\}$ and define $K'_T(a) = K'(a) \cap K_T$. As for the Cauchy problem, take $T = +\infty$ and thus the space K will be employed. Everything that ensues holds for $T < \infty$ if the K's are replaced by K_T's.

With these, a definition of a weak solution to the general mixed initial-boundary value problem can be given. A <u>weak solution of Eqs.</u> (3.1.1) - (3.1.3) <u>for the initial-boundary value problem</u>, is a pair (S,v) such that

$$\begin{aligned} 0 = \int_{\mathcal{R}} \{ & S\frac{\partial \phi_1}{\partial t} + Sv\frac{\partial \phi_1}{\partial z} - \psi\phi_1 + v\frac{\partial \phi_2}{\partial t} \\ & + \left(\frac{v^2}{2} + \tilde{p}\right)\frac{\partial \phi_2}{\partial z} + f\phi_2 + \nu v\frac{\partial^2 \phi_2}{\partial z^2} \} \, dz\,dt \\ & + \int_{\mathbb{R}} (S_0\phi_1 + v_0\phi_2)\Big|_{t=0} dz \quad + \quad \mathcal{B} \ , \end{aligned} \tag{3.3.11}$$

where

$$\mathcal{B} = -\int_{\mathbb{R}^+} \{Q\phi_1 + \tau\phi_2 + \nu v\frac{\partial \phi_2}{\partial z}\}\Big|_{z=0}^{z=L} dt \ , \tag{3.3.12}$$

and $Q, \mathcal{C}$ and $\vee : \{0,L\} \times [0,\infty) \longrightarrow \mathbb{R}$ are the prescribed boundary values of flow, apparent stress and velocity, respectively, and the ϕ_α's are chosen from particular spaces of test functions so that the boundary value problem makes sense. In addition, a weak solution may be required to satisfy boundary data of the form

$$\begin{aligned} S(0,t) &= \mathcal{A}(0,t) \,, \\ S(L,t) &= \mathcal{A}(L,t) \,, \\ v(0,t) &= \vee(0,t) \,, \\ v(L,t) &= \vee(L,t) \,, \end{aligned} \tag{3.3.13}$$

where $\mathcal{A} : \{0,L\} \times [0,\infty) \longrightarrow \mathbb{R}^+$ represents the prescribed boundary values of luminal area. Eqs. $(3.3.13)_{3,4}$ are stipulated, in addition to the inclusion of the $\vee$ term in $\mathcal{B}$, to cover the case in which $\nu = 0$ and velocity boundary data are given.

A few examples will be presented to clarify what this definition means.

Suppose $\nu = 0$. In this case two boundary data, one at each end, must be satisfied. Consider the following cases

$$\begin{aligned} &\text{(I)} \quad v(0,t) = \vee(0,t), \\ &\qquad\quad v(L,t) = \vee(L,t), \\ &\text{(II)} \quad v(0,t) = \vee(0,t), \\ &\qquad\quad S(L,t) = \mathcal{A}(L,t), \end{aligned}$$

$$\text{(III)} \quad \begin{aligned} u(0,t) &= v(0,t), \\ (Su)(L,t) &= Q(L,t), \end{aligned}$$

$$\text{(IV)} \quad \begin{aligned} \left(\frac{u^2}{2} + \tilde{p}\right)(0,t) &= \tau(0,t) > 0, \\ u(L,t) &= v(L,t), \end{aligned}$$

$$\text{(V)} \quad \begin{aligned} (Su)(0,t) &= Q(0,t), \\ \left(\frac{u^2}{2} + \tilde{p}\right)(L,t) &= \tau(L,t) > 0. \end{aligned}$$

There are eleven other permutations. Note also that no claims can be made for the well-posedness of various combinations, e.g., it would be ridiculous to expect anything but a short time result if $\psi = 0$ and Q was prescribed with opposite signs at each end. Physical insight will rule out most "bad" cases, but there may be others.

The term $\mathcal{B}$ accounts for the natural boundary conditions, i.e., an integration by parts yields

$$\int_{R^+} \Big\{ (Su - Q)\phi_1 + \left(\frac{u^2}{2} + \tilde{p} - \nu \frac{\partial u}{\partial z} - \tau\right)\phi_2 + \nu (u - v) \frac{\partial \phi_2}{\partial z} \Big\}_{z=0}^{z=L} dt. \tag{3.3.14}$$

The appropriate spaces of test functions are picked so that just the prescribed data of the particular case are satisfied and nothing is said about any other boundary value.

For the cases (I) - (IV), $\nu = 0$, the last term in Eq. (3.3.12) is absent. Therefore the

appropriate space of test functions for case (I) is $K(0,L)$ which wipes out Eq. (3.3.12) completely. In addition, (I) must be taken as part of the definition.

In case (II), $K(0,L)$ is also the appropriate space, and here (II) must be considered part of the definition.

For case (III), the appropriate spaces are $K(0)$ for the ϕ_1's and $K(0,L)$ for the ϕ_2's , and (III) must be part of the definition. In this case $\mathcal{B} = -\int_{\mathbb{R}^+} Q(L,t)\phi_1(L,t)\,dt$.

For case (IV), each ϕ_1 must be in $K(0,L)$, $K(L)$ is appropriate for the ϕ_2's , and (IV) is part of the definition; $\mathcal{B} = -\int_{\mathbb{R}^+} C(0,t)\phi_2(0,t)dt$.

For case (V), the ϕ_1's are in $K(L)$ and the ϕ_2's are in $K(0)$; $\mathcal{B} = -\int_{\mathbb{R}^+}\{Q(0,t)\phi_1(0,t) + C(L,t)\phi_2(L,t)dt$. The pattern should be clear.

When $\nu > 0$, three boundary data are to be specified. If v is one of these data it can be satisfied naturally, e.g., suppose the following conditions are given:

$$S(0,t) = s(0,t),$$
$$v(0,t) = v(0,t),$$
$$v(L,t) = v(L,t).$$

Then the appropriate space of test functions is $K(0,L)$ for both ϕ_1 and ϕ_2 ;

$$\mathcal{B} = +\int_{\mathbb{R}^+} \nu\left\{v(0,t)\frac{\partial\phi_2}{\partial z}(0,t) - v(L,t)\frac{\partial\phi_2}{\partial z}(L,t)\right\}dt .$$

The first condition must be accounted for as part of the definition. If instead

$$(Sv)(0,t) = Q(0,t) ,$$

$$\left(\frac{v^2}{2} + \tilde{p} - \nu \frac{\partial v}{\partial z}\right)(0,t) = \tau(0,t) ,$$

$$\left(\frac{v^2}{2} + \tilde{p} - \nu \frac{\partial v}{\partial z}\right)(L,t) = \tau(L,t) ,$$

then ϕ_1 is in $K(L)$, ϕ_2 is in $K'(0,L)$ and

$$\mathcal{B} = + \int_{\mathbb{R}^+} \{ Q(0,t)\phi_1(0,t) - \tau(L,t)\phi_2(L,t) + \tau(0,t)\phi_2(0,t) \} dt .$$

The pattern is clear and need not be labored further.

In analyzing the circulatory system it is often not clear how to specify boundary data. For example, in analyzing the aorta, distal boundary conditions must be specified. Where and what is the question.

The following technique* can be used to circumvent this issue for a limited class of problems. Assume the following:

(A) The system is governed by a pair of hyperbolic balance laws (e.g., Eq. (3.2.1)).

(B) Two independent boundary data are given at a fixed location, say $z = 0$.

(C) The boundary data are periodic.

---

* This approach manifested itself in a discussion with C. Peskin.

In addition, it will be assumed for simplicity that the problem involves smooth solutions so that the differential equations, rather than the weak forms, can be used. The above assumptions would hold for the natural pulse problem with $z=0$ taken as the aortic valve.

Carrying out the differentiation in Eq.(3.2.1) yields:

$$\frac{\partial \underset{\sim}{U}}{\partial t} + A(\underset{\sim}{U})\frac{\partial \underset{\sim}{U}}{\partial z} + \underset{\sim}{G}(\underset{\sim}{U}) = \underset{\sim}{0} \quad . \tag{3.3.15}$$

For the present case, Eqs. (3.1.1) - (3.1.3),

$$A = \begin{pmatrix} v & S \\ \tilde{P}_s & v \end{pmatrix}$$

and since $\det A = v^2 - c^2 \neq 0$ by assumption, A^{-1} exists. The eigenvalues of A^{-1} are the reciprocals of the eigenvalues of A . Thus the equation

$$\frac{\partial \underset{\sim}{U}}{\partial z} + A^{-1}\frac{\partial \underset{\sim}{U}}{\partial t} + A^{-1}\underset{\sim}{G} = \underset{\sim}{0} \ , \tag{3.3.16}$$

has the same properties as Eq. (3.3.15), with z viewed as the evolutionary parameter. A space-time picture for the case of two periodic data specified at $z=0$ is given by a semi-infinite cylinder with t running around the circumference and z along the

axis. Since the eigenvalues of A^{-1} are distinct, and one is positive and one is negative, this spatial Cauchy problem is well posed.

3.4 Consequences of the Discontinuity Conditions

Many local and global properties of solutions to Eqs. (3.1.1) - (3.1.3) can be immediately deduced from the discontinuity conditions, Eqs. (3.2.19). Recall that these apply at a point (ζ,τ) on a curve γ with tangent defined by $u = d\gamma/d\tau$ where (S,v) are assumed to be strong solutions on each side of γ, in a neighborhood of (ζ,τ). When $u = v^{\pm}$, a discontinuity in S, defined by Eqs. (3.2.19), is called a <u>contact discontinuity</u>. All other discontinuities in S and v are called <u>shocks</u>. In the analysis that follows, it is assumed that S and v are piecewise smooth but may experience finite discontinuities across smooth curves.

By the assumptions on $\tilde{p}$ it follows that

$$[D_1^i D_2^j D_3^k D_4^\ell \tilde{p}] = 0 , \tag{3.4.1}$$

where i,j,k,ℓ are integers ≥ 0, whenever the histories of S are the same on both sides of γ. In this case

$$\left[\frac{\partial \tilde{p}}{\partial \tau}\right] = \tilde{p}_s \left[\frac{\partial S}{\partial \tau}\right] ,$$
$$\left[\frac{\partial \tilde{p}}{\partial \zeta}\right] = \tilde{p}_s \left[\frac{\partial S}{\partial \tau}\right] , \quad \text{etc.} \tag{3.4.2}$$

Also, by the assumptions on $\mathcal{F}, \Psi$, it follows that

$$[S] = [v] = 0 \quad \Rightarrow \quad [f] = [\psi] = 0$$

$$[S] = [v] = \left[\frac{\partial S}{\partial z}\right] = \left[\frac{\partial S}{\partial t}\right] = \left[\frac{\partial v}{\partial z}\right] = \left[\frac{\partial v}{\partial t}\right] = 0$$

$$\Rightarrow \left[\frac{\partial f}{\partial z}\right] = \left[\frac{\partial f}{\partial t}\right] = \left[\frac{\partial \psi}{\partial z}\right] = \left[\frac{\partial \psi}{\partial t}\right] = 0 \text{ , etc.} \tag{3.4.3}$$

It is best to study the cases $\nu = 0$ and $\nu > 0$ separately since they have little in common. First recall the discontinuity conditions:

$$\begin{aligned} u[S] &= [Sv] \text{ ,} \\ u[v] &= \left[\frac{v^2}{2} + \tilde{p} - \nu \frac{\partial v}{\partial z}\right] \text{ ,} \\ 0 &= \nu [v] \text{ .} \end{aligned} \tag{3.2.19}$$

When $\nu > 0$, Eq. $(3.2.19)_3$ gives immediately that $[v] = 0$, which when used in Eqs. $(3.2.19)_{1,2}$ yields

$$\begin{aligned} (u - v)[S] &= 0 \text{ ,} \\ [\tilde{p}] &= \nu \left[\frac{\partial v}{\partial z}\right] . \end{aligned} \tag{3.4.4}$$

Now whenever $u \neq v$ it follows that $[S] = 0$, thus there can be no jumps in (S, v) as long as $u \neq v$. One can proceed further. The fact that the instantaneous response function is one-to-one gives $[S] = 0 \Leftrightarrow [\tilde{p}] = 0$ thus $[\partial v / \partial z] = 0$ from Eq. $(3.4.4)_2$. From the identity

$$\frac{d}{dt}[g] = \left[\frac{\partial g}{\partial t}\right] + u\left[\frac{\partial g}{\partial z}\right] \text{ ,} \tag{3.4.5}$$

where $g: \mathbb{R}^2 \to \mathbb{R}$ is differentiable on both sides of y, it follows that $[v] = [\partial v/\partial z] = 0$ implies $[\partial v/\partial t] = 0$. Taking the jump in Eq. (3.1.1) yields

$$[\partial S/\partial t] + v[\partial S/\partial z] = 0, \tag{3.4.6}$$

where use has been made of $[v] = [\partial v/\partial z] = 0$ and (3.4.3). Employing Eq. (3.4.5) with S substituted for g gives

$$[\partial S/\partial t] + u[\partial S/\partial z] = 0,$$

which when combined with Eq. (3.4.6) yields $[\partial S/\partial t] = [\partial S/\partial z] = 0$. Thus (S,v) are C^1. To proceed further, take the jump in Eq. (3.1.2):

$$\left[\frac{\partial \tilde{P}}{\partial z}\right] = \nu\left[\frac{\partial^2 v}{\partial z^2}\right],$$

where C^1-ness of v and continuity of f have been employed. From Eq. $(3.4.2)_2$ follows

$$\left[\frac{\partial \tilde{P}}{\partial z}\right] = \tilde{P}_S\left[\frac{\partial S}{\partial z}\right] = 0;$$

thus $[\partial^2 v/\partial z^2] = 0$. Using $\partial v/\partial t$ and $\partial v/\partial z$ for g in Eq. (3.4.5) gives then that $[\partial^2 v/\partial z \partial t] = [\partial^2 v/\partial t^2] = 0$; thus v is C^2. To garner the same for S, differentiate Eq. (3.1.1) with respect to z and t, and apply the jump operator:

$$\left[\frac{\partial^2 S}{\partial t^2}\right] = v\left[\frac{\partial^2 S}{\partial z \partial t}\right], \qquad \left[\frac{\partial^2 S}{\partial t \partial z}\right] = v\left[\frac{\partial^2 S}{\partial z^2}\right]. \tag{3.4.7}$$

Substitute $\partial S/\partial t$ and $\partial S/\partial z$ succesively for q in Eq. (3.4.5):

$$\left[\frac{\partial^2 S}{\partial t^2}\right] + u\left[\frac{\partial^2 S}{\partial z \partial t}\right] = 0 ,$$
$$\left[\frac{\partial^2 S}{\partial z \partial t}\right] + u\left[\frac{\partial^2 S}{\partial z^2}\right] = 0 . \qquad (3.4.8)$$

Combining Eqs. (3.4.7) with Eqs. (3.4.8) gives

$$\left[\frac{\partial^2 S}{\partial t^2}\right] = \left[\frac{\partial^2 S}{\partial z \partial t}\right] = \left[\frac{\partial^2 S}{\partial z^2}\right] = 0 ,$$

i.e., S is C^2 . Apparently this procedure can be carried on and on. Thus if $u \neq v$, (S, v) are C^∞ . In particular, <u>there are no shocks when</u> $\nu > 0$.

When $u = v$, Eq. $(3.4.4)_1$ is satisfied identically and Eq. $(3.4.4)_2$ remains as is. Although the existence of contact discontinuities is sometimes questioned, it does not seem possible to discount them via this approach.

<u>When</u> $\nu = 0$ <u>there are no contact discontinuities</u>, viz., with $[v] = u - v = 0$, Eq. $(3.2.19)_1$ is identically satisfied and Eq. $(3.2.19)_2$ becomes $[\tilde{p}] = 0$, which implies $[S] = 0$.

The case of prime interest is shocks when $\nu = 0$. In this case Eqs. (3.2.19) reduce to

$$u[S] = [Sv] ,$$
$$u[v] = \left[\frac{v^2}{2} + \tilde{p}\right] . \qquad (3.4.9)$$

In terms of the relative velocities $w^{\pm} = u - v^{\pm}$, Eqs. (3.4.9) can be put in invariant form, namely

$$0 = [Sw] \quad , \qquad (3.4.10)$$

$$0 = [\tfrac{1}{2}w^2 + \tilde{p}] \, .$$

It is of interest to solve these equations for the relative velocities.

3.5 Shock Wave Velocities

The quantity $V = (S\omega)^{\pm}$, which is well defined by Eq. $(3.4.10)_1$, represents the volume flow passing through the shock. Eqs. (3.4.10) combine to give

$$V[v] = \frac{[\tilde{p}]}{\langle 1/S \rangle} \quad , \tag{3.5.1}$$

where the bracket $\langle \cdot \rangle$ indicates an arithmetic mean value across the shock, i.e., $\langle 1/S \rangle = (1/S^- + 1/S^+)/2$. From the definitions it follows that

$$\begin{aligned} V[v] &= [S\omega v] \quad , \\ &= [S\omega(u-w)] \quad , \\ &= -[S\omega^2] \quad , \\ &= w^- w^+ [S] \quad , \end{aligned} \tag{3.5.2}$$

which when combined with Eq. (3.5.1) yields

$$w^- w^+ = \frac{1}{\langle 1/S \rangle} \frac{[\tilde{p}]}{[S]} \quad . \tag{3.5.3}$$

Employing Eq. $(3.4.10)_1$, Eq. (3.5.3) can be written in the alternative forms

$$\begin{aligned} (w^-)^2 &= \frac{(S^+/S^-)}{\langle 1/S \rangle} \frac{[\tilde{p}]}{[S]} \quad , \\ (w^+)^2 &= \frac{(S^-/S^+)}{\langle 1/S \rangle} \frac{[\tilde{p}]}{[S]} \quad . \end{aligned} \tag{3.5.4}$$

The content of Eqs. (3.5.4) is simply that the relative velocities of a shock depend only upon knowledge

of S^-, S^+ and the instantaneous values of $\tilde{p}$ at S^- and S^+. Note that if $S^- > S^+$, then

$$(w^+)^2 > w^+w^- > (w^-)^2 \quad , \tag{3.5.5}$$

whereas if $S^- < S^+$,

$$(w^+)^2 < w^+w^- < (w^-)^2 \quad . \tag{3.5.6}$$

3.6 Acceleration Wave Velocity

Any curve with velocity u such that $u \neq w^-$ or $u \neq w^+$ and across which S or v, or any of their derivatives, experiences a discontinuity is called a wave, e.g., a shock is a wave whereas a contact discontinuity is not. It has already been shown that when $\nu > 0$, no waves exist. However, when $\nu = 0$ waves of all orders can be shown to exist. A case of particular interest is acceleration waves, in which $[v] = 0$ whereas $[\partial v/\partial t] \neq 0$. It follows from Eqs. (3.4.9) that $[S] = [\tilde{p}] = 0$. From the basic identity, Eq. (3.4.5), and the assumption that $0 \neq u \neq \pm\infty$, one deduces that $[\partial v/\partial z] \neq 0$, since $[\partial v/\partial t] \neq 0$. Applying the jump operator to Eq. (3.1.1) yields

$$[\partial S/\partial t] + v[\partial S/\partial z] = -S[\partial v/\partial z] \neq 0 \quad , \tag{3.6.1}$$

by virtue of our previous assumptions on ψ. Substituting S into Eq. (3.4.5) and combining this with (3.6.1) gives $[\partial S/\partial t] \neq 0$, $[\partial S/\partial z] \neq 0$.

Thus in an acceleration wave the jump in (S,v) is zero, while the jump in each of the first derivatives is non-zero.

There are several ways of deriving the velocity expression for acceleration waves. The quickest, at this point, is to take the limits of Eqs. (3.5.3) and (3.5.4) as $[S]\to 0$. Since

$$\lim_{[S]\to 0} \frac{[\tilde{p}]}{[S]} = \tilde{p}_s \quad ,$$

$$\lim_{[S]\to 0} \langle 1/S \rangle = 1/S \quad ,$$

Eqs. (3.5.3) - (3.5.4) all go to

$$w^2 = S\tilde{p}_s \tag{3.6.2}$$

i.e., $w=\pm c$ and acceleration waves propagate at characteristic velocity.

For general quasi-linear hyperbolic systems this conslusion can be deduced as follows:

Apply the jump operator to Eq. (3.2.1) yielding

$$\left[\frac{\partial}{\partial t}\underset{\sim}{U}\right] + A(\underset{\sim}{U})\left[\frac{\partial}{\partial z}\underset{\sim}{U}\right] = \underset{\sim}{0} \quad , \tag{3.6.3}$$

where $A_{ij} = \partial F_i/\partial U_j$, and also use the identity, Eq. (3.4.5), on each entry in $\underset{\sim}{U}$ to obtain

$$\left[\frac{\partial}{\partial t}\underset{\sim}{U}\right] + w\left[\frac{\partial}{\partial z}\underset{\sim}{U}\right] = \underset{\sim}{0} \quad . \tag{3.6.4}$$

Subtracting Eq. (3.6.4) from Eq. (3.6.3) indicates that the velocities w are the eigenvalues of A ,

namely the characteristic velocities. The same conclusion holds for all higher-order waves.

The expression $c^2 = S\tilde{p}_S$, which has been shown to have several interpretations here, corresponds to various special cases of classical blood flow theory (e.g., the Bramwell-Hill equation and the Moens-Korteweg equation, see McDonald [46]).

3.7 Weak Shock Wave Velocities

It is useful to obtain approximate velocity expressions for weak shocks in terms of the characteristic velocity of the state into which the wave is propagating. Assuming suitable smoothness, $[\tilde{p}]$ may be expressed in terms of Taylor's formula

$$[\tilde{p}] = [S]\tilde{p}_S^+ + \frac{[S]^2}{2}\tilde{p}_{SS}^+ + o([S]^2) . \tag{3.7.1}$$

The following are used to eliminate S^- in favor of S^+ and $[S]$:

$$\begin{aligned} \frac{1}{\langle 1/S \rangle} &= S^+ + \frac{[S]}{2} + o([S]) , \\ S^-/S^+ &= 1 + \frac{[S]}{S^+} , \\ S^+/S^- &= 1 - \frac{[S]}{S^+} + o([S]) . \end{aligned} \tag{3.7.2}$$

Substituting Eqs. (3.7.1) - (3.7.2) into Eqs. (3.5.3) - (3.5.4) yields

$$w^- - w^+ = S^+ \tilde{P}_s^+ + \frac{[S]}{2}\left(S^+ \tilde{P}_{ss}^+ + \tilde{P}_s^+\right) + o([S])$$

$$(w^-)^2 = S^+ \tilde{P}_s^+ + \frac{[S]}{2}\left(S^+ \tilde{P}_{ss}^+ - \tilde{P}_s^+\right) + o([S])$$

$$(w^+)^2 = S^+ \tilde{P}_s^+ + \frac{[S]}{2}\left(S^+ \tilde{P}_{ss}^+ + 3\tilde{P}_s^+\right) + o([S]) \qquad (3.7.3)$$

These approximate formulas are consistent with the inequalities (3.5.5) - (3.5.6).

It is a consequence of a theorem due to Lax [47] that shock velocity is, to second-order in a measure of shock amplitude (e.g., $[S]$), the mean of the sound velocities in front and back:

$$u = \{v^- + v^+ + \alpha(c^- + c^+)\}/2 + O([S]^2) \qquad (3.7.4)$$

or equivalently,

$$w^- + w^+ = \alpha(c^- + c^+) + O([S]^2), \qquad (3.7.5)$$

where $\alpha = +1\ (-1)$ if the shock is facing right (left), respectively.

3.8 Shock Stability

Not all shocks which satisfy the compatibility conditions are physically admissible. In the following it is argued, following Bland [43], that dilative shocks are stable whereas constrictive shocks are not. These deductions are based on observed properties of arterial behavior, i.e., properties of the constitutive functional $\tilde{P}$.

If u is assumed to be positive, then a dilative shock is one in which $S^- > S^+$ and a constrictive shock is one for which $S^+ > S^-$. It is assumed that $\tilde{P}_{ss} \geq 0$, which, as was stated previously, is experimentally observed to hold for arteries. Consider the dilative shock profile depicted in Fig. 3.12. For this profile to be stable, small perturbations should tend to vanish. For example, consider the perturbations indicated in Fig. 3.13. Points a and d are acceleration waves. The profile abcd will tend to the profile $-+$ if (A) the propagation velocity of the acceleration wave at a is greater than the shock velocity u of bc and (B) the acceleration wave velocity at d is less than u. This insures that the perturbation at the crest catches up with the front, thus vanishes, and the perturbation at the root is caught and absorbed into the shock. Recall that acceleration waves travel at characteristic velocity, thus to establish (A) and (B) it is sufficient to show $v^- + c^- > u > v^+ + c^+$ since by virtue of the smallness of the perturbations $a \sim -$, $d \sim +$, and the shock $bc \sim -+$. The c's and v's are all taken to be positive. In words this is equivalent to the condition that dilative shock velocity is supersonic with respect to the state in front of the wave, and subsonic with respect to the state behind. Since $u = v^{\pm} + w^{\pm}$, this condition occurs if and only if $c^- > w^-$ and $w^+ > c^+$.

The condition $\tilde{p}_{ss} \geq 0$ implies $\tilde{p}_s^- \geq [\tilde{p}]/[S] \geq \tilde{p}_s^+$ (see Fig. 3.14). Using this, $S^- > S^+$, and Eqs. (3.5.3)-(3.5.4) enables one to compute

$$(w^+)^2 = \frac{2(S^-)^2}{(S^- + S^+)} \frac{[\tilde{p}]}{[S]} \geq \frac{2(S^-)^2}{(S^- + S^+)} \tilde{p}_s^+$$
$$> S^+ \tilde{p}_s^+ = (c^+)^2 \; ;$$

$$(w^-)^2 = \frac{2(S^+)^2}{(S^- + S^+)} \frac{[\tilde{p}]}{[S]} \leq \frac{2(S^+)^2}{(S^- + S^+)} \tilde{p}_s^-$$
$$< S^- \tilde{p}_s^- = (c^-)^2 \; .$$

Thus (A) and (B) are established. The same procedures could be carried out for infinitesimal shock perturbations as illustrated in Fig. 3.15. From this it may be conjectured that the result is independent of the class of perturbations. The stability condition $v^- + c^- > u > v^+ + c^+$, which is a condition on the right-facing characteristics $\lambda_+ : \frac{dz}{dt} = v + c$, is illustrated in Fig. 3.16. The analogous condition for a left-facing dilative shock, involving left-facing characteristics $\lambda_- : \frac{dz}{dt} = v - c$, is $v^- - c^- > u > v^+ - c^+$ (Fig. 3.17).

Now consider the case of a constrictive shock profile (Fig. 3.18) and a perturbed profile (Fig. 3.19) involving acceleration waves at a and d.

By arguments analogous to the preceding it can be shown that since $\tilde{P}_s^+ \geq [\tilde{P}]/[S] \geq \tilde{P}_s^-$ (switch - and + in Fig. 3.14), and

$$(w^+)^2 \leq \frac{2(S^-)^2}{(S^- + S^+)} \tilde{P}_s^+ < S^+ \tilde{P}_s^+ = (c^+)^2;$$

$$(w^-)^2 \geq \frac{2(S^+)^2}{(S^- + S^+)} \tilde{P}_s^- > S^- \tilde{P}_s^- = (c^-)^2;$$

that $v^- + c^- < u < v^+ + c^+$, and thus points a and d move, respectively, slower and faster than the shock. This implies that each perturbation permanently erodes the front or, equivalently, that the shock is unstable. The characteristics picture is the opposite of Figure 3.16; similarly the picture is opposite Fig. 3.17 for a left-facing constrictive shock. Employing infinitesimal shock perturbations (Fig. 3.20) yields again the same conclusion. Thus in summary it is deduced that in arteries dilative shocks are stable whereas constrictive shocks are unstable, hence the latter are not physically realizable. Thus wave profiles akin to Fig. 3.18 will not be seen in arteries.

Note that this result is not universally applicable to flow in distensible tubes. It depends intimately upon the qualitative nature of $\tilde{P}$. For

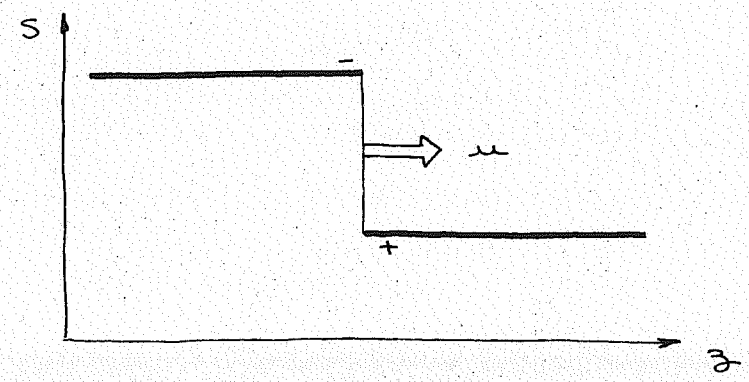

Figure 3.12

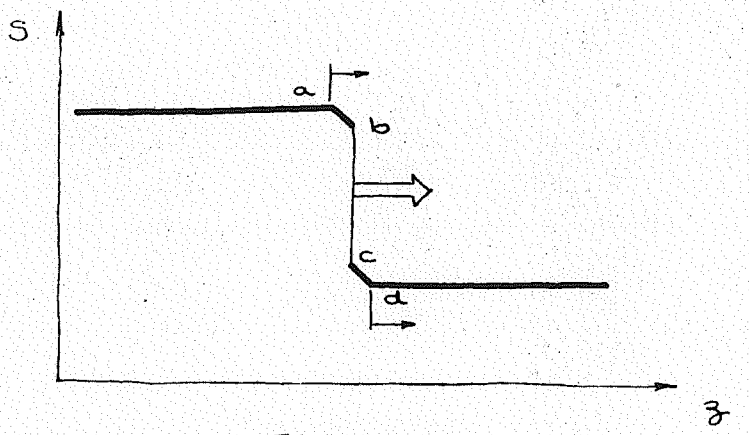

Figure 3.13

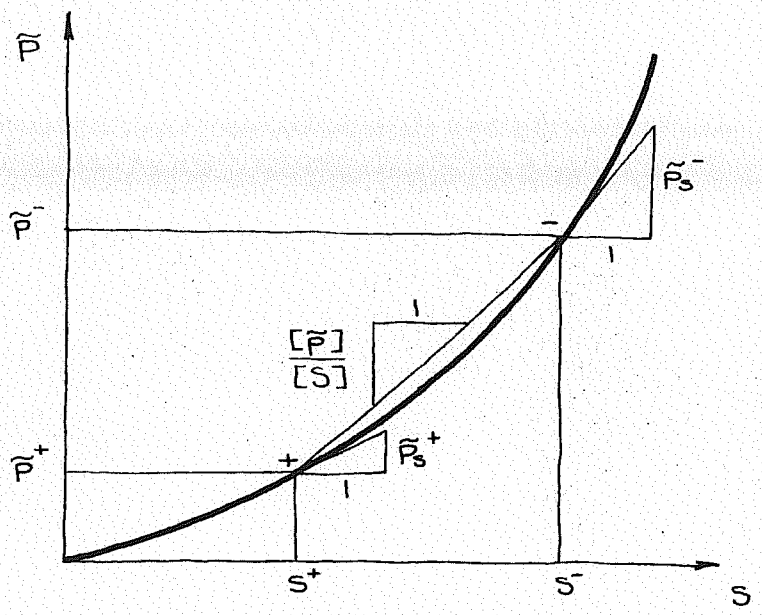

Figure 3.14

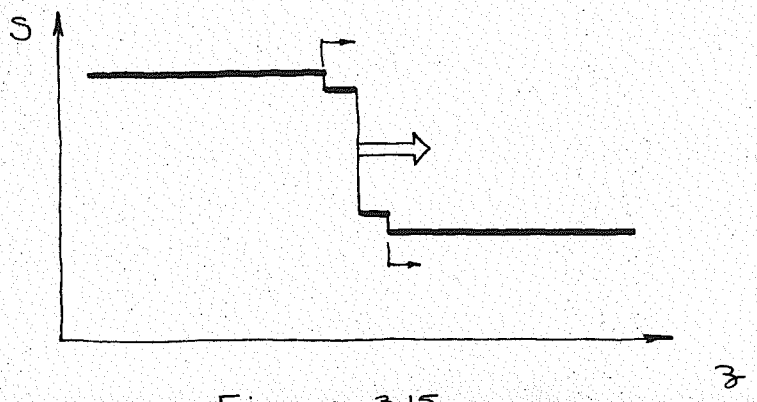

Figure 3.15

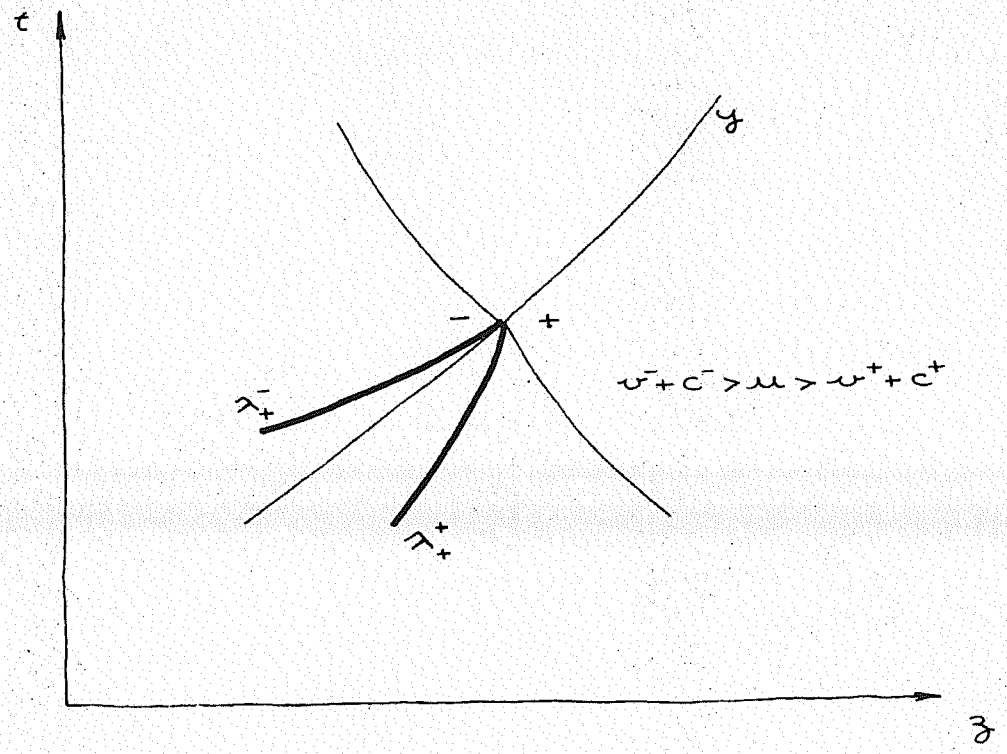

Figure 3.16

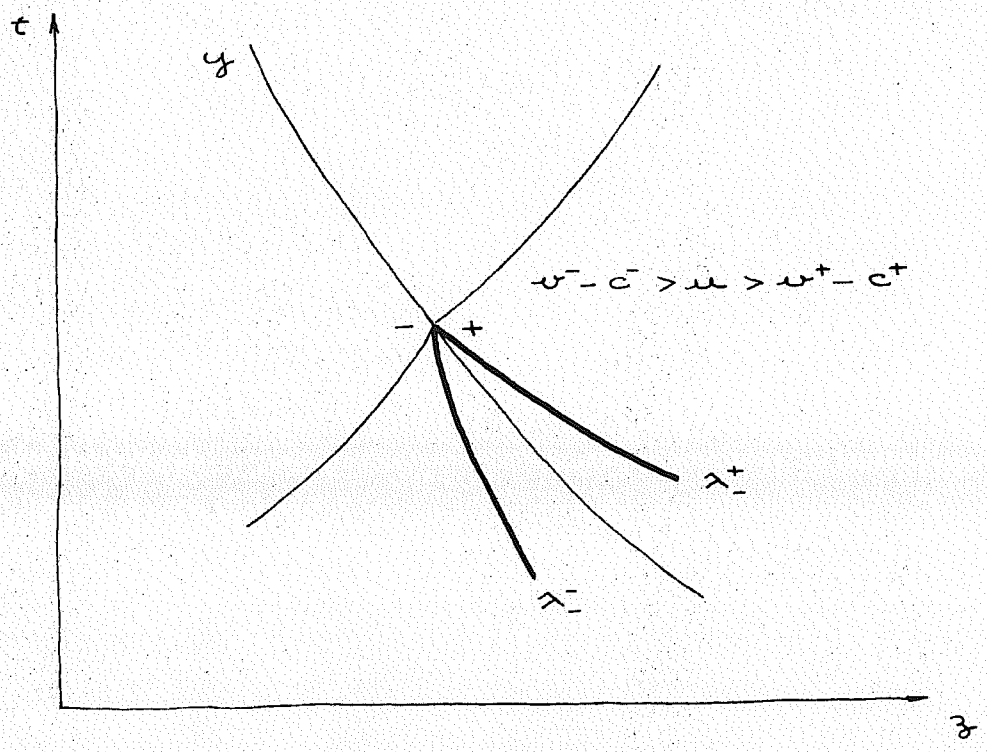

Figure 3.17

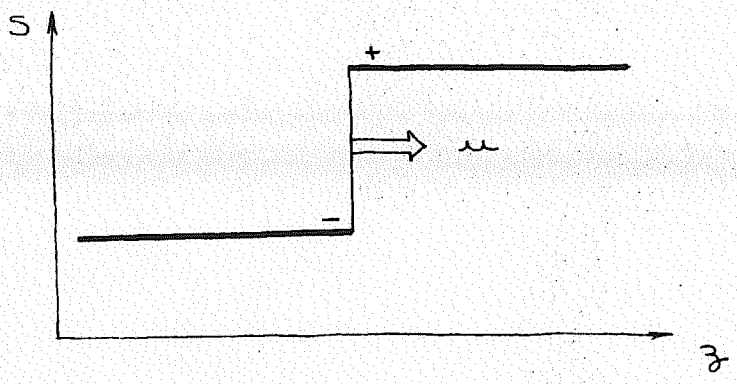

Figure 3.18

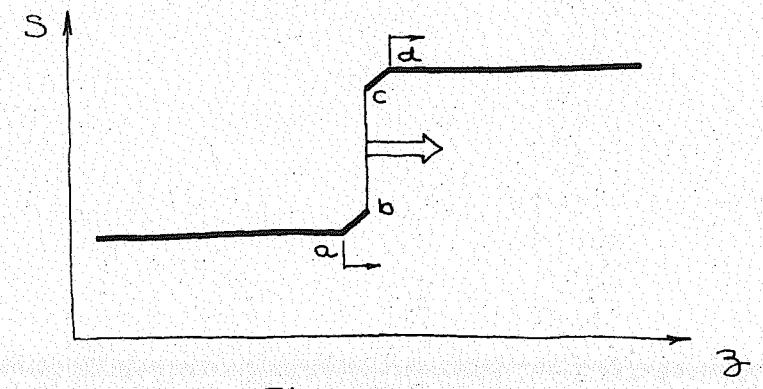

Figure 3.19

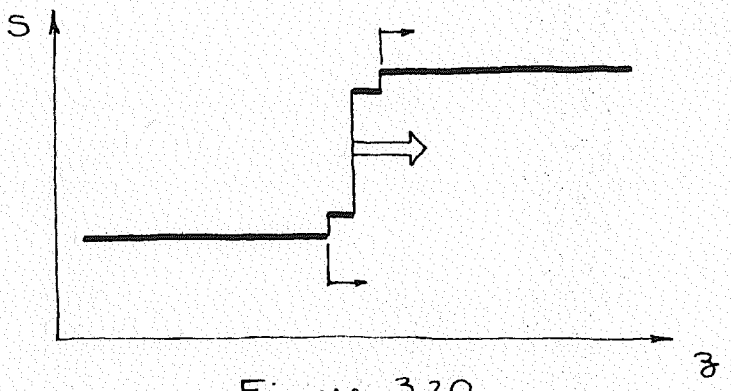

Figure 3.20

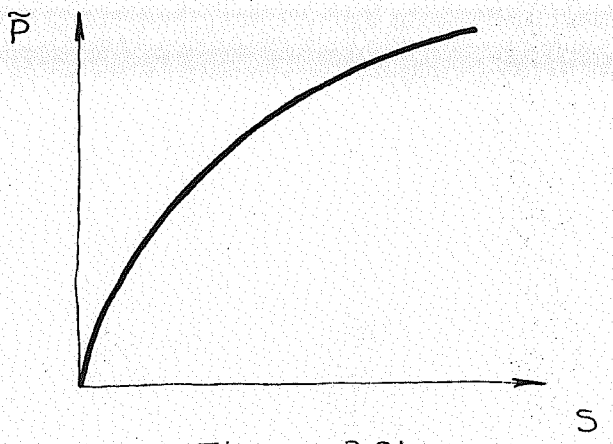

Figure 3.21

instance, if the material curve was concave (Fig. 3.21, e.g., metals) to a great enough degree, an opposite conclusion would hold. The weak shock velocity expressions, Eqs. (3.7.3), give an indication of what type of local inequality would be necessary for $\bar{P}$ to be concave enough.

3.9 Shock Admissibility Criterion

This was formerly called the entropy condition by Lax who proposed it [47]. For a conservation law in one dependent variable it is simply a statement that shock velocity s is supersonic with respect to the state in front and subsonic with respect to the state in back, e.g.,(3.2.25). For Eqs. (3.1.1) - (3.1.3) this condition can take two forms:

$$\text{(I)} \quad v^+ + c^+ < s < v^- + c^- ,$$
$$v^- - c^- < s ,$$

$$\text{(II)} \quad v^+ - c^+ < s < v^- - c^- ,$$
$$s < v^+ + c^+ .$$

If either (I) or (II) is satisfied the discontinuity is deemed admissible. Thus the shock admissibility criterion is also a condition on the slopes of characteristics (Figs. 3.22 - 3.23), but is somewhat stronger than the shock stability argument due to $(I)_2$ and $(II)_2$. However, the same conclusions hold as before if the condition $|v|^{\pm} < c^{\pm}$ is invoked. This condition has already been assumed in conjunction with the mixed initial-boundary value problem and is anticipated in

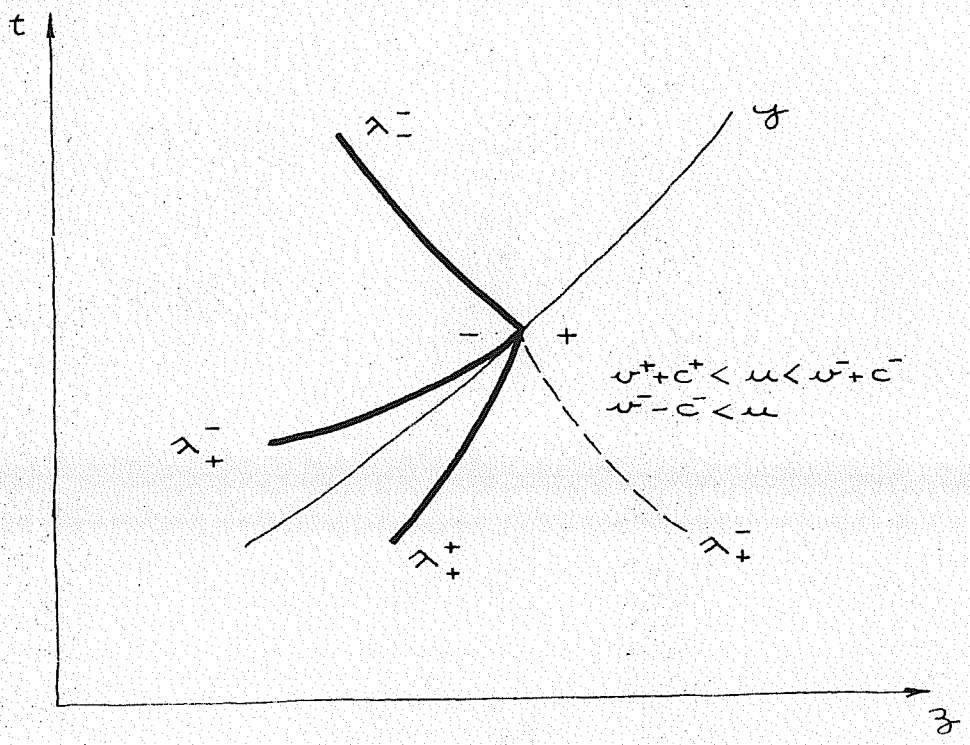

Figure 3.22

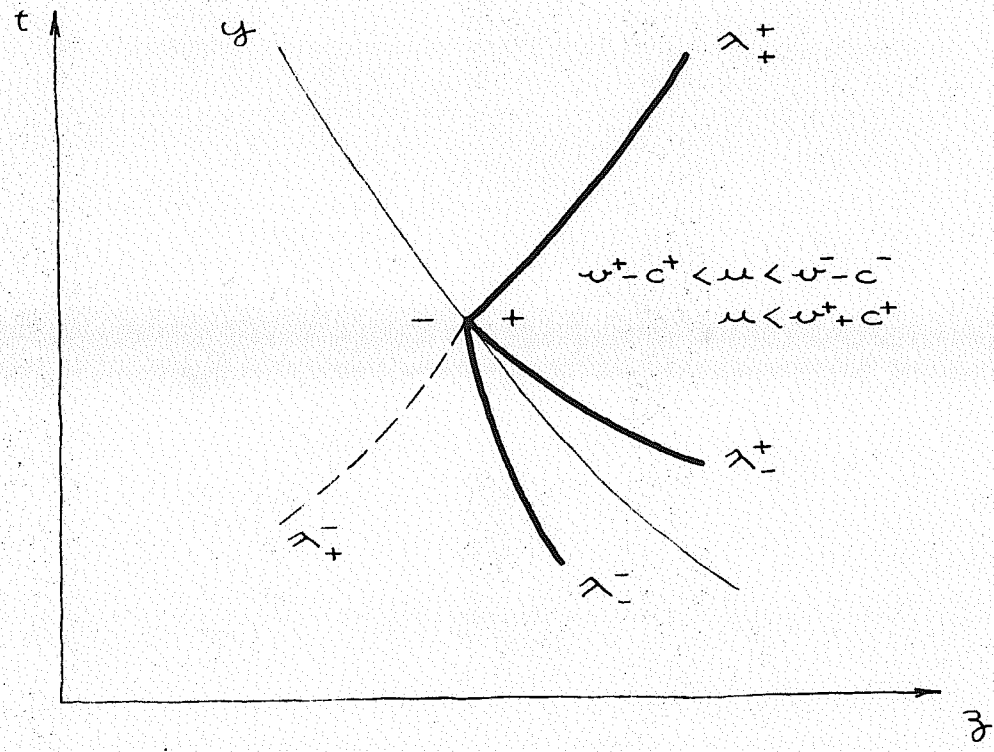

Figure 3.23

practice; this guarantees $(I)_2$ and $(II)_2$ are satisfied.

3.10 Local Qualitative Behavior of Shock Waves*

3.10a Preliminaries. In this section, the local qualitative growth and decay characteristics of a dilative shock wave are considered. The wave is assumed to propagate into a quiescent region, i.e., one in which the fluid is at rest and the pressure is constant. The vessel is assumed to possess an arbitrary degree of static taper. It is found that there exist critical values of taper in terms of which the local behavior may be expressed.

In the analysis of shocks it is convenient to employ a system of Lagrangian or material coordinates. The system to be used is described as follows. The motion $\chi : \mathbb{R}^2 \to \mathbb{R}$, defined by

$$z = \chi(Z,t) = \chi_t(Z) , \tag{3.10.1}$$

gives the location z of a fluid particle at time t which was located at Z at time 0. Thus χ_t is a map: $\mathbb{R} \to \mathbb{R}$, from the initial configuration (time 0) to the present configuration (time t). The pair (Z,t) are the Lagrangian coordinates employed here. It is clear that if χ is differentiable, then

$$v(z,t) = v(z(Z,t),t) = \dot{\chi}(Z,t) \overset{\text{def.}}{=} \left.\frac{\partial \chi}{\partial t}(Z,t)\right|_{Z = \text{const.}} \tag{3.10.2}$$

---

* See Chen [48], Chen and Gurtin [49] and Nunziato and Walsh [50].

The deformation gradient is defined as

$$F = \left.\frac{\partial \chi}{\partial Z}\right|_{t=\text{const.}} \qquad (3.10.3)$$

If χ_t is invertible, then by Eq. (3.10.1), functions of (z,t) may be alternatively represented as functions of (Z,t) and vice versa. This is taken to be the case, in fact it is assumed χ_t is a homeomorphism* from $\mathcal{U}$ open in $\mathbb{R}$ to $\chi_t(\mathcal{U})$. If $\chi_t(\mathcal{U})$ contains a shock at $y(t)$, χ_t is merely continuous at $Y(t) = \chi_t^{-1}(y(t))$. In considering shocks, $\chi_t(\mathcal{U})$ is taken to be an open interval containing $y(t)$. On $\mathcal{U} \sim Y(t)$, χ_t is assumed differentiable. Thus (3.10.2) and (3.10.3) make sense on both sides of the shock.

No additional notations will be introduced to facilitate changes of variables and thus dependent variables may be considered to be functions of either pair, e.g., if $v = \dot{\chi}$ is written, the meaning is given by Eq. (3.10.2).

The shock wave is assumed to propagate into a quiescent region $\{(z,t) \mid z > y(t)\}$ characterized by

$$\begin{aligned} &z = Z \qquad (\Rightarrow v = 0\,,\ F = 1)\,, \\ &\rho p = \pi = \text{const.}\,, \qquad S(z,t) = s(z)\,, \\ &\psi = 0\,. \end{aligned} \qquad (3.10.4)$$

Eq. $(3.10.4)_3$ motivates the definition of a dimension-

---

* One-to-one, continuous and the same for $\chi_t^{-1} : \chi_t(\mathcal{U}) \to \mathcal{U}$.

less area variable $\sigma = S/s$. With this and $(3.10.4)_2$ some new constitutive relations are defined which adapt themselves nicely when a distinguished configuration is available, e.g., the initial one.

It is assumed that there exists a unique equilibrium state independent of the history of S, i.e., if $\rho p(z,t) = \Pi$ = constant for all t greater than some fixed value, then there exists a function $s(z,t) = s(z)$, independent of S^r, such that as $t \to \infty$, $S(z,t) \to s(z)$ where S satisfies $\Pi = \tilde{p}$. The function s of course depends upon Π. Suppose the equilibrium state has been reached. The instantaneous response function in terms of σ for the equilibrium state is denoted

$$\begin{aligned} &\hat{p}(\cdot, \sigma^r - 1; z, t) : \mathbb{R} \to \mathbb{R}, \\ &\hat{p}(\sigma^t - 1, \sigma^r - 1; z, t) = \tilde{p}(S^t, S^r; z, t), \\ &\Pi = \hat{p}(0, \sigma^r - 1; z, t) \end{aligned} \tag{3.10.5}$$

The tangent modulus is denoted by $E = D_1\hat{p} = s\, D_1\tilde{p}$ and the second-order tangent modulus by $\tilde{E} = D_1^2\hat{p} = s^2 D_1^2\tilde{p}$. The secant modulus is $E_\Lambda = [\hat{p}]/[\sigma]$. See Fig. 3.24 for an illustration of these definitions.

For future use it is necessary to rewrite Eq. (3.1.1) in terms of Lagrangian coordinates. To do this, multiply Eq. (3.1.1) by F, make use of the chain rule $(\partial/\partial Z = F\,\partial/\partial z)$ and the identity $\partial v/\partial Z = \dot{F}$ to get

$$\dot{\overline{FS}} + F\psi = 0 . \tag{3.10.6}$$

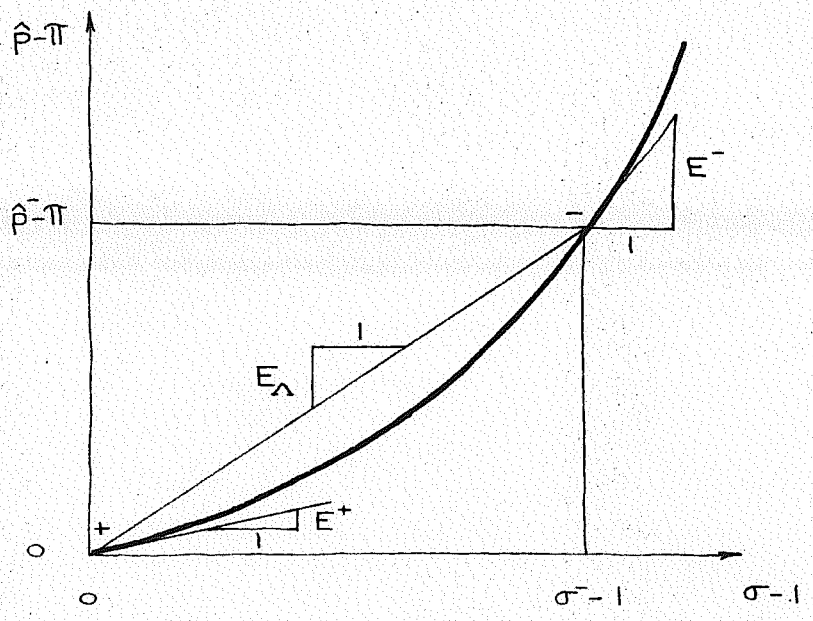

Figure 3.24

Integrating with respect to t , holding Z fixed, and employing Eqs. (3.10.4) yields

$$s(Z) = (SF)(Z,t) + \int_0^t (\psi F)(Z,t')dt' . \qquad (3.10.7)$$

Recalling that χ_t is invertible, the material path of the shock $Z = Y(t)$ is defined by

$$y(t) = \chi_t(Y(t)) , \qquad (3.10.8)$$

and its intrinsic velocity is $U = Y'(t)$ (assumed greater than zero). It follows from differentiating Eq. (3.10.8) that

$$w^{\pm} = UF^{\pm} . \qquad (3.10.9)$$

Thus from Eqs. (3.10.4)

$$u = w^{+} = U. \qquad (3.10.10)$$

Eq. (3.4.10) , in the present notation, becomes

$$[\sigma F] = 0 ;$$

thus from Eqs. (3.10.4)

$$\sigma^{-}F^{-} = 1 . \qquad (3.10.11)$$

Using Eqs. (3.5.3) - (3.5.4) and (3.10.4) results in

$$U^2 = \frac{(\sigma^{-})^2}{\langle \sigma \rangle} E_{\wedge} . \qquad (3.10.12)$$

The Lagrangian shock compatibility condition, dual to Eq. (3.4.5), follows from differentiating $g: \mathbb{R}^2 \to \mathbb{R}$ on both sides of the shock and subtracting:

$$\frac{d}{dt}[g] = [\dot{g}] + U[\partial g/\partial Z] . \qquad (3.10.13)$$

Substituting $g=\chi$ in the above, noting that $[\chi]=0$, and employing Eqs. (3.10.2) - (3.10.4) results in

$$\upsilon^- = [\upsilon] = -U[F] \,. \tag{3.10.14}$$

With the aid of Eqs. (3.10.4), (3.10.11) and (3.10.14), the shock strength, Δ, may be expressed in the following alternative forms:

$$\Delta \overset{\text{def.}}{=} [S]/S^- = [\sigma]/\sigma^- = [F] = \upsilon^-/U. \tag{3.10.15}$$

The range of interest of Δ, corresponding to dilative shocks, is $(0,1)$. Eqs. (3.10.12) and (3.10.15) combine to give

$$U^2 = (\hat{p}^- - \Pi)/\Delta(1-\Delta/2) \,, \tag{3.10.16}$$

and thus for the usual arterial conditions illustrated in Fig. 3.14 ($\tilde{E}\geq 0$, $E^- > E_\Lambda > E^+$), Eqs. (3.10.15) - (3.10.16) imply

$$E^-/(1-\Delta)(1-\Delta/2) \;> U^2 >\; E^+/(1-\Delta)(1-\Delta/2) \,. \tag{3.10.17}$$

The speed of sound in this notation is given by $c^\pm = (E^\pm)^{1/2}$

3.10b Evolution of the Shock. The aim is to derive an expression governing the evolution of Δ. Substituting $g=F$ and $g=\upsilon$ in Eq. (3.10.13), noting that $\dot{\upsilon} = \partial\upsilon/\partial\tau + \upsilon\,\partial\upsilon/\partial z$, making use of Eqs. (3.1.2) and (3.10.15) and assuming $[f]=0$ results in

$$2U\frac{d\Delta}{dt} + \Delta\frac{dU}{dt} + \frac{1}{\rho}[\partial p/\partial z] + U^2[\partial F/\partial Z] = 0 \qquad (3.10.18)$$

In turn, expressions will be obtained for $[\partial F/\partial Z]$, $[\partial p/\partial z]$ and dU/dt.

The results get somewhat messy for the fully general case so initially the following simplifications are made:

$$\begin{aligned} \psi &= 0 \quad \text{(no outflow)}, \\ D_2\hat{p} &= 0 \quad \text{(elastic)}, \\ D_3\hat{p} &= 0 \quad \text{(axial homogeneity)}, \\ D_4\hat{p} &= 0 \quad \text{(no induced changes in the artery)}. \end{aligned} \qquad (3.10.19)$$

Eq. (3.10.7), when differentiated by Z, operated upon by $[\cdot]$, and combined with Eq. (3.10.15), becomes

$$[\partial F/\partial Z] = -(1-\Delta)^3\,\partial\sigma^-/\partial z \qquad (3.10.20)$$

where the notation $\partial\sigma^-/\partial z = (\partial\sigma/\partial z)^-$ is used.

An equation for $[\partial p/\partial z]$ is derived by differentiating $\hat{p}$ with respect to z, using Eqs. (3.10.4), and applying the jump operator to the result:

$$\frac{1}{\rho}[\partial p/\partial z] = \frac{1}{\rho}\partial p^-/\partial z = E^-\partial\sigma^-/\partial z. \qquad (3.10.21)$$

dU/dt is obtained by differentiating Eq. (3.10.16) and employing Eqs. (3.10.4)

$$U\frac{dU}{dt} = \frac{\alpha}{2(1-\Delta)^2(1-\Delta/2)}\,\frac{1}{\Delta}\,\frac{d\Delta}{dt}, \qquad (3.10.22)$$

where

$$\alpha = E^- - U^2(1-\Delta)^3.$$

Note that (3.10.17) implies $\alpha > 0$, from which it follows that

$$\frac{dU}{dt} \gtreqless 0 \quad \Leftrightarrow \quad \frac{d\Delta}{dt} \gtreqless 0 \qquad (3.10.23)$$

Substituting Eqs. (3.10.20) - (3.10.22) into Eq. (3.10.18) and rearranging, results in the equation governing the shock strength,

$$d\Delta/dt = A(\Delta)\, \partial\sigma^-/\partial\zeta ,$$
$$A(\Delta) = \frac{-(2-\Delta)(1-\Delta)^2 U \alpha}{(E^- + U^2(3-\Delta)(1-\Delta)^2)} . \qquad (3.10.24)$$

It follows that $A < 0$, thus

$$\frac{\partial\sigma^-}{\partial\zeta} \gtreqless 0 \quad \Leftrightarrow \quad \frac{d\Delta}{dt} \lesseqgtr 0 . \qquad (3.10.25)$$

Note that in Eq. (3.10.24) the non-dimensional area gradient behind the wave front, $\partial\sigma^-/\partial\zeta$, can be expressed as

$$\partial\sigma^-/\partial\zeta = (\partial S^-/\partial\zeta - \lambda)/A ,$$
$$\lambda = (\partial A/\partial Z)/(1-\Delta)^2 , \qquad (3.10.26)$$

from which it follows that

$$\frac{\partial\sigma^-}{\partial\zeta} \gtreqless 0 \quad \Leftrightarrow \quad \frac{\partial S^-}{\partial\zeta} \gtreqless \lambda . \qquad (3.10.27)$$

For obvious reasons the functions $\partial A/\partial Z$, $\partial S^-/\partial\zeta$, $\partial\sigma^-/\partial\zeta$ and λ are called the <u>static taper</u>, <u>dynamic taper</u>, <u>relative dynamic taper</u>, and <u>critical taper</u>, respectively. From Eq. $(3.10.26)_2$, $|\lambda| > |\partial A/\partial Z|$. The local evolution relationship between $[\sigma]$ and the

shock strength can be determined by noting that Eq. (3.10.15) is equivalent to $[\sigma] = \Delta(1-\Delta)$ from which it follows that

$$\frac{d[\sigma]}{dt} = \frac{1}{(1-\Delta)^2}\frac{d\Delta}{dt} \quad , \tag{3.10.28}$$

and therefore

$$\frac{d[\sigma]}{dt} \begin{matrix} \leq \\ = \\ > \end{matrix} 0 \iff \frac{d\Delta}{dt} \begin{matrix} \leq \\ = \\ > \end{matrix} 0. \tag{3.10.29}$$

The physical content of Eqs. (3.10.23) - (3.10.29) is depicted in Fig. 3.25. The use of $\sigma-1$ as ordinate in Fig. 3.25, as opposed to $S-\Delta$, considerably simplifies the diagrams.

Example. Take the case of an induced dilative shock wave in the aorta propagating in a direction away from the heart. Assume laboratory circumstances that conform to the analytical assumptions. For example, assume the aortic branches have been occluded to prevent outflow and that cardiac activity has been arrested for a period of time prior to the arrival of the shock, so that the static conditions (3.10.4) are created. The aorta is tapered distally such that $\partial\Delta/\partial Z < 0$. These conditions and (3.10.23) - (3.10.29) imply that $\lambda < \partial\Delta/\partial Z < 0$ and if $\partial\bar{S}/\partial\zeta < \lambda$, then $d\Delta/dt$, dU/dt, and $d\bar{\sigma}/dt$ are all > 0, which corresponds to condition (i) in Fig. 3.25, whereas if $\partial\bar{S}/\partial\zeta > \lambda$, then $d\Delta/dt$, dU/dt and $d\bar{\sigma}/dt$ are all < 0, corresponding to condition

(ii) in Fig. 3.25.

Now the simplifying assumptions (3.10.19) will be removed. In this case

$$[\partial F/\partial Z] = -(1-\Delta)^3 \frac{\partial \sigma^-}{\partial \zeta} + \frac{(1-\Delta)^2}{\Delta U} \psi^- \quad , \tag{3.10.30}$$

$$\frac{1}{\rho}[\partial p/\partial \zeta] = \frac{1}{\rho}\frac{\partial p^-}{\partial \zeta} = E^- \frac{\partial \sigma^-}{\partial \zeta} + \left(D_2 \hat{p} \cdot \frac{\partial \sigma}{\partial \zeta}\right)^- + D_3 \hat{p}^- \quad , \tag{3.10.31}$$

$$\frac{1}{\rho}\frac{d[p]}{dt} = \frac{1}{\rho}\frac{dp^-}{dt} = E^- \frac{d\sigma^-}{dt} + U D_3 \hat{p}^- + D_4 \hat{p}^- \quad , \tag{3.10.32}$$

$$U\frac{dU}{dt} = \frac{\alpha}{2\Delta(1-\Delta/2)(1-\Delta)^2}\frac{d\Delta}{dt} + (U D_3 \hat{p}^- + D_4 \hat{p}^-)/(2\Delta(1-\Delta/2)) \quad . \tag{3.10.33}$$

The amplitude equation is

$$\frac{d\Delta}{dt} = A(\Delta)\left\{\frac{\partial \sigma^-}{\partial \zeta} - \tau\right\} \quad , \tag{3.10.34}$$

where τ , the relative critical taper, is given by

$$\tau = -\{(D_2 \hat{p} \cdot \frac{\partial \sigma}{\partial \zeta})^- + D_3 \hat{p}^- + (U D_3 \hat{p}^- + D_4 \hat{p}^-)/(2U(1-\Delta/2)) + \frac{U(1-\Delta)^2}{\Delta}\psi^-\}/\alpha \quad . \tag{3.10.35}$$

The sign of τ is problem dependent. It would generally be assumed

$$(D_2 \hat{p} \cdot \frac{\partial \sigma}{\partial \zeta}) \geq 0 \quad ,$$

$$\psi^- \geq 0 \quad ,$$

but $D_3 \hat{p}^-$, $D_4 \hat{p}^-$ would depend upon particular circumstances. For the example of a wave propagating

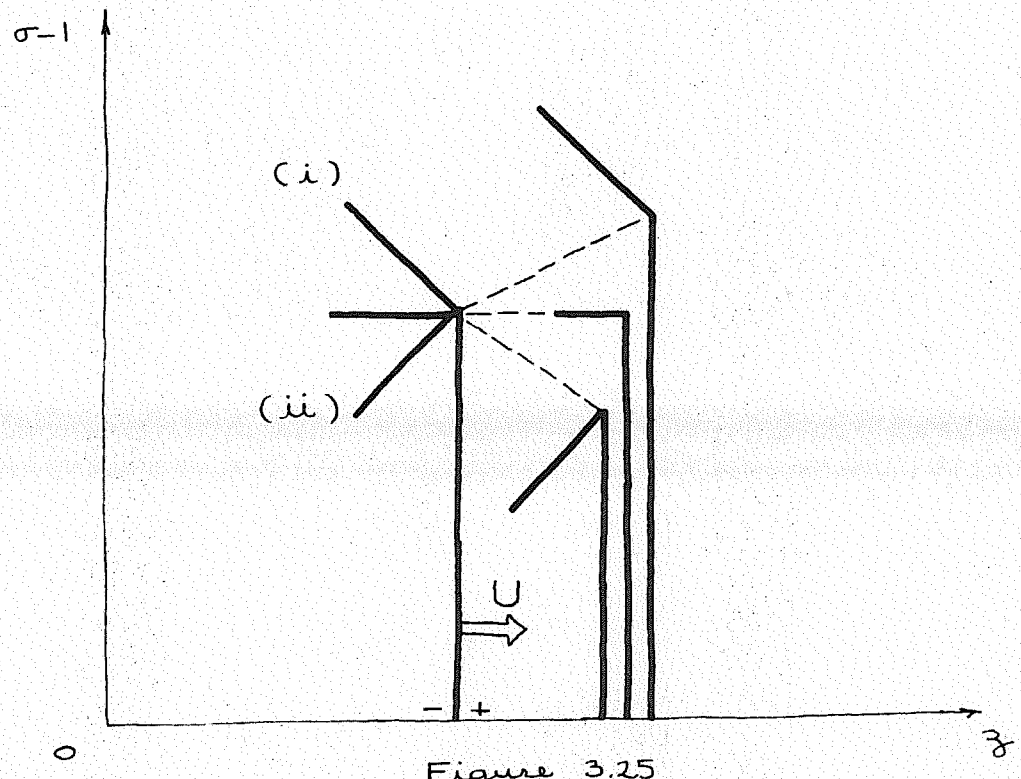

Figure 3.25

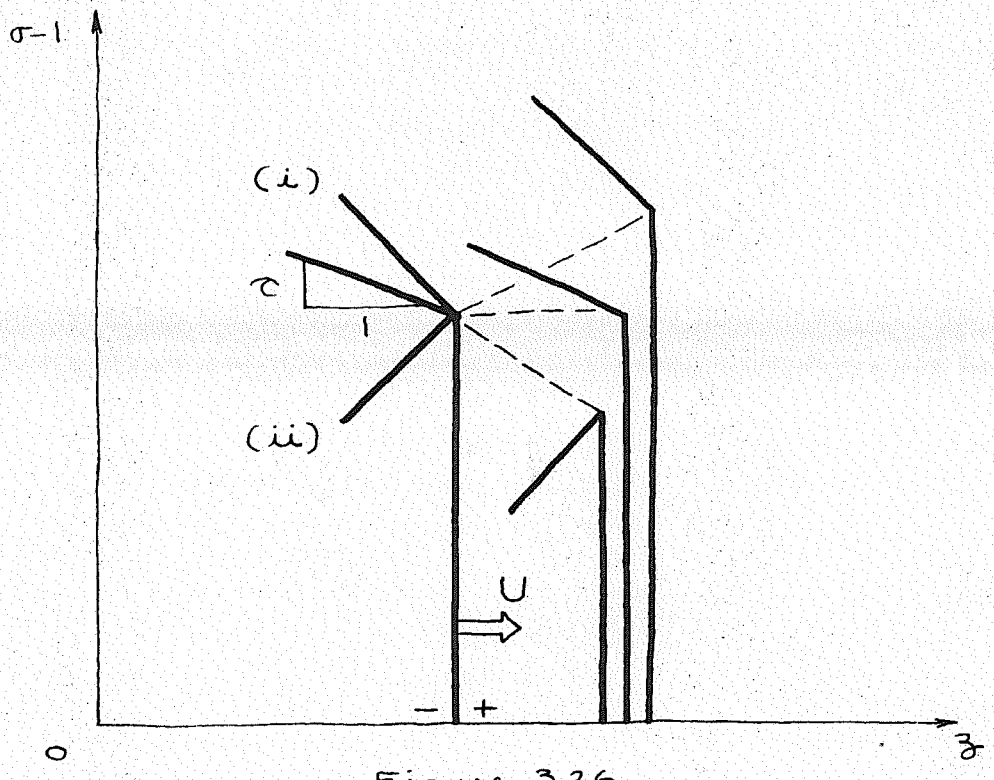

Figure 3.26

distally in the aorta it is well known that $D_3\hat{p} > 0$. Nevertheless, the local qualitative behavior is still expressed concisely for all possible $\mathcal{C}$:

(A) (3.10.23) no longer holds; similar type deductions must be made from (3.10.33) for each case.

(B) (3.10.25) should be replaced by

$$\frac{\partial \sigma^-}{\partial \mathcal{Z}} \lesseqgtr \mathcal{C} \iff \frac{d\Delta}{dt} \gtreqless 0 . \qquad (3.10.36)$$

(C) (3.10.27) and (3.10.29) remain the same.

Example. Let everything be as in the previous example except this time take account of the neglected effects as follows. Assume

$$\begin{aligned} \left(D_2\hat{p}\,\frac{\partial \sigma}{\partial \mathcal{Z}}\right)^- &\geq 0 , \\ \mathcal{V}^- &\geq 0 , \\ D_3\hat{p}^- &\geq 0 , \\ D_4\hat{p}^- &= 0 . \end{aligned} \qquad (3.10.37)$$

The last condition could be changed to $D_4\hat{p}^- \geq 0$ without changing the argument, but this seems to have little physical significance. It follows from (3.10.37) and the previous assumptions that $\mathcal{C} < 0$. Thus the situations are as illustrated in Fig. 3.26. It can be garnered from Eq. (3.10.33), and the assumptions, that the propagation velocities are, in fact, qualitatively correct in Fig. 3.26, since from (3.10.29)

$$\frac{d[\sigma]}{dt} \gtreqless 0 \Rightarrow \frac{dU}{dt} \gtreqless 0 . \qquad (3.10.38)$$

Conditions (i) and (ii) this time correspond to the

cases $\partial\bar{\sigma}/\partial\zeta < \tau$ and $\partial\bar{\sigma}/\partial\zeta > \tau$, respectively. These can be expressed in terms of λ via (3.10.26).

3.11 Comparison with Experimental Work

Landowne's experiments [51,52] afford an opportunity to check some of the qualitative features of the present theory. Briefly, Landowne employed a mechanical impactor to induce (non-invasively) waves in human brachial and radial arteries. The impactor was applied to the overlying skin of the brachial artery at the midhumerus. Recordings of luminal arterial pressure were taken in the radial artery at the wrist and in the brachial artery at the antecubital space (Fig. 3.27). A typical impact wave pressure recording superposed on the natural pulse is schematically reproduced in Fig.3.28 after Landowne, [51], p.596. Landowne's findings were:

(A) The propagation velocity of impact waves increased with ambient arterial pressure.

(B) Impact waves riding on a rising ambient pressure did not travel measurably faster than on a falling ambient pressure.

(C) The propagation velocity of impact waves at diastolic pressure was greater than the velocity of cardiac pulse waves. Simultaneous measurements in five subjects yielded 16.1 to 11.6 meters/sec., respectively.

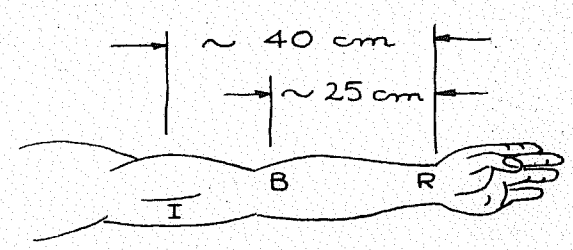

Figure 3.27 Locations of radial (R) and brachial (B) pressure transducers and impactor (I) in Landowne's experiments.

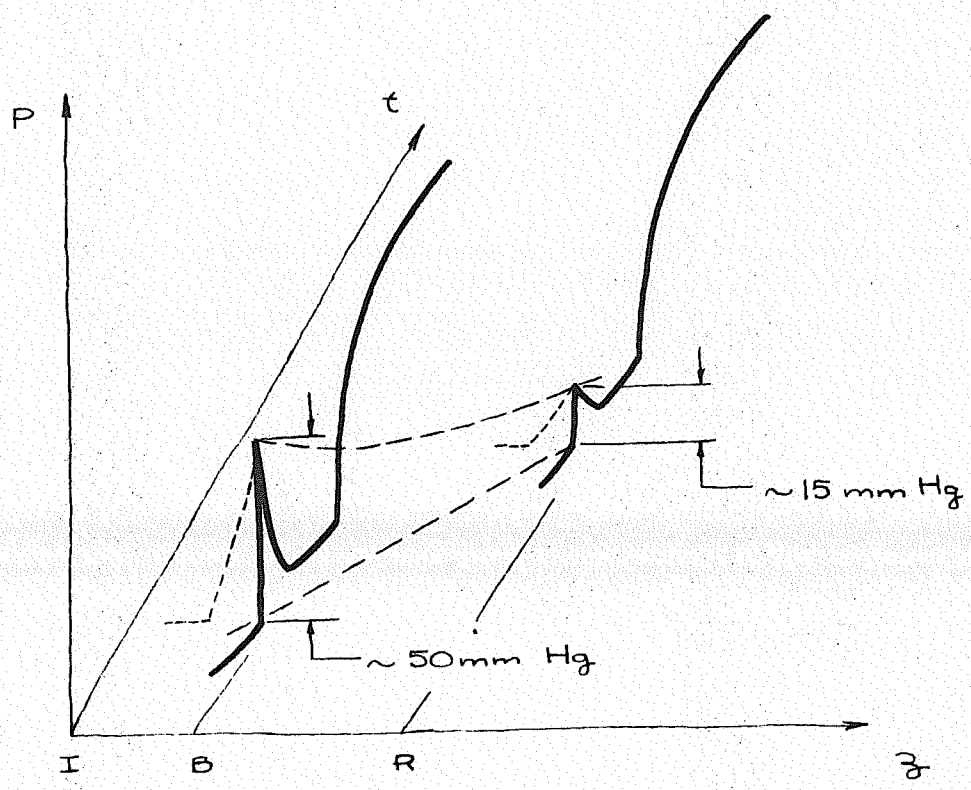

Figure 3.28

(D) The amplitude (pressure rise) of impact waves decreased as they propagated distally (see Fig. 3.28).

Phenomenon (A) is consistent with either an acceleration wave or shock wave interpretation (see Eqs. (3.5.3) - (3.5.4), (3.6.2) and (3.7.4) - (3.7.5)) along with the basic material assumption (2.4.19). Phenomenon (B) is also consistent with either an acceleration wave or shock wave interpretation as the slope of ambient data does not appear in either velocity expression (Eqs. (3.5.3) - (3.5.4) and (3.6.2)).

Phenomenon (C) is compelling evidence for interpreting the impact waves as shocks in the context of the present theory. The argument goes like this. All data, except shocks, propagate at characteristic velocity. Thus wavelets comprising the natural pulse travel at characteristic velocity. Characteristic velocity depends only upon the ambient state (Eq.(3.6.2)) whereas shock velocity depends upon the state behind the front (Eqs. (3.5.3) - (3.5.4)). The fact that the velocity of the impact wave is greater than that of the cardiac pulse at the same ambient pressure indicates that it must be a shock. This interpretation is consistent with the inequality (3.10.17) for dilative shocks. The thickness of the front at the brachial recording location can be estimated from the velocity (16.1 meters/sec) and the time duration between the

front and peak (5 msec, p.92, [52]):

$$\text{thickness} \approx (16.1 \text{ m/sec}) \times (5. \times 10^{-3} \text{ sec}) = 8.05 \text{ cm.}$$

For comparison purposes, a similar calculation for the cardiac pulse (based on Fig. 3, p.596, [51]) gives:

$$\text{thickness} \approx (11.6 \text{ m/sec}) \times (.3 \text{ sec}) = 3.48 \text{ m.}$$

Thus the ratio of front thickness of impact to cardiac pulse wave at the brachial recording location is approximately 1:40. The amplitudes are approximately the same, about 50 mm Hg.

To compare the results of Section 3.10b with phenomenon (D), assume the following:

(1) A graph for σ is qualitatively the same as Fig. 3.28.

(2) The conditions (3.10.37) apply for the present case.

(3) The diastolic ambient conditions do not alter the validity of the results based upon the static ambient conditions, (3.10.4). Then, since $\partial\sigma/\partial\zeta > 0$, (ii) of Fig. 3.26 applies and is consistent with Fig. 3.28, interpreted in terms of (1). With account for the preceding assumptions, phenomenon (D) is consistent with a shock interpretation.

3.12 Identification

The theory can only be put to practical numerical use if the material properties, namely $\tilde{P}$, can be quantitatively evaluated. In this section some simple procedures are presented for identifying $\tilde{P}$ via wave propagation experiments, assuming several specific forms for $\tilde{P}$. The procedures are ad hoc, i.e., they make no pretense to be optimal and do not avail themselves of the considerable methodology of identification theory. For more sophisticated approaches along these lines the reader is referred to the forthcoming thesis of E. Llinas.

3.12a Identification of an Elastic Constitutive Model via Acceleration or Shock Wave Data. The first case considered is when $\tilde{P}$ models an elastic artery. In this case $\tilde{P} = \tilde{P}(S, \mathfrak{Z}, t)$ and a very simple identification algorithm can be constructed employing either shock or acceleration wave propagation data.

The first method derives from the velocity expression for an acceleration wave, $c^2 = S\tilde{P}_S$, which may be considered an ordinary differential equation for $\tilde{P}$ parameterized by $\mathfrak{Z}$ and t . The velocity c is assumed to be a function of S, $\mathfrak{Z}$ and t , which is obtained from experimental data. Integration of $c^2 = S\tilde{P}_S$ yields the constitutive equation

$$\tilde{P}(S;\mathfrak{Z},t) = \tilde{P}(S_o;\mathfrak{Z},t) + \int_{S_o}^{S} \frac{c(S';\mathfrak{Z},t)^2}{S'}\, dS' \qquad (3.12.1)$$

Most likely $\tilde{p}(S_o; z, t)$ would be chosen as a constant and $S_o : \mathbb{R} \longrightarrow \mathbb{R}$ would be the corresponding area function.

This approach has been used by Rockwell [17]. He reversed the roles of p and S from that employed here, i.e., he used $S = \tilde{S}(p; z)$, $c^2 = S/\rho \tilde{S}_p$ which integrates to

$$\tilde{S}(p; z) = S_o(z)\, e^{\int_{p_o}^{p} \frac{dp'}{\rho c(p'; z)^2}} \qquad (3.12.2)$$

The expression assumed for the velocity was

$$c = (c_0 + c_1 p)(c_2 + c_3 z).$$

The constants, c_i, $i = 0,1,2,3$, were chosen to fit data obtained from wave propagation experiments on dogs (see Section 5.6). The wave he used is the front of the cardiac pulse, which may be reasonably considered an acceleration wave, although he did not make this interpretation.

A plot of his data, Fig. 3.29, for several stations indicates, for the most part, qualitative agreement with the properties indicated in Fig. 2.2. The only area of disagreement ($\tilde{p}_{ss} < 0$) is for $p < 100$ mm Hg in a neighborhood of the aortic valve, $z = 0$ cm .

Another simple way to determine $\tilde{p}$ for an elastic artery is via the shock velocity relations (3.5.3) - (3.5.4). The simple case where assumptions

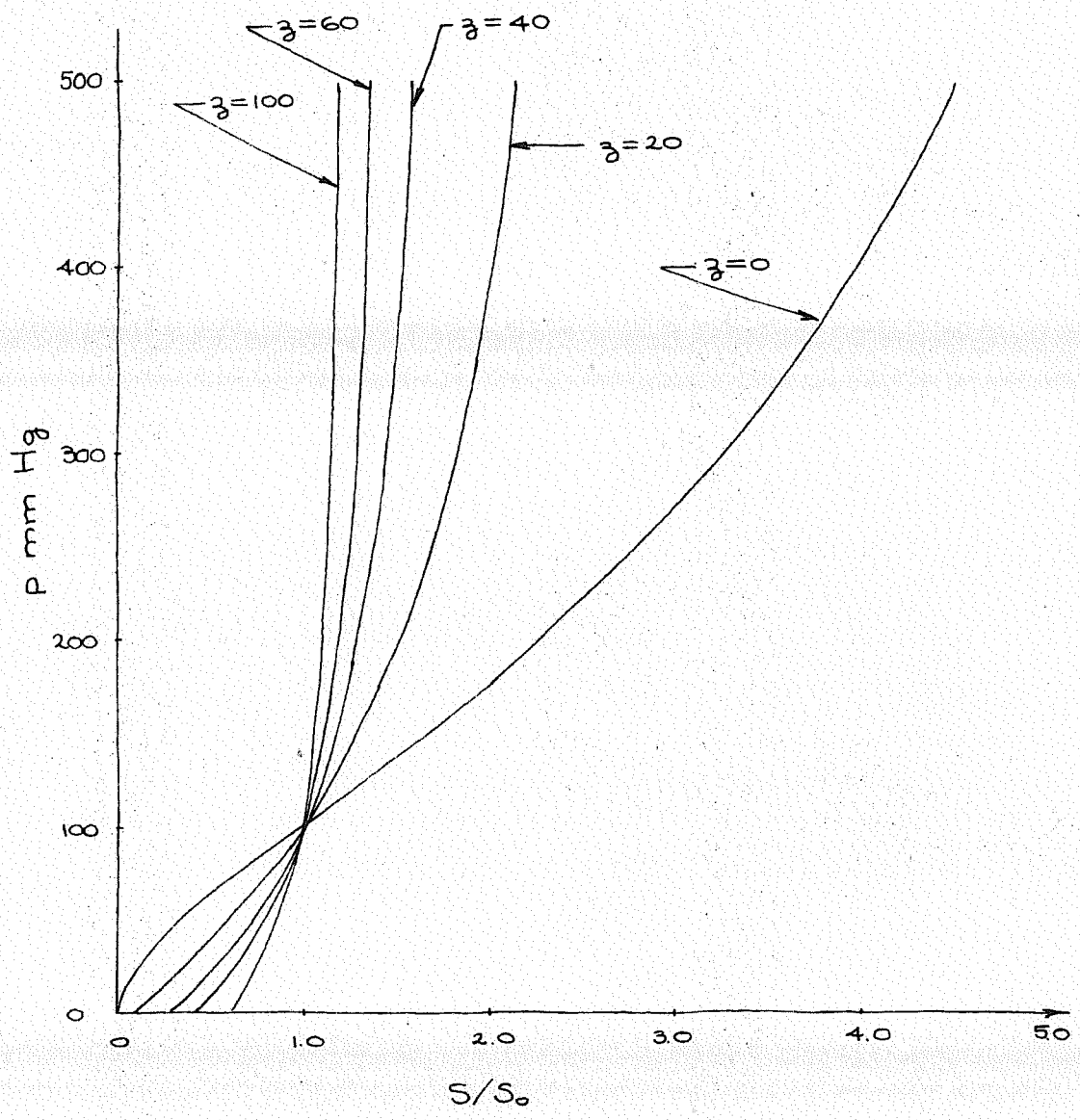

Figure 3.29 Pressure (p) vs. normalized area (S/S_o) from Rockwell's data [17]; z is the distance in cm from the aortic valve.

(3.10.4) are made is illustrative. If in Eq. (3.10.16) the superscript $(-)$ is suppressed and the equation is solved for $\hat{p}$, then

$$\hat{p}(\sigma-1;z,t) = \pi + U(\sigma;z,t)^2\frac{(\sigma^2-1)}{2\sigma^2} \quad . \tag{3.12.3}$$

The values $U(\sigma;z,t)$ are put together from experimental data. Note that this can come directly through measurements of U and σ, or indirectly via measurements of U and v by using Eq. (3.10.15) which reduces to

$$\sigma = 1/(1-v/U) \quad . \tag{3.12.4}$$

These techniques, for identifying the elastic artery, are remarkably simple and underlie the significance of the propagation velocity expressions. However, it is well known that arteries exhibit viscoelastic behavior. The identification problem for constitutive equations of this form represents a considerable increase in difficulty. The first step in performing a viscoelastic identification is pinning down the form of the constitutive equation, as there are many different ways to manifest dissipative effects.

3.12b A Simple Non-Linear Viscoelastic Constitutive Model.* Let $\alpha=\sigma-1$ and assume a constitutive equation of the form:

$$\hat{p}(\alpha^t,\alpha^r;z,t) = \hat{p}_o(\alpha^t;z,t) + \\ + K(\alpha^t;z,t)\int_0^\infty e^{-r/\tau(z,t)}\,\alpha(z,t-r)\,dr \quad . \tag{3.12.5}$$

* See Schuler and Walsh [53].

For simplicity the explicit dependence upon χ and t will be suppressed in what follows, i.e., Eq. (3.12.5) will be written as

$$\hat{p}(\alpha(t),\alpha^r) = \hat{p}_0(\alpha(t)) + K(\alpha(t))\int_0^\infty e^{-r/\tau}\alpha(t-r)\,dr. \qquad (3.12.6)$$

Note that as $\tau > 0$ approaches zero, the second term, representing viscous effects, becomes small and the constitutive equation approaches the elastic form. If a constant history $\alpha(t-r) = a$, $\forall r \in (0,\infty)$ is substituted into the second term of Eq. (3.12.6), a function, called the instantaneous response function for the history a , is defined

$$\hat{p}_a(\alpha(t)) = \hat{p}_0(\alpha(t)) + a\tau K(\alpha(t)). \qquad (3.12.7)$$

Thus $\hat{p}_0$ is the instantaneous response function for the 0 history. This corresponds to $S(\chi,t-r) = s(\chi)$, $\forall r \in (0,\infty)$. Although such situations do not occur in practice, the preceding notion is important since the exponential term causes the second term in Eq. (3.12.6) to remember in essence only the "immediate past." Thus a constant history for some finite time (which depends on the magnitude of τ) is adequate to define instantaneous response functions in practical circumstances. As usual, it is assumed $D_1\hat{p}_a > 0$ and $D_1^2\hat{p}_a \geq 0$ for all a in the range of physical behavior. In general K is assumed to be negative, which can be interpreted by

assuming a step function for the history

$$\alpha(t) = a\, H(t) \quad ; \qquad (3.12.8)$$

see Fig. 3.30. The slope of the $\hat{p}$ curve at $t=0$ is computed assuming the dependence on t in the fourth slot is absent.

3.12c Identification of the Viscoelastic Model via Shock Data.

(A) Computing $\hat{p}_0$:

Suppose the initial state is given by (3.10.4) and has been in equilibrium long enough so that the integral in Eq. (3.12.6) can be neglected. Then $\hat{p}_0$ can be constructed from shock wave propagation data in exactly the same way as the elastic function was constructed (Eq. (3.12.3)). In terms of α , and suppressing the dependence on the last two slots, the counterpart of Eq. (3.12.3) is

$$\hat{p}_0(\alpha) = \pi + U(\alpha)^2 \left\{ \frac{\alpha(\alpha+2)}{2(\alpha+1)^2} \right\} \qquad (3.12.9)$$

where $\alpha = \alpha^-$.

(B) Computing τK:

A steady wave is a solution of Eqs. (3.1.1) - (3.1.3) which depends only on the single variable $\xi = z - \bar{u}t$; $\bar{u}$ is called the steady wave velocity (cf. the analysis in Section 3.2). A steady shock wave is a steady wave with a shock front, (e.g., see Fig. 3.31). The analysis in Section 3.2 indicates that

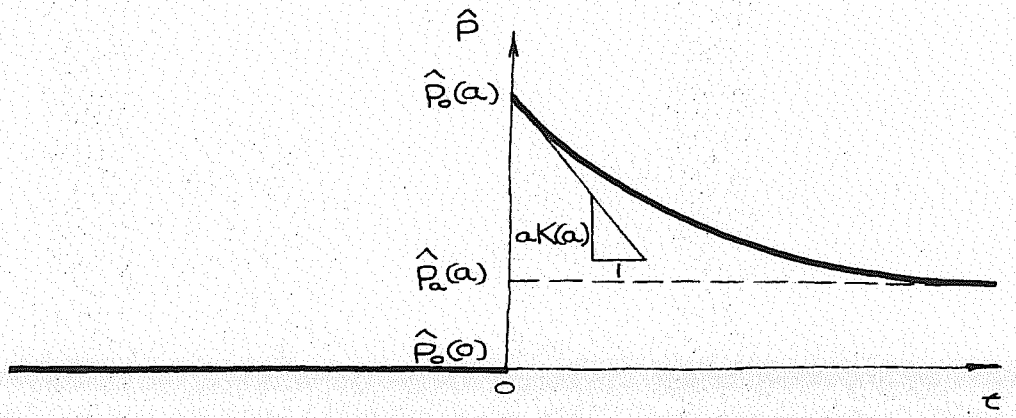

Figure 3.30

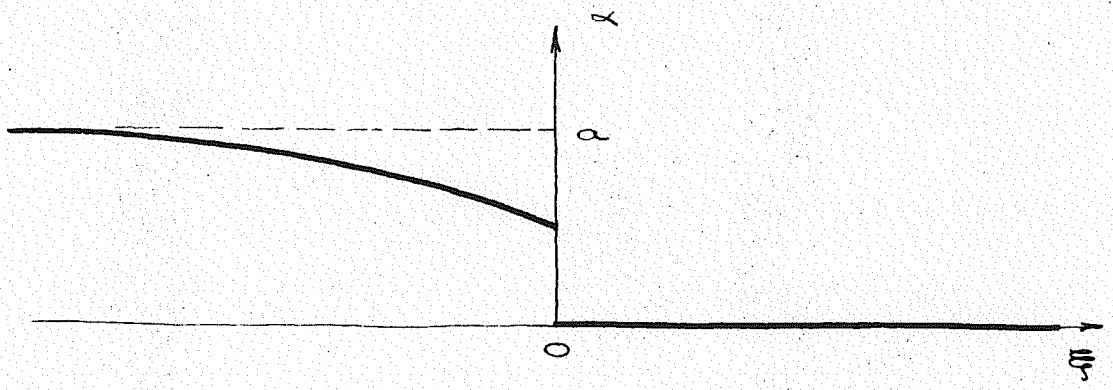

Figure 3.31

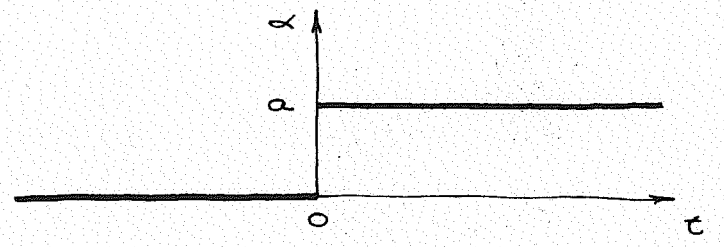

Figure 3.32

steady waves satisfy conditions identical in form to the shock jump conditions, but have a different interpretation. These conditions will be written here as

$$S^{(-\infty)}\,\overline{w}^{(-\infty)} = S^{(+\infty)}\,\overline{w}^{(+\infty)}$$

$$\frac{\left(\overline{w}^{(-\infty)}\right)^2}{2} + \frac{p}{\rho}^{(-\infty)} = \frac{\left(\overline{w}^{(+\infty)}\right)^2}{2} + \frac{p}{\rho}^{(+\infty)} \qquad (3.12.10)$$

where $\overline{w}^{(\pm\infty)} = F^{(\pm\infty)}\,\overline{U}^{(\pm\infty)} = \overline{u} - w^{(\pm\infty)}$

is the <u>relative steady wave velocity</u>, $\overline{U}$ is the <u>intrinsic steady wave velocity</u>, and the superscripts $(\pm\infty)$ correspond to $\xi_j \longrightarrow (\pm\infty)$. Suppose the wave is as depicted in Fig. 3. 1, and the state to the right of the shock front is given by

$$\begin{aligned} \rho p &= \rho p^{+} = \rho p^{(+\infty)} = \pi \,, \\ S = S^{+} &= S^{(+\infty)} = s \iff \alpha = \alpha^{+} = \alpha^{(+\infty)} = 0, \\ w &= w^{+} = w^{(+\infty)} = 0 \,. \end{aligned} \qquad (3.12.11)$$

Also suppose the superscripts on the $\xi_j \longrightarrow -\infty$ state are suppressed:

$$\begin{aligned} p^{(-\infty)} &= p \,, \quad S^{(-\infty)} = S \,, \quad F^{(-\infty)} = F \,, \\ w^{(-\infty)} &= w \,, \quad \overline{U}^{(-\infty)} = \overline{U} \,, \\ \alpha^{(-\infty)} &= a \iff \sigma^{(-\infty)} = \sigma = a+1 \,. \end{aligned} \qquad (3.12.12)$$

With these, the following relations can be computed:

$$\begin{aligned}\overline{u} &= u^{(+\infty)} + \overline{u'}^{(+\infty)} = \overline{U}^{(+\infty)} \\ &\overset{\text{def.}}{=} U \ ; \\ \overline{u} &= u^{(-\infty)} + \overline{u'}^{(-\infty)} \\ &= u + F\overline{U} \\ &= u + \frac{\overline{U}}{\sigma} \\ &= u + \frac{\overline{U}}{(a+1)} \ ;\end{aligned} \tag{3.12.13}$$

and finally

$$\hat{p}_a(a) = \pi + \frac{1}{2}\left\{ U^2 - (U-u)^2(a+1)^2 \right\} . \tag{3.12.14}$$

Thus measurements of U, u as functions of a determine $\hat{p}_a(a)$. From $\hat{p}_a(a)$ and $\hat{p}_o(a)$, $\tau K(a)$ can be computed via Eq. (3.12.7):

$$\tau K(a) = (\hat{p}_a(a) - \hat{p}_o(a))/a . \tag{3.12.15}$$

(C) Computing τ :

By assumption, τ does not depend on α . Thus it can be determined from pressure and area data as indicated in the following example:

Suppose α at some site z is a step function with amplitude a , Fig. 3.32, and suppose the pressure data at z is as sketched in Fig. 3.33. Use the history depicted in Fig. 3.33 to integrate the

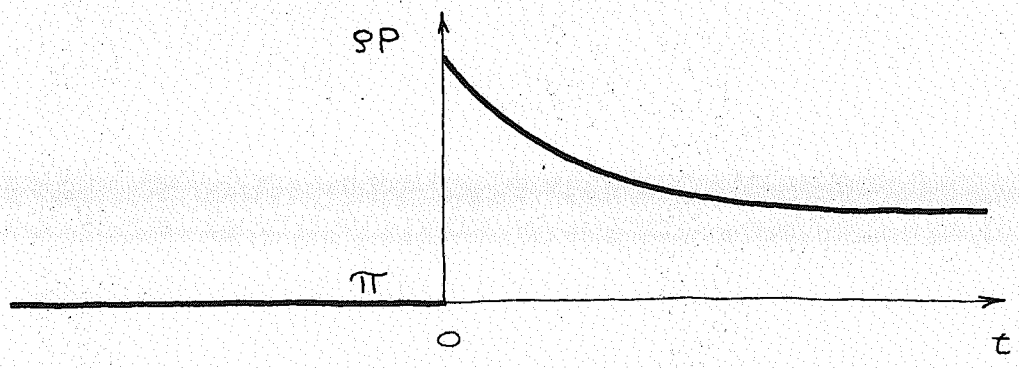

Figure 3.33

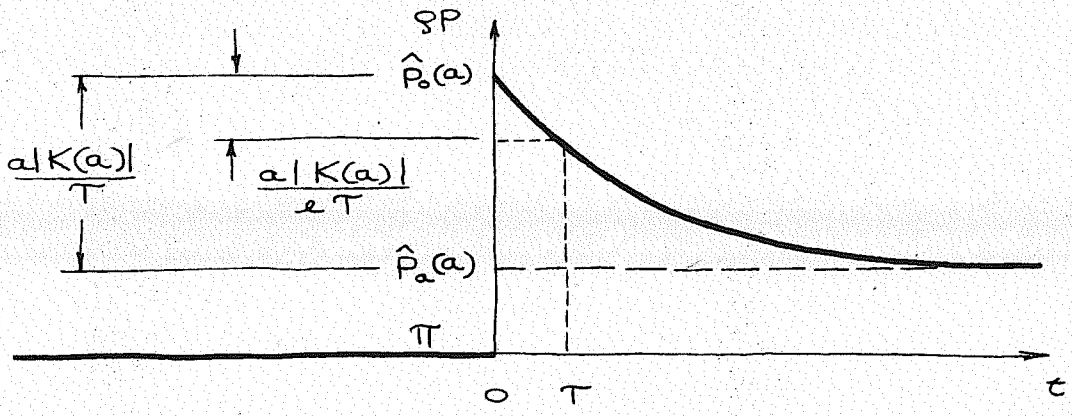

Figure 3.34

second term in Eq. (3.12.6):

$$\rho p = \begin{cases} \pi , & t < 0 \\ \hat{p}_0(a) + \dfrac{a K(a)}{\tau}\left(1 - e^{-t/\tau}\right), & t \geq 0 \end{cases} \qquad (3.12.16)$$

which enables the interpretation of Fig. 3.33 and the computation of τ (see Fig. 3.34).

For more complicated profiles the procedure for computing is essentially the same, namely represent the data parametrically and perform the integration in Eq. (3.12.6). The resulting relation, akin to Eq. (3.12.16), is then used in conjunction with the pressure data to deduce τ as in Fig. 3.34. Note that this procedure doesn't depend on the wave being steady, however it is considerably simpler if it is.

Notes. The use of steady shock waves provides a simple analytical technique for the identification of a viscoelastic arterial model. The technique does not require bona fide steady waves, as long as equilibrium manifests itself in the experimental data; a zero derivative in graphs such as Figs. 3.32 - 3.34 is indicative.

The dependence of $\hat{p}$ on z and t in the last two slots was suppressed as the notation was becoming cumbersome. To construct the dependence on z, data must be measured at different sites and the analysis of steps (A)-(C) carried out for each site.

An interpolation of the results gives the dependence. The dependence on t, e.g., before and after the administration of a drug affecting the cardiovasculature, is deduced simply by performing the whole sequence of experiments at different times.

The experimental work of Landowne [51,52] indicates that shock-like waves can be induced in the circulatory system. Thus there is some hope that a procedure such as the one just described may be used to identify viscoelastic properties.

3.13 Smooth Pulses and the Shock Relations

In this section the way in which the shock relations approximate the behavior of smooth pulses is studied.

A smooth pulse is a C^2 mapping

$$\varphi : [\xi_1, \xi_2] \subset \mathbb{R} \longrightarrow \mathbb{R}$$

such that $D\varphi(\xi_1) = D\varphi(\xi_2) = 0$, $D^2\varphi(\xi_1) \leq 0$, $D^2\varphi(\xi_2) \geq 0$ and $D\varphi(\xi) < 0$, for all $\xi \in (\xi_1, \xi_2)$; see Fig 3.35. The front of φ is its graph, $\{(\xi, \varphi(\xi)) \mid \xi \in [\xi_1, \xi_2]\}$. The front thickness $\varepsilon = \xi_2 - \xi_1$ and the amplitude $[\varphi] = \varphi(\xi_1) - \varphi(\xi_2)$, where $\varphi(\xi_1)$ and $\varphi(\xi_2)$ are the maximum and minimum of φ , respectively.

Consider an equation of the form:

$$\frac{\partial U_i}{\partial t} + \frac{\partial F_i}{\partial z}(\underset{\sim}{U}) + G_i(\underset{\sim}{U}) = \nu \frac{\partial^2 U_i}{\partial z^2} . \qquad (3.13.1)$$

Let $(\xi(z,t), \eta(z,t))$ define a rotated orthogonal coordinate system such that, for η fixed, $U_i(\cdot, \eta)$ is a smooth pulse. To pin down the definition of the coordinate system, suppose η is tangent to the right-facing characteristic (setting $\nu = 0$ in (3.13.1)) through the point $(\bar{\xi}, \bar{\eta})$, where $\bar{\xi}$ satisfies

$U_i(\bar{\xi}, \bar{\eta}) = \frac{1}{2}\{U_i(\xi_1, \bar{\eta}) + U_i(\xi_2, \bar{\eta})\}$; see Fig. 3.36. A particular system which satisfies these conditions is given by

$$\xi = z - \bar{u}t \quad , \qquad \eta = z + \bar{u}t \quad , \qquad (3.13.2)$$

where $\tilde{u}$ is the velocity of the right-facing characteristic at $(\bar{\xi},\bar{\eta})$. In this coordinate system, Eq. (3.13.1) becomes:

$$-\tilde{u}\left(\frac{\partial}{\partial\xi}-\frac{\partial}{\partial\eta}\right)U_i+\left(\frac{\partial}{\partial\xi}+\frac{\partial}{\partial\eta}\right)F_i+G_i = \nu\left\{\frac{\partial^2 U_i}{\partial\xi^2}+2\frac{\partial^2 U_i}{\partial\xi\,\partial\eta}+\frac{\partial^2 U_i}{\partial\eta^2}\right\}. \tag{3.13.3}$$

Integrating with respect to ξ over $[\xi_1,\xi_2]$ yields

$$\tilde{u}[U_i]-[F_i]+\varepsilon\left\{\frac{\partial}{\partial\eta}(\tilde{u}\bar{U}_i+\bar{F}_i)+\bar{G}_i\right\} = \nu\left\{2\left[\frac{\partial U_i}{\partial\eta}\right]+\varepsilon\frac{\partial^2\bar{U}_i}{\partial\eta^2}\right\}, \tag{3.13.4}$$

where the superposed bar indicates mean value, e.g., $\bar{U}_i=\left(\int_{\xi_1}^{\xi_2}U_i\,d\xi\right)/\varepsilon$, and the jump operator $[\cdot]$ is defined by $[U_i]=U_i(\xi_1,\eta)-U_i(\xi_2,\eta)$. Eq. (3.13.4) is understood to be evaluated at $\bar{\eta}$. The first two terms on the left hand side of (3.13.4) are the smooth pulse analogs of the shock relations. The remaining terms were neglected in the analysis of Section 3.2, pp. 33-38.

To see when the shock relations hold to a good approximation, introduce the length scales

$$\lambda_1=\left\{\tilde{u}[U_i]/\left\{\frac{\partial}{\partial\eta}(\tilde{u}\bar{U}_i+\bar{F}_i)\right\}\right\}\Big|_{\bar{\eta}},$$

$$\lambda_2=\left\{\tilde{u}[U_i]/\bar{G}_i\right\}\Big|_{\bar{\eta}},$$

and the coordinate change $\xi = \eta/\lambda_1$. With these, Eq. (3.13.4) can be written as

$$\left(1 - \frac{[F_i]}{\bar{u}[U_i]}\right) + \varepsilon_1 + \varepsilon_2 = \tilde{\nu}\left\{\left(2\left[\frac{\partial U_i}{\partial \xi}\right] + \varepsilon_1 \frac{\partial^2 \bar{U}_i}{\partial \xi^2}\right)/[U_i]\right\}, \qquad (3.13.5)$$

where $\varepsilon_1 = \varepsilon/\lambda_1$, $\varepsilon_2 = \varepsilon/\lambda_2$ and $\tilde{\nu} = \nu/(\bar{u}\lambda_1)$ are non-dimensional parameters. Thus the shock relations are seen to hold to $O(\varepsilon_1 + \varepsilon_2 + \tilde{\nu})$ for smooth pulses. Roughly speaking, the parameters $\varepsilon_1, \varepsilon_2$ and $\tilde{\nu}$ are measures of the tangential variation of the pulse, lower-order effects and viscosity, respectively.

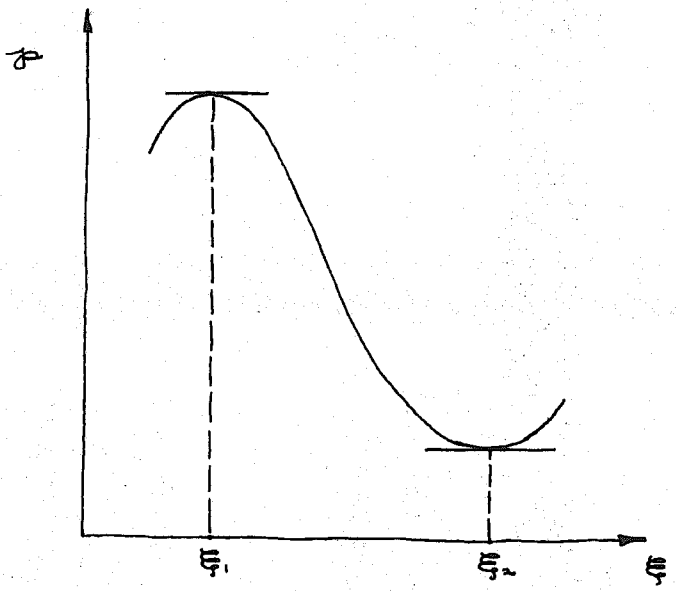

Figure 3.35

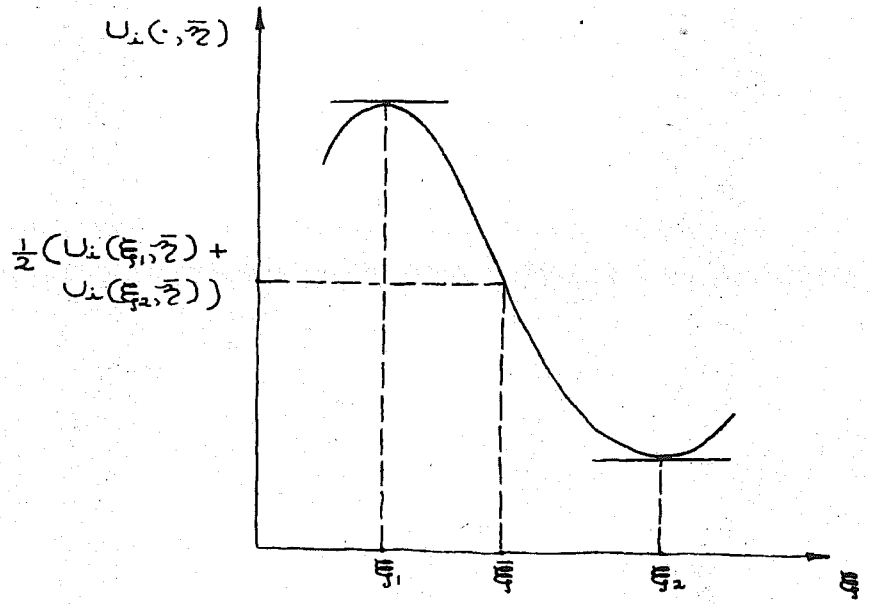

Figure 3.36

IV. NO-SLIP THEORY

4.1 Introduction

On the basis of the assumptions made in the construction of the flat-profile and no-slip theories, the latter is physically more realistic. In the present section some of the features of this theory are analyzed and compared with the flat-profile theory. The only difference in the two theories is in the momentum equation, which for the no-slip profile is

$$\frac{\partial S\upsilon}{\partial t} + \frac{\partial}{\partial z}(1+\delta)(S\upsilon^2) + \frac{S}{\rho}\frac{\partial p}{\partial z} = Sf + \omega N + \nu\frac{\partial^2 S\upsilon}{\partial z^2} \tag{4.1.1}$$

Assuming S and υ are smooth enough, Eq. (3.1.1) can be used to put (4.1.1) in a form amenable to comparison with the flat-profile momentum balance, Eq. (3.1.2):

$$\frac{\partial \upsilon}{\partial t} + \frac{\partial}{\partial z}\left(\frac{\upsilon^2}{2} + \frac{p}{\rho}\right) + \frac{1}{S}\frac{\partial}{\partial z}\delta(S\upsilon^2) = f + \frac{\upsilon}{S}(\psi + N) + \frac{\nu}{S}\frac{\partial^2 S\upsilon}{\partial z^2} \tag{4.1.2}$$

Eq. (4.1.2) is the velocity form of the momentum equation for the no-slip theory. There are three terms in this equation which are not in Eq. (3.1.2), and one which has changed form.

The N term represents the contribution to viscous forces resulting from the slope of the velocity

profile at the luminal surface. This term does not vanish, as does the second-order viscous term, in the limiting approximations of [7,15] and [18] . Historically, a viscous term has been added ad hoc to the flat-profile theory. The no-slip theory thus includes this more rationally. The significance of this term has been explored numerically by Rockwell [17]. His results indicate that for reasonable values of the viscosity, μ , the effect of N is small up to, and including, the bifurcation. However, beyond the bifurcation, where the luminal area decreases rapidly causing an increase in magnitude of $\upsilon N/S$, the effects of varying μ are quite noticeable. As μ increases both the pressure and velocity pulses tend to decrease in amplitude in the region distal to the bifurcation.

The inclusion of the outflow term ψ in Eq. (4.1.2) for the no-slip theory was first pointed out in [27]. Since both it and N multiply υ/S , its significance is easy to deduce. It tends to mitigate the effect of viscous forces $(+1 = \operatorname{sgn}\psi = -\operatorname{sgn}N)$. Thus for the analyses considered by Rockwell one would anticipate changes in the post-bifurcation region. This hypothesis was verified numerically (see Fig. 4.1). A detailed description of the analysis is contained in Section 5.6.

The δ term represents a correction to the axial momentum due to the fact that the velocity

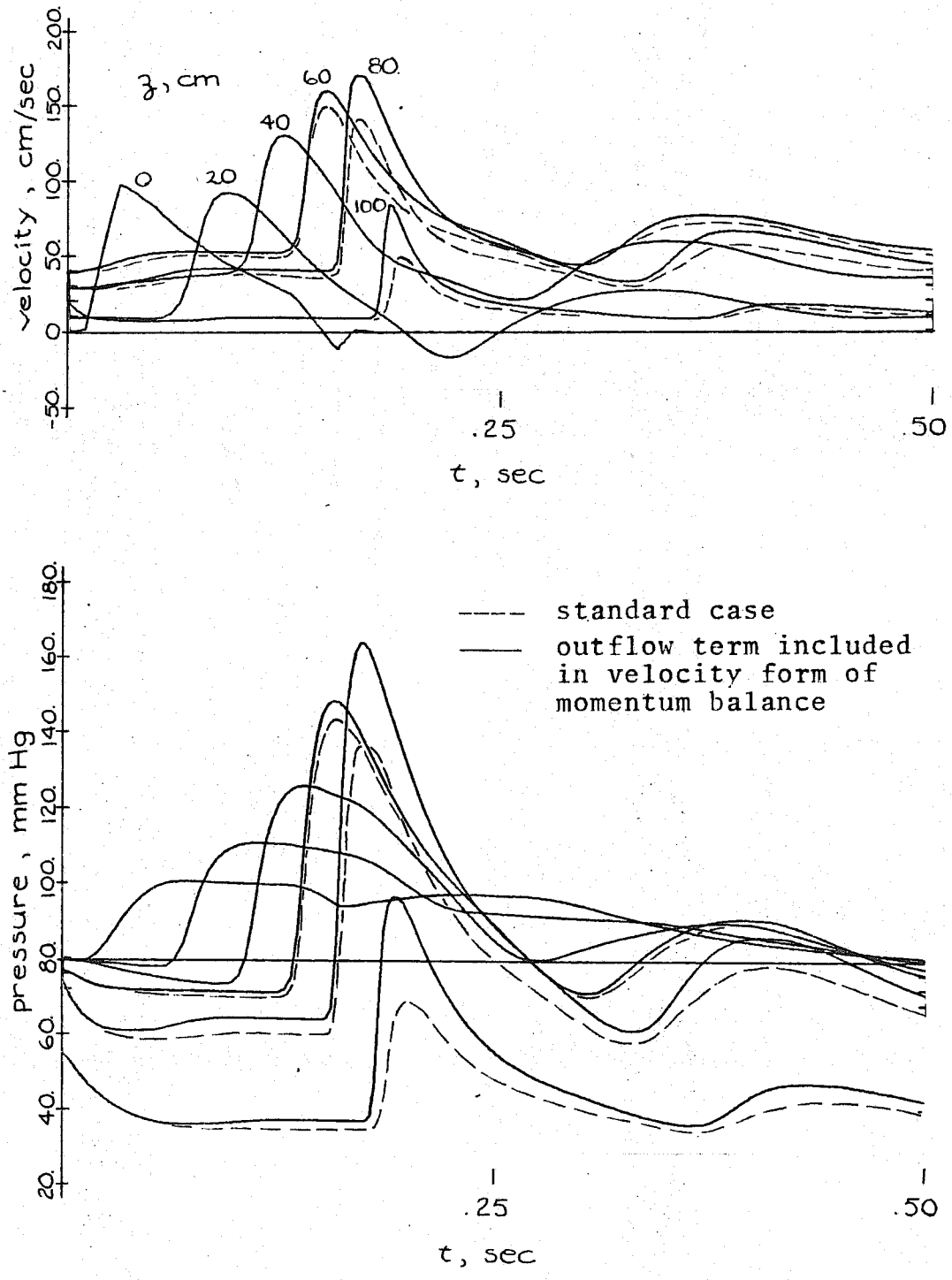

Figure 4.1 Effect of outflow term in momentum balance

profile isn't flat. Although experimental work indicates its value is small (say $0<\delta<1/3$), its quantitative significance has not been established. To assess its effect, a calculation has been made based upon Rockwell's data (see Fig. 4.2). The details of the analysis are described in Section 5.6. The results indicate that there is negligible effect prior to $z = 60\ cm$. However, for $z > 60\ cm$ the differences become noticeable. This suggests that the effect of δ may be important in the smaller vessels.

The second-order viscous term is interesting. The form it takes indicates that the appropriate discontinuity conditions, as motivated by the arguments for the flat-profile theory*, will be different than the flat profile conditions. The appropriate weak form of the equations for the mixed initial-boundary value problem will then be

$$
\begin{aligned}
0 = \int_{\mathcal{R}} \Big\{ & S\frac{\partial \phi_1}{\partial t} + Sv\frac{\partial \phi_1}{\partial z} - \psi\phi_1 \\
& + Sv\frac{\partial \phi_2}{\partial z} + \Big((1+\delta)Sv^2 + \int_S^{S} s'\bar{p}_s\, ds'\Big)\frac{\partial \phi_2}{\partial z} \\
& + (Sf + vN + \mathcal{S})\phi_2 + \nu Sv\frac{\partial^2 \phi_2}{\partial z^2}\Big\} dz\,dt \\
& + \int_{\mathcal{R}} (S_0\phi_1 + S_0 v_0 \phi_2)\Big|_{t=0} dz + \mathcal{B},
\end{aligned}
\tag{4.1.3}
$$

---

* Cf. pp. 33-38.

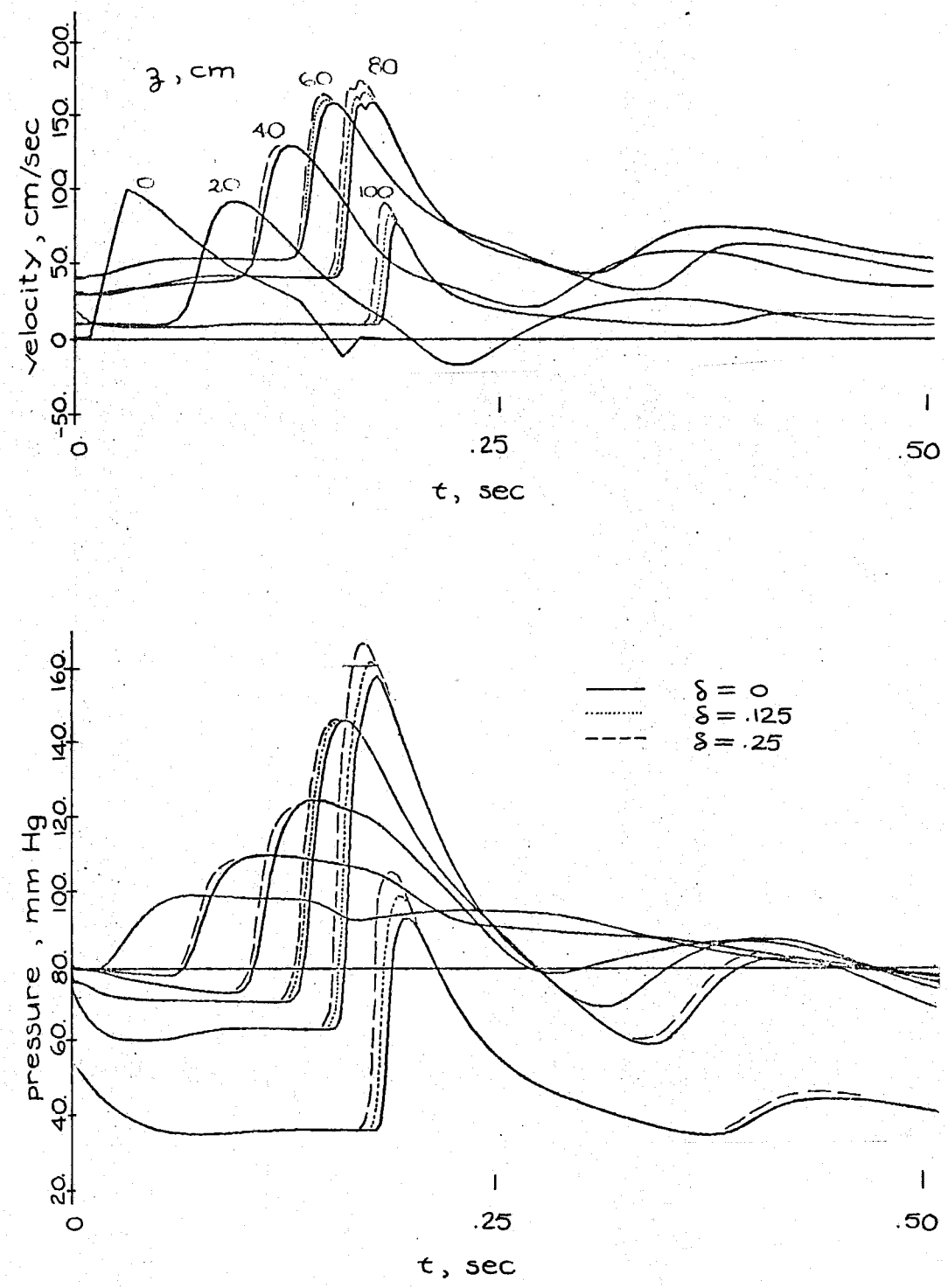

Figure 4.2 Effect of no-slip velocity profiles

where

$$\mathcal{S} = \int^{S} S'\left(D_2\tilde{P}_S \cdot \frac{\partial S^r}{\partial \zeta} + D_3\tilde{P}_S\right) dS'$$

$$- SD_2\tilde{P} \cdot \frac{\partial S^r}{\partial \zeta} - SD_3\tilde{P} \,, \qquad (4.1.4)$$

$$\mathcal{B} = -\int_{\mathbb{R}^+} \left\{ Q\phi_1 + \mathcal{F}\phi_2 + \nu Q \frac{\partial \phi_2}{\partial \zeta} \right\}\Big|_{\zeta=0}^{\zeta=L} dt \,,$$

and $\mathcal{F} = SC$ is the <u>apparent force</u>. The term $\mathcal{S}$ is zero if wall viscosity and inhomogeneity are neglected. The discussion of appropriate boundary data follows along the lines of Section 3.3. Note though that here the last term of $\mathcal{B}$ contains Q instead of V as before. Since this is redundant, it might as well be insisted that $\phi_2 \in K'(0,L)$. Thus even when $\nu > 0$, the specification of V constitutes an essential boundary condition, unlike the case for Eqs. (3.3.11) - (3.3.12). The argument for writing the momentum balance in this weak form is that if N is fixed and the full equations are solved for various values of ν , then in the limit as $\nu \to 0$, the class of weak solutions arrived at is that defined by Eqs. (4.1.3) - (4.1.4) with ν formally set to zero. Note that if δ and N are formally set to zero, weak solutions obtained by satisfying Eqs. (4.1.3) - (4.1.4) do not in general satisfy Eqs. (3.3.11) - (3.3.12). This can be seen by looking at the discontinuity conditions for Eqs. (4.1.3) - (4.1.4) :

$$
\begin{aligned}
u[S] &= [Sv] \,, \\
u[Sv] &= [(1+\delta)(Sv^2)] + \sum_{S^+}^{S^-} S\tilde{p}_s \\
&\quad - \nu \left[\frac{\partial Sv}{\partial z} \right] \,, \\
0 &= \nu [Sv] \,,
\end{aligned}
\tag{4.1.5}
$$

and comparing them with Eqs. (3.2.19). However, when δ, N and ν are set to zero, strong solutions of one theory are strong solutions of the other. This implies that differences will be seen in numerical analysis of the theories, when shock-like pulses are involved, even when δ, N and ν are set to zero.

It is interesting that the assumption of the flat-profile or the no-slip profile turns out to be crucial in that two different classes of weak solutions result.

4.2 Consequences of the Discontinuity Conditions

The discontinuity conditions for the no-slip theory, Eqs. (4.1.5), are somewhat different than those for the flat-profile theory, Eqs. (3.2.19). In the following analysis use is made of some of the notions of Section 3.4. In addition, it is assumed $[\delta] = 0$.

If $\nu > 0$, Eq. $(4.1.5)_3$ gives $[Sv] = 0$, which reduces Eqs. $(4.1.5)_{1,2}$ to

$$
\begin{aligned}
u[S] &= 0, \\
0 &= (Sv)^{\pm} [(1+\delta)v] + \sum_{S^+}^{S^-} S\tilde{p}_s - \nu \left[\frac{\partial Sv}{\partial z} \right] .
\end{aligned}
\tag{4.2.1}
$$

If $u \neq 0$, $[S]=0$ which implies $[v]=0$; thus from Eq. $(4.2.1)_2$ $\left[\frac{\partial Sv}{\partial z}\right]=0$. Taking the jump of Eq. (3.1.1) thus gives $[\partial S/\partial t]=0$, and from the compatibility relation, Eq. (3.4.5), with $g=S$, one obtains $[\partial S/\partial z]=0$. By expanding $[\partial Sv/\partial z]=0$ one gets $[\partial v/\partial z]=0$, and using Eq. (3.4.5) with $g=v$ then gives $[\partial v/\partial t]=0$. Therefore (S,v) are C^1 and <u>there are no shock waves for $\nu>0$</u> . It is no problem to proceed further; thus if $u \neq 0$, (S,v) are C^∞ .

If the assumption $u \neq 0$ is dropped, Eq. $(4.2.1)_2$ remains as is, Eq. $(4.2.1)_1$ is satisfied identically, and little more can be said.

When $\nu=0$, Eqs. (4.1.5) reduce to

$$\begin{aligned} u[S] &= [Sv] , \\ u[Sv] &= [(1+\delta)Sv^2] + \int_{S^+}^{S^-} S\tilde{p}_S \end{aligned} \qquad (4.2.2)$$

In terms of the relative velocity w these become

$$\begin{aligned} 0 &= [Sw] , \\ 0 &= [Sw^2] + \int_{S^+}^{S^-} S\tilde{p}_S + \delta[Sv^2] \end{aligned} \qquad (4.2.3)$$

At first glance it appears that unless $\delta=0$, Eq. (4.2.3) is not properly invariant in that v cannot be eliminated in favor of w . This appearance is only illusory however, as a moment's reflection reveals. The condition that v_3 satisfy the no-slip boundary condition, and the condition that the arterial wall experiences no longitudinal motion imply $v_3\big|_C = 0$

(cf. (F) and (E_2), p. 16). This selects out a special observer, namely, one sitting on a fixed point (ξ) in the artery wall. Thus v takes on an invariant meaning; it is the mean fluid velocity with respect to the artery wall. Another one-dimensional observer translating along at some constant velocity $\bar{u}$ would measure mean fluid velocity to be $v-\bar{u}$, but he would also measure artery wall velocity as $-\bar{u}$. The difference v is thus the same for all one-dimensional Galilean observers, and Eq. $(4.2.3)_2$ is in fact Galilean invariant.

It is of interest to consider the possibility of a contact discontinuity. In this case $w=0$ and Eq. $(4.1.7)_1$ is identically satisfied, whereas Eq. $(4.1.7)_2$ becomes

$$0 = \int_{S^+}^{S^-} S\tilde{p}_s + \delta v^2 [S].$$

Suppose $S^- > S^+$, then both terms on the right are greater than zero, as $S, \tilde{p}_s, \delta, v^2$ are all greater than zero. If $S^- < S^+$, then the right hand side is strictly negative. Thus the only possibility is $[S]=0$, and <u>there are no contact discontinuities for all</u> $\delta \geq 0$ when $\nu = 0$.

4.3 Shock and Acceleration Wave Velocities

The counterpart of Eq. (3.5.3) for the no-slip velocity profile is

$$\omega^{-}\omega^{+} = \frac{1}{[S]} \int_{S^{+}}^{S^{-}} S\tilde{P}_s \; + \; + \delta(v^{-}v^{+} + v^{-}\omega^{+} + v^{+}\omega^{-}) \qquad (4.3.1)$$

The counterparts of Eqs. (3.5.4) - (3.5.5) just involve using $\omega^{-}/\omega^{+} = S^{+}/S^{-}$, i.e., Eq. (4.2.3). The conclusions (3.5.5) - (3.5.6) follow from Eq. (4.2.3), and thus hold in this case also.

Acceleration wave velocity (= characteristic velocity) can be obtained from Eq. (4.3.1) by taking the limit $\omega^{\pm} \longrightarrow \omega$; $S^{\pm} \longrightarrow S$, viz.,

$$\omega^{2} = S\tilde{P}_s + \delta(v^{2} + 2v\omega) \qquad (4.3.2)$$

Note that the shock velocity expression for the present case, Eq. (4.3.1), is different than Eq. (3.5.3) even when $\delta \longrightarrow 0$. This corresponds to the different classes of discontinuous solutions picked out by the two theories. On the other hand, as $\delta \longrightarrow 0$, the acceleration wave velocity for the no-slip profile is the same as for the flat profile.

When comparing predictions made by the no-slip and flat-profile theories, the following notations will be used: $(\cdot)^{N}$, to indicate a no-slip theory quantity, and $(\cdot)^{F}$, a flat-profile theory quantity. Some physical interpretations of Eq. (4.3.2) are immediate:

(A) The velocity of acceleration waves

propagating into quiescent regions, i.e., where $v=0$, is the same for both theories.

(B) Assume $v, w > 0$. Then if experimental acceleration wave data are used to identify $\tilde{p}$, $(\tilde{p}_s)^F > (\tilde{p}_s)^N$; that is, the neglect of the δ term makes the artery appear to be instantaneously stiffer. Equality occurs if the data are obtained from tests where the acceleration waves propagate into regions where $v = 0$. Otherwise Eq. (4.3.2) should be resorted to for identification purposes, unless of course it can be established $\delta(v^2 + vw) \ll w^2$. This is the usual case for the major vessels.

(C) Assuming $v, w > 0$, and $\tilde{p}_s$ and δ have been obtained exactly by some independent means, then $(w)^N > (w)^F$; that is, the predicted acceleration wave velocity for the no-slip theory is greater than that for the flat-profile theory.

The shock velocity expression is more difficult to decipher. First consider the case where $\delta = 0$. Assume that $S^- > S^+$. Then to conclude that $(w^- w^+)^N > (w^- w^+)^F$, it is necessary to show that $\int_{S^+}^{S^-} S\tilde{p}_s > [\tilde{p}] / \langle 1/S \rangle$.

First notice that if $S^- = S^+$ both sides are zero. Thus it suffices to show that

$$\frac{d}{dS^-} \int_{S^+}^{S^-} S\tilde{p}_s > \frac{d}{dS^-} \frac{[\tilde{p}]}{\langle 1/S \rangle}.$$

Compute:

$$\frac{d}{dS^-}\int_{S^+}^{S^-} S\tilde{p}_s = S^-\tilde{p}_s^- > \frac{2(S^+)^2}{(S^-+S^+)}\tilde{p}_s^- ,$$

$$\geq \frac{2(S^+)^2}{(S^-+S^+)}\frac{[\tilde{p}]}{[S]} ;$$

$$\frac{[S]S^-\tilde{p}_s^-}{(S^-+S^+)} = \frac{(S^-+S^+-2S^+)}{(S^-+S^+)} S^-\tilde{p}_s^- ,$$

$$= \left(1 - \frac{2S^+}{(S^-+S^+)}\right) S^-\tilde{p}_s^- ,$$

$$\geq \frac{2(S^+)^2}{(S^-+S^+)^2}[\tilde{p}] ;$$

$$S^-\tilde{p}_s^- \geq \frac{2S^+}{(S^-+S^+)}\left(S^-\tilde{p}_s^- + \frac{S^+}{(S^-+S^+)}[\tilde{p}]\right) ,$$

$$= \frac{2S^-S^+}{(S^-+S^+)}\left(\tilde{p}_s^- + \frac{S^-S^+}{(S^-+S^+)}\frac{1}{(S^-)^2}[\tilde{p}]\right),$$

$$= \frac{1}{\langle 1/S\rangle}\left(\tilde{p}_s^- - \frac{[\tilde{p}]}{\langle 1/S\rangle}\frac{1}{2}\frac{d}{dS^-}\left(\frac{1}{S^-}\right)\right),$$

$$= \frac{\tilde{p}_s^-}{\langle 1/S\rangle} + [\tilde{p}]\frac{d}{dS^-}\left(\frac{1}{\langle 1/S\rangle}\right),$$

$$= \frac{d}{dS^-}\frac{[\tilde{p}]}{\langle 1/S\rangle} .$$

Note that since $(w^-/w^+)^N = (w^-/w^+)^F = S^+/S^-$, the preceding result also implies $(w^{-2})^N > (w^{-2})^F$ and $(w^{+2})^N > (w^{+2})^F$. Since the inequalities are strict, they hold for δ small enough.

Thus suppose $w^- > w^+ \geq 0$ and $S^- > S^+$.

Then for all $\delta \geq 0$ it can be concluded that

$$(w^- - w^+)^N > (w^- - w^+)^F ,$$

$$(w^{-2})^N > (w^{-2})^F ,$$

$$(w^{+2})^N > (w^{+2})^F ,$$

i.e., the shock velocities predicted by the no-slip theory are greater than those for the flat-profile theory. In particular, shock velocity predictions of the two theories are different even if $\delta = 0$.

4.4 Previous Shock Conditions Appearing in the Literature

Four papers dealing with one-dimensional shock conditions have come to my attention. All have the same jump condition for the continuity equation, namely $[Sw] = 0$. However, each presents a different jump condition for the momentum equation:

(i) Lambert [1]: $[Sw^2 + S\bar{p}] = 0$,

(ii) Bird and Bodley [6]: $[Sw^2] + \langle S \rangle [\bar{p}] = 0$,

(iii) Beam [13]: $[Sw^2] + \sum_{S^+}^{S^-} S\bar{p}_s = 0$, (4.4.1)

(iv) Seymour and Varley [18]: $[\frac{w^2}{2} + \bar{p}] = 0$.

In light of the theory presented here, Beam's result is seen to correspond to the no-slip theory with (Eq. (4.1.1)), and Seymour and Varley's to the flat-profile theory (Eq. (3.1.2)).

It is of interest to compare these formulas. As a basis of comparison, $(\bar{w}\bar{\rho})$ will be expanded in powers of $[S]$:

(i) $\tilde{u}^{-}\tilde{u}^{+} = \dfrac{[S\tilde{p}]}{[S]} = (S^{+}\tilde{p}_{s}^{+} + \tilde{p}^{+}) + O([S])$,

(ii) $\tilde{u}^{-}\tilde{u}^{+} = \dfrac{\langle S\rangle}{[S]}[\tilde{p}] = S^{+}\tilde{p}_{s}^{+} + \dfrac{[S]}{2}(S\tilde{p}_{s})_{s}^{+} +$
$+ \dfrac{[S]^{2}}{3!}(S^{+}\tilde{p}_{sss}^{+} + \dfrac{3}{2}\tilde{p}_{ss}^{+}) + O([S]^{3})$,

(iii) $\tilde{u}^{-}\tilde{u}^{+} = \dfrac{1}{[S]}\int_{S^{+}}^{S^{-}} S\tilde{p}_{s} = S^{+}\tilde{p}_{s}^{+} + \dfrac{[S]}{2}(S\tilde{p}_{s})_{s}^{+}$
$+ \dfrac{[S]^{2}}{3!}(S^{+}\tilde{p}_{sss}^{+} + 2\tilde{p}_{ss}^{+}) + O([S]^{2})$,

(iv) $\tilde{u}^{-}\tilde{u}^{+} = \dfrac{1}{\langle 1/S\rangle}\dfrac{[\tilde{p}]}{[S]} = S^{+}\tilde{p}_{s}^{+} + \dfrac{[S]}{2}(S\tilde{p}_{s})_{s}^{+}$
$+ \dfrac{[S]^{2}}{3!}(S^{+}\tilde{p}_{sss}^{+} + \dfrac{3}{2}(\tilde{p}_{ss}^{+} - \tilde{p}_{s}^{+}/S^{+}))$
$+ O([S]^{3})$

Note first of all that (i) does not agree with the other forms even to terms of order 1 (acceleration wave velocity). Examination of Lambert's derivation reveals that he uses an erroneous form of the global momentum balance for the case at hand, inconsistent even with his (correct) differential equations.

The derivation of Bird and Bodley seems nothing more than an assertion. However, their formula (ii) represents a convenient approximation to (iii) as it can be obtained by replacing the integral in (iii) by its trapezoidal-rule approximation.

Coherent shock theories stemming from weak forms of the equations can only be given for (iii) and (iv). That these agree up to terms of $O([S]^{2})$ (i.e., weak shocks) justifies the preceding detailed study of

the simpler flat-profile theory shock structure. There is thus a range of shock behavior in which the two forms, flat and no-slip profile, agree. However, reasons will now be given why the no-slip theory is to be preferred when the predictions of the theories differ:

(A) A simple analysis indicates that the shock conditions, Eqs. (4.1.5), imply, under appropriate circumstances, that momentum is conserved, whereas the shock conditions, Eqs. (3.2.19), imply, under similar circumstances, mean velocity is conserved. For example, assume that ν, ψ, f and δ are zero, $\tilde{p} = \tilde{p}(S)$ and v, S, p are identical at the fixed locations z_1 and z_2; $z_2 > z_1$. Assume also that a shock wave exists at $y \in (z_1, z_2)$ and integrate the two momentum equations between z_1 and z_2:

$$0 = \frac{d}{dt}\int_{z_1}^{z_2} Sv\,dz - u[Sv] + [Sv^2] + \int_{S^+}^{S^-} S\tilde{p}_S \,,$$
$$0 = \frac{d}{dt}\int_{z_1}^{z_2} v\,dz - u[v] + \left[\frac{v^2}{2} + \tilde{p}\right] \,, \qquad (4.4.3)$$

thus corroborating the assertion. Since the former condition is consistent with the mechanical axiom underlying the equation, it is preferred.

A similar analysis for Eq. (3.1.1) shows that it is consistent with mass conservation:

$$0 = \frac{d}{dt}\int_{z_1}^{z_2} S\,dz - u[S] + [Sv] \,. \qquad (4.4.4)$$

(B) The conjectures enunciated on p.44 imply

that (for a Newtonian fluid, p. 12) the shock conditions of the momentum form are consistent with the no-slip theory, whereas the shock conditions of the velocity form are consistent with the flat-profile theory. Since the no-slip profile is physically more realistic, this also implies that the momentum from is preferable to the velocity form.

(C) When δ = constant $\neq 0$, the velocity form of the equations cannot be put in conservation form. This is because the term $\frac{\delta}{S}\frac{\partial}{\partial z}(S v^2)$ does not derive from a potential, i.e., does not equal $\partial \Phi(S, v)/\partial z$ for any Φ. Thus it does not seem possible to construct a coherent shock theory for the velocity form, free of ad hoc assumptions, unless $\delta = 0$.

Based upon these remarks, when there is a difference in the predictions of the formulas, the momentum form should be viewed as correct. (A similar situation exists for the shallow-water equations [54]).

To assess the quantitative differences between the two forms of the shock relations, the following has been observed:

Given a constitutive relation for P, the shock relations involve five pieces of data $(\mu, S^-, S^+, v^-, v^+)$. If three are specified, the other two may be computed from the shock relations. To get reasonable magnitudes on data, the results of Rockwell [17] have been employed. In each of the following two examples,

p^+, p^-, v^+ are taken from Rockwell's data and v^- and μ are computed from the shock relations, employing the constitutive equation (Eq. (3.12.2)).

The first set of data is for his so-called standard case and is presented in Fig. 4.3. As can be seen from this, for shocks of the approximate amplitude of the natural pulse, the effects of the different shock relations and varying the profile parameter δ are relatively small.

The next set of data is for the case of aortic insufficiency and is presented in Fig. 4.4. For shocks of this amplitude the difference between the velocity and momentum forms is seen to be considerable. In addition, the effect of δ is seen to be substantial.

This is an indication that when computing large amplitude shock-like pulses, algorithms faithful to the momentum form of the equations should be employed. At the same time, in view of the many simplifications made in Chapter II, it should be noted that for strong shock, the realm of applicability of the theory is being severely stretched.

4.5 Shock Stability

The same conclusions for the no-slip theory hold as for the flat-profile theory (Section 3.8) if it can be verified that

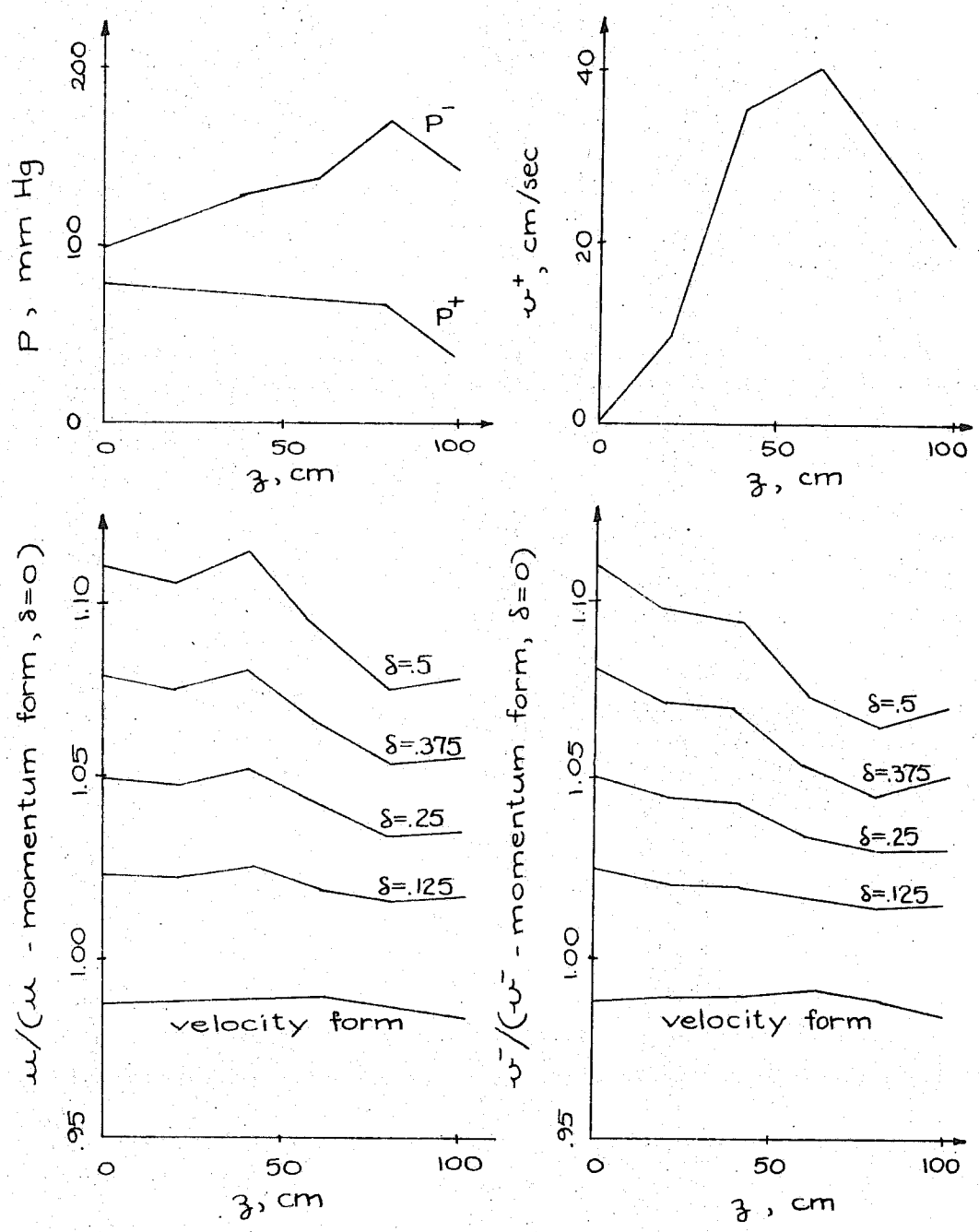

Figure 4.3 Comparison of v^- and u computed from velocity and momentum forms of the shock relations for data (P^+, P^-, v^+) taken from Rockwell's standard case [17], p.33.

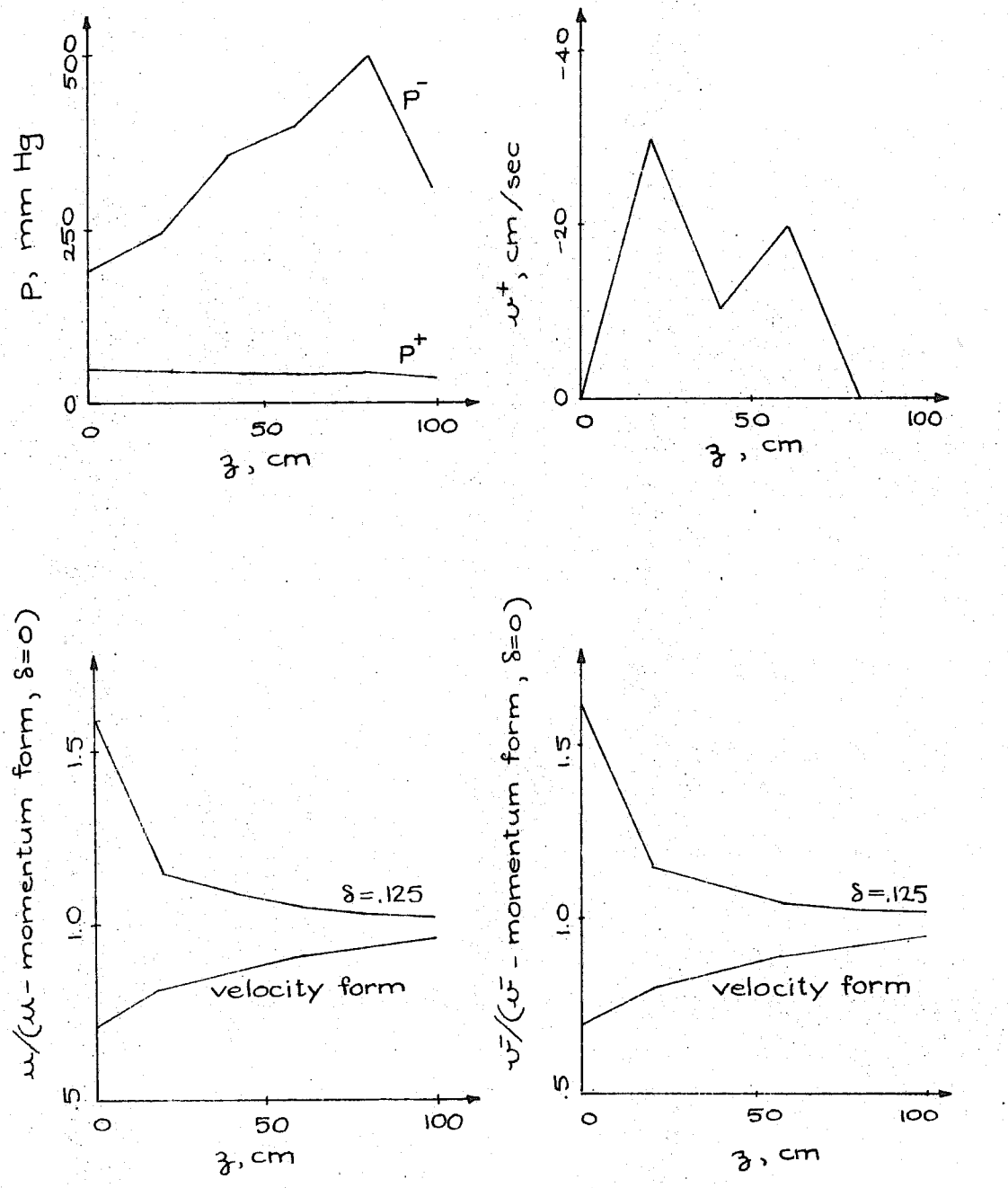

Figure 4.4 Comparison of v^- and u computed from velocity and momentum forms of the shock relations for data (P^+, P^-, v^+) taken from Rockwell's aortic insufficiency case [17], pp. 97-98.

(A) for a dilative shock

$$(\omega^+)^2 > (c^+)^2 \ , \qquad (\omega^-)^2 < (c^-)^2 \ , \tag{4.5.1}$$

(B) for a constrictive shock

$$(\omega^+)^2 < (c^+)^2 \ , \qquad (\omega^-)^2 > (c^-)^2 \ ,$$

when $\delta = 0$. Consider the four above cases in turn:

(A) Recall that here $S^- > S^+$ and $\omega^- < \omega^+$. The mean-value theorem and monotonicity of $\tilde{\rho}_s$ imply

$$S^-\tilde{\rho}_s^- > \frac{1}{[S]}\int_{S^+}^{S^-} S\tilde{\rho}_s > S^+\tilde{\rho}_s^+ \ ,$$

from which it follows that

$$\begin{aligned}(\omega^+)^2 &= \frac{(S^-/S^+)}{[S]}\int_{S^+}^{S^-} S\tilde{\rho}_s \\ &> \frac{1}{[S]}\int_{S^+}^{S^-} S\tilde{\rho}_s \\ &> S^+\tilde{\rho}_s^+ = (c^+)^2 \ ;\end{aligned}$$

$$\begin{aligned}(\omega^-)^2 &= \frac{(S^+/S^-)}{[S]}\int_{S^+}^{S^-} S\tilde{\rho}_s \\ &< \frac{1}{[S]}\int_{S^+}^{S^-} S\tilde{\rho}_s \\ &< S^-\tilde{\rho}_s^- = (c^-)^2 \ .\end{aligned}$$

(B) Here $S^- < S^+$ and $w^- > w^+$. This time the mean-value theorem and monotonicity of $\tilde{p}_s$ give

$$S^- \tilde{p}_s^- < \frac{1}{[S]} \int_{S^+}^{S^-} S\tilde{p}_s < S^+ \tilde{p}_s^+ .$$

Therefore

$$(w^+)^2 = \frac{(S^-/S^+)}{[S]} \int_{S^+}^{S^-} S\tilde{p}_s$$

$$< \frac{1}{[S]} \int_{S^+}^{S^-} S\tilde{p}_s$$

$$< S^+ \tilde{p}_s^+ = (c^+)^2 ;$$

$$(w^-)^2 = \frac{(S^+/S^-)}{[S]} \int_{S^+}^{S^-} S\tilde{p}_s$$

$$> \frac{1}{[S]} \int_{S^+}^{S^-} S\tilde{p}_s$$

$$> S^- \tilde{p}_s^- = (c^-)^2 .$$

Since these inequalities are strict it follows that (4.5.1) hold in the general case ($\delta \geq 0$) as long as δ is small enough.

4.6 Local Qualitative Behavior of Shocks

In this section the local qualitative behavior of shocks is determined for the momentum form (no-slip theory) of the shock relations, and in the process it is verified that this behavior is the same as that computed previously for the velocity form.

This assertion is established for the case $\delta = 0$. The same pace is taken as in Section 3.10, i.e., the results are first deduced for the case when (3.10.19) is in force, then the more general situation is considered. Note that all of (3.10.1) - (3.10.11), and (3.10.13) - (3.10.15) are taken to hold here.

With these the no-slip counterpart of Eq. (3.10.16) is

$$U^2 = \frac{1}{\Delta} \int_1^{(1-\Delta)^{-1}} \sigma E \, d\sigma \quad . \tag{4.6.1}$$

With the assumptions (3.10.19) and $\mathcal{F} = N = 0$, Eqs. (3.10.18), (3.10.20) and (3.10.21) remain intact, but Eq. (3.10.22) must be replaced by

$$U \frac{dU}{dt} = \frac{\alpha}{2(1-\Delta)^3} \frac{1}{\Delta} \frac{d\Delta}{dt} \quad , \tag{4.6.2}$$

which follows from differentiating Eq. (4.6.1) and using Eqs. (3.10.15) and (3.10.19). Note that from (4.5.1) it follows that

$$\begin{aligned} E^- = (c^-)^2 &> (w^-)^2 = (F^- U)^2 \\ &= U^2 (1-\Delta)^2 \\ &> U^2 (1-\Delta)^3 \quad , \end{aligned} \tag{4.6.3}$$

and so $\alpha > 0$ for the no-slip case also. Thus (3.10.23) holds, and if $A(\Delta)$ is replaced in Eq. (3.10.24) by

$$A(\Delta) = \frac{-2U(1-\Delta)^3 \alpha}{(E^- + 3(1-\Delta)^3 U^2)} \quad , \tag{4.6.4}$$

Eq. (3.10.24) holds as well as (3.10.25). Conditions (3.10.27) and (3.10.29) hold and thus the example on pp. 95-96.

The results will now be generalized for the case when (3.10.19) is not in effect and $N \neq 0$. The first change occurs in Eq. (3.10.18):

$$2U\frac{d\Delta}{dt} + \Delta\frac{dU}{dt} + \frac{1}{\rho}\left[\frac{\partial p}{\partial z}\right] + U^2\left[\frac{\partial F}{\partial Z}\right] = \left[\frac{\upsilon}{S}(\psi + N)\right]. \tag{4.6.5}$$

Eqs. (3.10.30) - (3.10.32) hold and from the definitions

$$\left[\frac{\upsilon}{S}(\psi + N)\right] = \frac{U\Delta(1-\Delta)}{\Delta}(\psi^- + N). \tag{4.6.6}$$

Eq. (3.10.33) must be modified to account for the different velocity expression, Eq. (4.6.1):

$$U\frac{dU}{dt} = \frac{\alpha}{2(1-\Delta)^3}\frac{1}{\Delta}\frac{d\Delta}{dt} + \frac{1}{2\Delta}\int_1^{(1-\Delta)^{-1}} \sigma\{U D_3 E + D_4 E\}\, d\sigma. \tag{4.6.7}$$

Combining Eqs. (4.6.5) - (4.6.7) and (3.10.30) - (3.10.31) results in Eq. (3.10.34), where $A(\Delta)$ is defined by Eq. (4.6.4), and τ becomes

$$\mathcal{C} = -\{(D_2\hat{p}\cdot\frac{\partial\sigma}{\partial\zeta})^{-} + D_3\hat{p}^{-} + \\ + \frac{1}{2U}\int_1^{(1-\Delta)^{-1}}\sigma(UD_3E + D_4E)\,d\sigma + \\ + \frac{U(1-\Delta)(1-2\Delta)}{a}\psi^{-} - \frac{U\Delta(1-\Delta)}{a}N\}/\alpha\,. \tag{4.6.8}$$

With these conditions, (3.10.36) holds. For the example on pp. 98-99 take $(3.10.37)_{1,2,3}$ and

$$\begin{aligned} D_3E &> 0\,, \\ D_4E &= 0\,, \\ N &< 0\,, \end{aligned} \tag{4.6.9}$$

In addition assume $\Delta<1/2$. Then $\mathcal{C}<0$ and the conditions are as illustrated in Fig. 3.15.

4.7 Identification

In this section it is assumed that $\delta=0$.

With this assumption, the identification procedure via the acceleration wave velocity expression (Eqs. (3.12.1) - (3.12.2)) holds for the no-slip case. The shock wave analysis, of course, requires modification due to the different velocity expression for the momentum form. When the assumptions (3.10.4) are made, the analog of Eq. (3.12.3) for the momentum form becomes

$$P(\sigma-1;\mathcal{Z},t) \overset{\text{def.}}{=} \int_1^\sigma \sigma' E(\sigma'-1;\mathcal{Z},t)\,d\sigma' = U(\sigma-1;\mathcal{Z},t)^2\,(\sigma-1)/\sigma \tag{4.7.1}$$

The physical interpretation of the function P for $\mathcal{Z},t$ fixed is illustrated in Fig. 4.5, where it is represented by the shaded area. This can be seen by performing an integration by parts in Eq. (4.7.1). One can deduce $\hat{p}$ from P by playing with Eq. (4.7.1):

$$\hat{p}(\sigma-1;\mathcal{Z},t) = \Pi + \int_1^\sigma \frac{1}{\sigma'} D_1 P(\sigma'-1;\mathcal{Z},t)\,d\sigma' \tag{4.7.2}$$

However, note that it is P which appears in the momentum form of the momentum equation. The analog of Eq. (3.12.9) consists simply of Eqs. (4.7.1) and (4.7.2) with $\sigma=\alpha+1$:

$$\begin{aligned} P_o(\alpha) &= \frac{\alpha}{1+\alpha}\,U(\alpha)^2 \\ \hat{P}_o(\alpha) &= \Pi + \int_1^{\alpha+1} \frac{1}{(\alpha'+1)} D_1 P_o(\alpha')\,d(\alpha'+1) \end{aligned} \tag{4.7.3}$$

Finally, only the counterpart of Eq. (3.12.14) is needed:

$$\begin{aligned} P_a(a) &= U^2 - (U-v)^2/(a+1) \\ \hat{P}_a(a) &= \Pi + \int_1^{a+1} \frac{1}{(a'+1)} D_a P_{a'}(a')\,d(a'+1) \end{aligned} \tag{4.7.4}$$

The rest of the analysis proceeds as before.

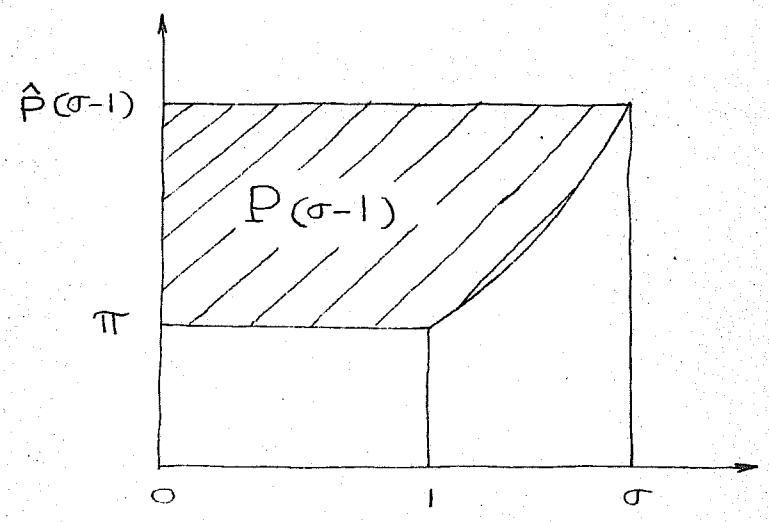

Figure 4.5

4.8 Growth and Decay of Acceleration Waves

4.8a Preliminaries. Acceleration waves have been defined in Section 3.6. Expressions for the propagation velocities for the flat-profile and no-slip theories are given in Eqs. (3.6.2) and (4.3.2), respectively. The usefulness of these expressions for material identification purposes has been indicated in Section 3.12a. In this section, the evolution of acceleration waves is discussed in the context of the present theories. The analysis is carried out for the no-slip theory, Eqs. (3.1.1), (3.1.3) and (4.1.1), from which the flat-profile results can be deduced.

Assume the constitutive equation takes the form

$$\frac{\partial p}{\partial t} = \mathcal{E}\frac{\partial S}{\partial t} + H \tag{4.8.1}$$

where

$$\begin{aligned} \mathcal{E} &= \mathcal{E}(S, p, z, t) \\ H &= H(S, p, z, t) \end{aligned} \tag{4.8.2}$$

are continuously differentiable functions of all their arguments.

Equation (4.8.1) is the most general quasi-linear constitutive equation of the first-order for a viscoelastic material of rate type. This form of the constitutive equation is preferred, rather than the functional relationship used previously, since, for

acceleration wave analysis, it simplifies derivations but represents no loss in generality. In this regard one can exhibit a one-to-one relationship between moduli of the two constitutive models which affect acceleration wave evolution. A correspondence of this sort has been shown for one-dimensional acceleration waves in materials with memory [55].

Recall that in an acceleration wave at $z = y(t)$,

$$[S] = [v] = [p] = 0 \quad , \tag{4.8.3}$$

whereas

$$\begin{aligned} &[\partial v/\partial t] \neq 0 \quad , \quad [\partial v/\partial z] \neq 0 , \\ &[\partial S/\partial t] \neq 0 \quad , \quad [\partial S/\partial z] \neq 0 , \\ &[\partial p/\partial t] \neq 0 \quad , \quad [\partial p/\partial z] \neq 0 , \end{aligned} \tag{4.8.4}$$

The assumptions on ψ, f, N imply that if Eqs. (4.8.3) hold then

$$[\psi] = [f] = [N] = 0 . \tag{4.8.5}$$

The <u>amplitude</u>, a, of an acceleration wave is defined as

$$a = [\dot{v}] . \tag{4.8.6}$$

Recall $\dot{(\ )}$ represents the material time derivative, i.e., $\dot{v} = \partial v/\partial t + v \partial v/\partial z$. Employing (3.1.1) and (4.1.1), the following jumps may be related to the amplitude a :

$$[\partial S/\partial z] = [\partial S/\partial t]/(-w) = -Sa/w^2 ,$$

$$[\partial v/\partial z] = [\partial v/\partial t]/(-w) = -a/w ,$$

$$\begin{aligned} [\partial p/\partial z] &= [\partial p/\partial t]/(-w) , \\ &= -\rho a(1-\delta(2+v/w)v/w) , \\ &= -a\epsilon S/w^2 \end{aligned} \qquad (4.8.7)$$

It therefore suffices to determine a to compute all jumps in first derivatives.

From relations (4.8.3) and (4.8.4) it can be seen that an acceleration wave corresponds to a discontinuity in slope in the v vs. t , S vs. t , and p vs. t graphs for a fixed site z . With reference to Fig. 4.6, there appear to be two distinct features of the natural pulse which are akin to these circumstances. The first is the front of the pulse which arises from the opening of the aortic valve and the second is the dicrotic notch or incisura which, it is now generally agreed, coincides with the closure of the valve.

Applying the jump operator to Eq. (4.8.1) yields

$$[\partial p/\partial t] = \epsilon [\partial S/\partial t] , \qquad (4.8.8)$$

which, when combined with Eqs. (4.8.7), determines

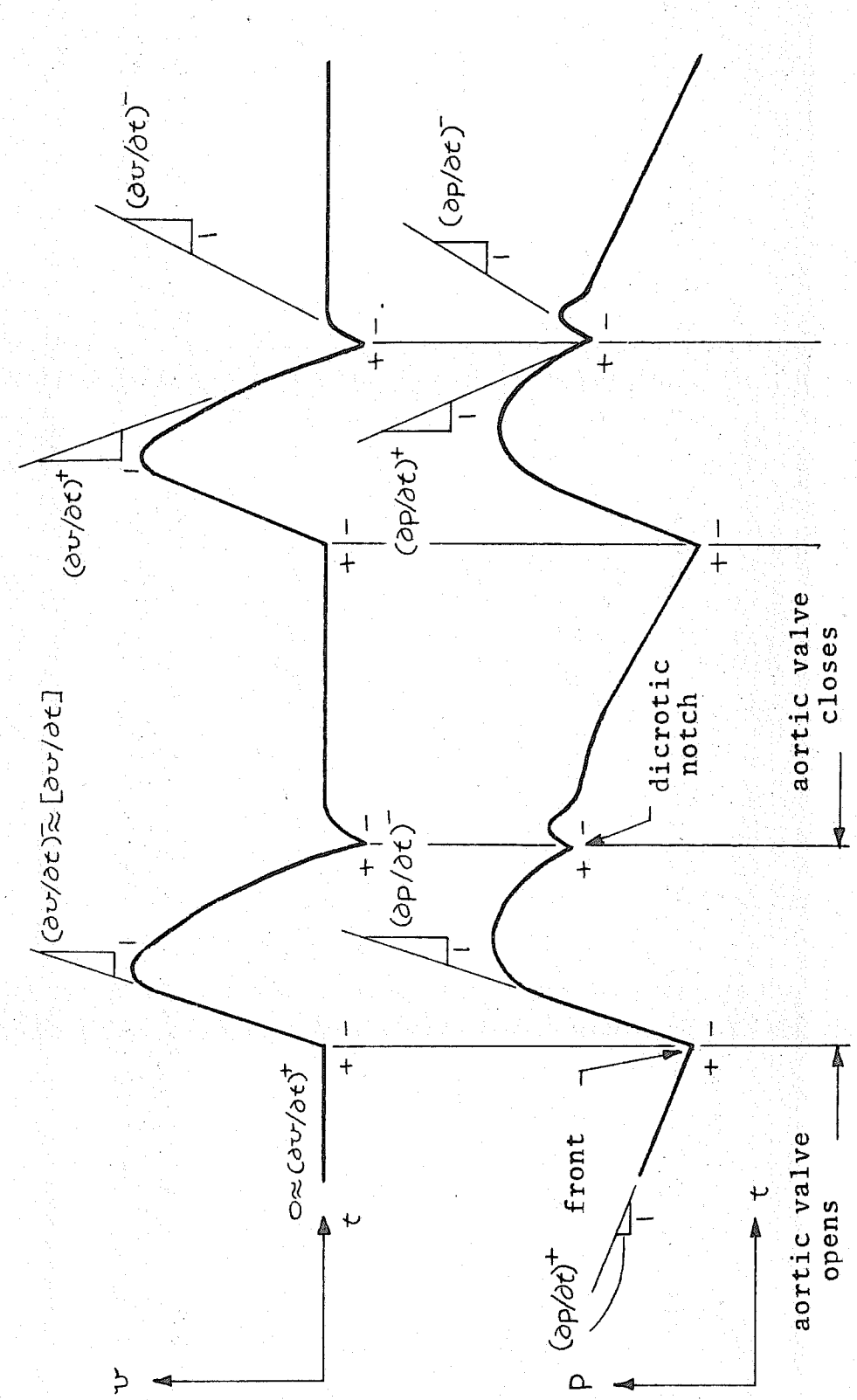

Figure 4.6 Acceleration waves associated with the front and dicrotic notch of the natural pulse in the ascending aorta of a dog measured about 4 cm above the aortic valve; redrawn after Falsetti et al. [29].

the expression for the relative velocity of an acceleration wave, namely

$$w^2 = \mathcal{E}S/\rho + \delta(u^2 - w^2) \qquad (4.8.9)$$

which is equivalent to Eq. (4.3.2) with the identification $\mathcal{E} \longrightarrow \tilde{P}_S$.

4.8b Evolution of the Amplitude. The equation governing the evolution of a can be derived by several procedures (see for example Coleman et al. [32], Lubliner [56], and Seymour and Varley [18]).

For quasi-linear hyperbolic systems, perhaps the most general technique goes as follows:

Recall that from Section 3.6, the velocities of acceleration waves are given by the eigenvalues of A , where

$$\frac{\partial U_i}{\partial t} + A_{ij}\frac{\partial U_j}{\partial z} + G_i = 0 . \qquad (4.8.10)$$

Differentiate Eq. (4.8.10) with respect to t and apply the jump operator:

$$\left[\frac{\partial^2 U_i}{\partial t^2}\right] + A_{ijk}\left[\frac{\partial U_j}{\partial z}\frac{\partial U_k}{\partial t}\right] +$$

$$+ A_{ij}\left[\frac{\partial^2 U_j}{\partial t\,\partial z}\right] + B_{ij}\left[\frac{\partial U_j}{\partial t}\right] = 0 , \qquad (4.8.11)$$

where $A_{ijk} = \partial^2 F_i/\partial U_j\,\partial U_k$, and $B_{ij} = \partial G_i/\partial U_j$.

Let $g = \partial U_i/\partial t$ in Eq. (3.4.5), and combine the result with Eq. (4.8.10):

$$\frac{d}{dt}\left[\frac{\partial U_i}{\partial t}\right] + (A_{ij} - u\,\delta_{ij})\left[\frac{\partial^2 U_j}{\partial z\,\partial t}\right] +$$

$$+ A_{ijk}\left[\frac{\partial U_j}{\partial z}\,\frac{\partial U_k}{\partial t}\right] + B_{ij}\left[\frac{\partial U_j}{\partial t}\right] = 0 \qquad (4.8.12)$$

Take the inner product of Eq. (4.8.12) with a left eigenvector, ℓ_i, of A_{ij}, and use Eq. (4.8.10) to eliminate $\partial U_j/\partial z$:

$$\ell_i \frac{d}{dt}\left[\frac{\partial U_i}{\partial t}\right] = \ell_i A_{ijk} C_{jl}\left\{\cdot\right.$$

$$\left.\cdot\left[\frac{\partial U_l}{\partial t}\,\frac{\partial U_k}{\partial t}\right] + G_l\left[\frac{\partial U_k}{\partial t}\right]\right\} \qquad (4.8.13)$$

$$- \ell_i B_{ij}\left[\frac{\partial U_j}{\partial t}\right],$$

where $C = A^{-1}$. Applying Eq. (4.8.13) to the present case, and making use of the relations (4.8.7), yields the amplitude equation (Bernoulli's equation):

$$\frac{da}{dt} = -\mu a + \beta a^2 \qquad (4.8.14)$$

The coefficients $\mu(t)$ and $\beta(t)$ for the general case of an acceleration wave propagating into an inhomogeneous region are contained in the Appendix, Section 4.8f. Some of the well known, important properties of solutions of Eq. (4.8.14) and some observations pertaining specifically to blood flow will be recapitulated here.

The coefficient of the linear term in Eq. (4.8.14), μ , is in general a complicated function of almost all parameters in the theory and also depends upon the state immediately in front of the wave. On the other hand β depends only upon the nonlinearities of the governing equations and the nonlinear elastic response of the vessel. From (4.8.38), it can be seen that it is independent of fluid viscosity, outflow, and the viscous properties of the wall. The sign of β tells a great deal about the nature of the solution.

It is observed for arteries that $\beta > 0$ at typical working pressures. Defining the local critical acceleration

$$\lambda = \mu / \beta \quad , \tag{4.8.15}$$

Eq. (4.8.14) can be rewritten as

$$\frac{da}{dt} = \beta a (a - \lambda) \; ; \tag{4.8.16}$$

then

$$\frac{d|a|}{dt} \begin{matrix} < \\ = \\ > \end{matrix} 0 \iff a \begin{matrix} < \\ = \\ > \end{matrix} \lambda \quad , \tag{4.8.17}$$

From the results of Rockwell [17] for the standard case, and the case of postcardiac arrest, one gets that at the front $\mu > 0$ and $a > \lambda > 0$. Therefore the last condition of (4.8.17) is the one that applies. Since

μ is increasing with distance away from the heart, Eq. (4.8.7) implies $[\partial p/\partial t]$ is increasing, which corresponds to the results of Rockwell [17]. Eq.(4.8.7) implies that

$$\frac{d}{dt}\left[\frac{\partial v}{\partial t}\right] \gtrless 0 \Leftrightarrow \frac{1}{a}\frac{da}{dt} \lessgtr \frac{\mu}{w}\frac{d}{dt}\left(\frac{w}{\mu}\right) . \quad (4.8.18)$$

Since $w=\mu$ for the case of postcardiac arrest, $d(w/\mu)/dt=0$ and therefore by (4.8.18) $d[\partial v/\partial t]/dt > 0$, which is consistent with Rockwell's results.

His data also indicate that $d[\partial v/\partial t]/dt > 0$ for the standard case which, as he points out, is inconsistent with results quoted by McDonald [46]. From (4.8.18) this is seen to correspond to $(\mu/w)d(w/\mu)/dt$ being too small. Many factors could change this situation.

The solution of Eq. (4.8.14) is

$$a(t) = \frac{e^{-\int_0^t \mu(\tau)d\tau}}{\left(\frac{1}{a(0)} - \int_0^t \beta(\tau) e^{-\int_0^\tau \mu(\sigma)d\sigma} d\tau\right)} . \quad (4.8.19)^*$$

Since for the natural pulse $a(0) > 0$, and with μ, β both > 0, the numerator and denominator of (4.8.19) are each monotonically approaching zero. Therefore if

$$\alpha = 1/\left(\int_0^{\bar{t}} \beta(t) e^{-\int_0^t \mu(\tau)d\tau} dt\right), \quad (4.8.20)$$

---

* a may equally well be considered a function of z by employing $t = y^{-1}(z)$

where $\bar{t}$ is the arrival time of the acceleration wave at the periphery of the systemic circulation, the following conditions exist:

(A) If $a(0)<\alpha$ then $a(t)$ remains bounded for $t\in[0,\bar{t})$.

(B) If $a(0)>\alpha$ then there exists a unique finite time t_∞ such that

$$a(0) = 1/\left(\int_0^{t_\infty} \beta(t)\, e^{-\int_0^t \mu(\tau)\,d\tau}\, dt\right), \qquad (4.8.21)$$

and $\lim a(t) = \infty$ as $t \uparrow t_\infty$. Thus α is a critical initial amplitude which determines whether or not a shock will form for a particular set of circumstances (see Fig. 4.7).

Under normal physiological conditions shocks do not form. An example of a case when one can form is aortic insufficiency, where the aortic valve fails to close properly and regurgitates (Fig. 4.8). The slope of the front for the incompetent case is much larger than under normal conditions. This causes $a(0)$ to increase to the point where t_∞ may be within $(0,\bar{t})$ and a shock-like situation will occur.

It is interesting to consider the formally linearized system (i.e., $\beta=0$); then

$$a(t) = a(0)\, e^{\int_0^t \mu(\tau)\,d\tau}. \qquad (4.8.22)$$

From (4.8.22) it can be seen that linearizing

(A) precludes shock formation in a finite time (distance) since $a(t)$ is bounded for all $t<\infty$ and

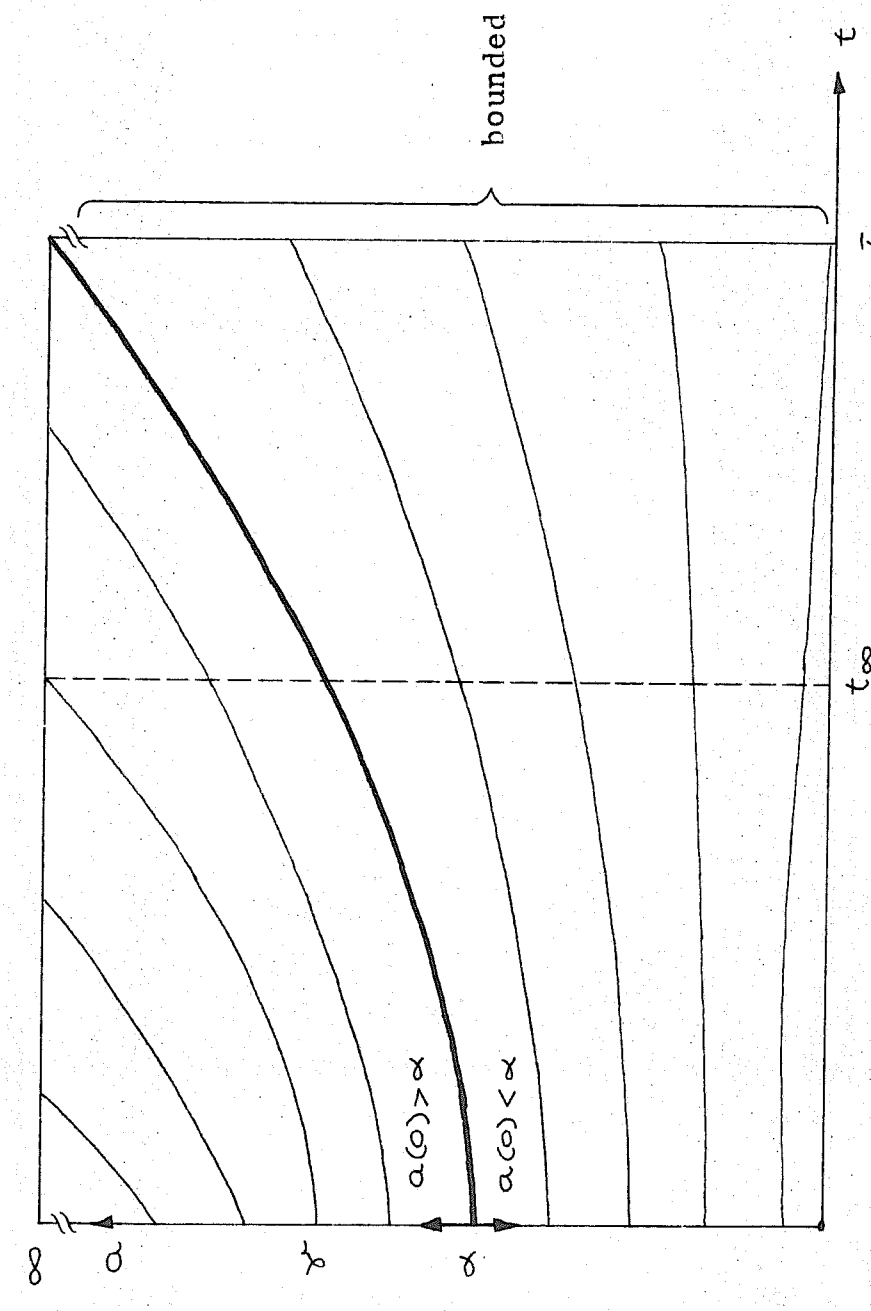

Figure 4.7 Critical initial amplitude (α) of acceleration waves in arteries. If $a(0) < \alpha$, a remains bounded. If $a(0) > \alpha$, a shock commences at t_∞ which depends upon the initial condition $a(0) = \gamma$.

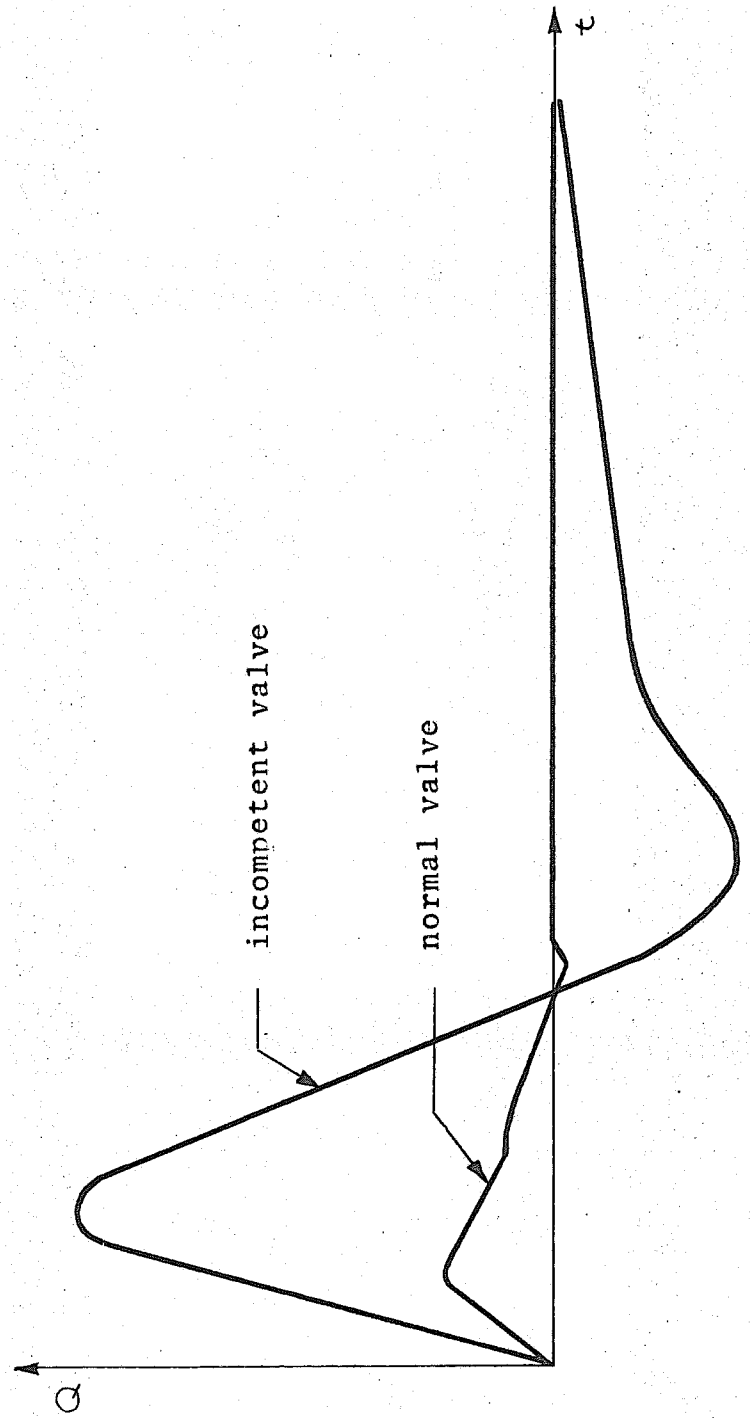

Figure 4.8 Volume flow (Q) at the aortic valve for normal and incompetent valves after Rockwell [17].

(B) implies that if $\mu > 0$, $a(t)$ decreases with increasing t, which contradicts the results of the non-linear analysis.

It is clear from (4.8.19) that (4.8.22) is a reasonable approximation only if $a(0) \ll \alpha$.

4.8c Résumé of Previous Work. It seems Barnard et al. [8] were the first to apply acceleration-wave theory to the one-dimensional theory of blood flow. They noted in their study, using physiologically realistic data, that the steepening of the pressure pulse and flattening of the velocity pulse were consistent with the one-dimensional theory. They established the amplitude equation for the case of an elastic, homogeneous vessel ($p = \tilde{p}(S)$), with no outflow ($\psi = 0$) and a front propagating into a region of steady flow, i.e., one in which the $\partial(\cdot)/\partial t$ terms in (3.1.1) and (4.1.1) are set equal to zero. The solution of Eq. (4.8.14) was not obtained in this work.

Seymour and Varley [18] have established Eq. (4.8.14) for the case of Eqs. (3.1.1), (4.1.1) and (4.8.1) with $\psi = f = \delta = N = 0$, where they assumed that $\omega/\mu \sim 1$, t is absent as a dependent variable of $\mathcal{E}$ and H, and that the acceleration front travels into a region of steady flow. With these they are able to write

$$\mu = \mu\left(L_r^{-1} + \tfrac{1}{2}\left(L_s^{-1} + L_t^{-1}\right)\right), \qquad (4.8.23)$$

where

$$L_r = -2\mu(H_p + H_s/\varepsilon)^{-1} \quad , \qquad (4.8.24)^*$$

is a measure of the tube rate dependence,

$$L_s = \left(\frac{1}{w}\frac{dw}{dz}\right)^{-1} \quad , \qquad (4.8.25)$$

is a measure of the axial changes in stiffness of the wall and

$$L_\epsilon = \left(\frac{1}{S}\frac{dS}{dz}\right)^{-1} \quad , \qquad (4.8.26)$$

is a measure of taper. This is a tremendous simplification of the μ for the general case and roots out three effects of interest. The β that they obtain is simplified only to the extent that the terms involving δ are absent. They present the solution to Eq. (4.8.14) and discuss the local critical acceleration (4.8.15) and shock formation. They reiterate the observation of Barnard et al. [8] by noting the relation (4.8.7), when differentiated with respect to z, yields a result that is qualitatively consistent with physiological observations of the front of the cardiac pulse, namely

$$\frac{d}{dz}[\partial p/\partial t] = \rho\left\{\frac{dw}{dz}[\partial v/\partial t] + w\frac{d}{dz}[\partial v/\partial t]\right\} \quad , \qquad (4.8.27)$$

---

* See the Appendix for notational definitions.

where

$$\begin{aligned} w &> 0 , \\ [\partial v/\partial t] &> 0 , \\ \frac{d}{dz}[\partial p/\partial t] &> 0 , \\ \frac{d}{dz}[\partial v/\partial t] &< 0 , \\ \frac{dw}{dz} &> 0 . \end{aligned} \tag{4.8.28}$$

Seymour [20], in commenting upon Rudinger's article [19], discussed specific cases of the amplitude equation and emphasized the critical initial acceleration (4.8.20) for shock formation.

The local and global properties of Eq. (4.8.14), discussed by Seymour and Varley [18] and Seymour [20], have been dealt with in generality by Bailey and Chen [57,58]

4.8d Asymptotic Formulas. Bailey and Chen [58] have derived several asumptotic formulas for Eq. (4.8.14) which are recapitulated for the present case:

(A) If $a(0)>\alpha$, then as $t \uparrow t_\infty$

$$a(t) \approx \frac{1}{\beta(t_\infty)(t-t_\infty)} . \tag{4.8.29}$$

(B) If $a(0)>\alpha$, then shock formation time is

$$t_\infty \approx \frac{1}{a(0)\beta(0)} \quad \text{as} \quad a(0) \uparrow \infty . \tag{4.8.30}$$

The corresponding formula for shock formation distance

is

$$z_\infty \approx \frac{u(0)}{a(0)\beta(0)} \quad \text{as} \quad a(0) \uparrow \infty . \tag{4.8.31}$$

Combining (A) and (B),

$$a(t) \approx \frac{1}{\beta(1/a(0)\beta(0))\,(t - t_\infty)} , \tag{4.8.32}$$

as $t \uparrow t_\infty$ and $a(0) \uparrow \infty$, where t_∞ is given by (4.8.30).

(C) If $a(0) < \alpha$, then

$$a(t) \approx \frac{a(0)\, e^{-\int_0^t \mu(\tau)\,d\tau}}{\left(1 - \frac{a(0)}{\alpha}\right)} \tag{4.8.33}$$

at $t \uparrow t_d$ or $a(0) \downarrow 0$. For the latter case it can be seen that the linearized solution (4.8.22) becomes a good approximation. Parts (A) and (B) govern the asymptotic behavior of strong acceleration waves $(a(0) > \alpha)$ whereas (C) corresponds to weak ones $(a(0) < \alpha)$.

Formula (4.8.31) permits the estimation of whether or not a shock will form within physiologically meaningful distances. As an example of its application let it be evaluated for the front of the cardiac pulse where $u(0) \approx 0$. For simplicity, assume $\delta = 0$ and $S = \tilde{S}(\rho, z, t)$ in place of (4.8.7). Then it follows that $\partial\tilde{S}/\partial\rho = 1/\varepsilon(\rho, z, t)$ and using (4.8.36), (4.8.47) and (4.8.48) gives

$$\beta = \frac{1}{2c}(3 + S\varepsilon_\rho) = \frac{1}{c}\left(1 + \rho c \frac{\partial c}{\partial \rho}\right) , \tag{4.8.34}$$

which when substituted in (4.8.31) yields

$$\gamma_\infty = \frac{c(0)^2}{a(0)\left(1 + \rho c(0) \frac{\partial c}{\partial p}(0)\right)} \qquad (4.8.35)$$

This result with $a(0) \approx ((\partial p/\partial \epsilon)(\bar{\sigma}))/\rho c(0)$ from (4.8.7) was originally derived by Rudinger [19], who used a power-series expansion technique and invoked several simplifications in the basic equations.

4.8e The Dicrotic Notch. The origin of the dicrotic notch is the abrupt closing of the aortic valve in diastole. This causes a discontinuity in the slope of the volumetric flow vs. time curve and thus an acceleration wave commences, Fig. 4.6. With this interpretation, the explanation prevalent in physiology texts (e.g., Steen and Montagu, [59]) that the dicrotic notch is attributable to backflow may be dismissed. What is essential is that the valve closes rapidly enough to cause a discontinuous slope in the volumetric flow vs. time curve. This also explains why no dicrotic notch is visible in the case of aortic insufficiency. Here the valve never closes properly and the dicrotic limb of the pulse is initially and persistently smooth. These observations are consistent with the numerical studies of Rockwell [17]. The existence of the dicrotic wave seems to be another matter.

4.8f Appendix. The functions μ and β for the general case of an acceleration wave propagating into an arbitrary state are:

$$\mu = \gamma_3/\gamma_1^* \quad , \qquad \beta = -\gamma_2^*/\gamma_1^* \quad , \tag{4.8.36}$$

$$\gamma_1^* = -\left(\frac{u+v}{w} + \eta\right) + \delta\frac{v^2}{w^2} \quad , \tag{4.8.37}$$

$$\gamma_2^* = \frac{u}{w^2}\left\{3 + S\eta\left(\varepsilon_S/\varepsilon + \varepsilon_P\right) + 2\delta\left(1 - \frac{v}{w} - \frac{1}{2}\frac{v^2}{w^2}\right)\right\} \tag{4.8.38}$$

$$\gamma_3 = \omega_1 + \delta\omega_2 \quad , \tag{4.8.39}$$

$$\begin{aligned}\omega_1 = -\Big\{&\frac{vw}{uS}\frac{d}{dt}\left(\frac{uS}{w^2}\right) + \frac{d}{dt}\left(\frac{u}{w}\right) + \frac{(w-v)}{S}\zeta \\ &- \frac{v}{S}\xi + \frac{1}{S}\left(uS_3^+ - S_\epsilon^+\right) + \frac{2}{w}\left(uv_3^+ - v_\epsilon^+\right) + \\ &+ \frac{1}{u}\frac{d}{dt}(u\eta) - \frac{u}{S}\left(1 - \frac{v}{w}\right)(\nu + N)\Big\} + \\ &+ \frac{\eta}{\varepsilon}\Big\{2S_\epsilon^+\left(\varepsilon_S + \varepsilon\varepsilon_P\right) + \varepsilon_\epsilon + H_S + \\ &+ (\varepsilon H)_P\Big\} \quad ,\end{aligned} \tag{4.8.40}$$

$$\omega_2 = \frac{v^2}{uS}\frac{d}{dt}\left(\frac{uS}{w^2}\right) + 2\frac{v}{S}\zeta + \frac{v^2}{w^2}\frac{u}{S}S_3^+ + 2\frac{u}{w}\left(\frac{v}{w} - 1\right)v_3^+ + \frac{2}{w}v_\epsilon^+ - \frac{v}{wS}\left(2 + \frac{v}{w}\right)S_\epsilon^+ \tag{4.8.41}$$

In (4.8.36) - (4.8.41) the following notations have been used:

$$\varkappa = \varepsilon S/\rho\omega^2 \ , \tag{4.8.42}$$

$$\varepsilon_s = D_1\varepsilon \ , \quad \varepsilon_p = D_2\varepsilon \ , \quad \varepsilon_t = D_4\varepsilon \ , \tag{4.8.43}$$
$$H_s = D_1 H \ , \quad H_p = D_2 H \ ,$$

$$\zeta a = [\partial\psi/\partial t] \ , \tag{4.8.44}$$

$$\xi_j a = [\partial N/\partial t] \ , \tag{4.8.45}$$

$$g_z^+ = g_z^+(t) = \frac{\partial g}{\partial z}(z,t)\Big|_{z=y^+(t)} \ ,$$
$$g_t^+ = g_t^+(t) = \frac{\partial g}{\partial t}(z,t)\Big|_{z=y^+(t)} \ , \tag{4.8.46}$$

where g in (4.8.46) represents S, v or p . Considerable simplification in (4.8.36) - (4.8.41) is engendered for particular circumstances. For instance, suppose the flat-profile theory is employed. Then $\varkappa = 1, S = N = \xi_j = 0$, and the contributions of Eq. (4.1.1) to the ψ and ζ terms in (4.8.40) are also equal to zero and thus:

$$\gamma_1^* = -2\frac{\mu}{c} \ , \tag{4.8.47}*$$

$$\gamma_2^* = \frac{\mu}{c^2}\{3 + S(\varepsilon_s/\varepsilon + \varepsilon_p)\} \ , \tag{4.8.48}$$

---

* Recall $\omega = c$ in the flat-profile case.

$$\gamma_3 = \omega_1 = -\left\{ \frac{vc}{\mu S}\frac{d}{dt}\left(\frac{\mu S}{c^2}\right) + \frac{d}{dt}\left(\frac{\mu}{c}\right) + \frac{c}{S}\zeta + \frac{1}{S}\left(\mu S_z^+ - S_t^+\right) + \frac{2}{c}\left(\mu v_z^+ - v_t^+\right) + \frac{1}{\mu}\frac{d\mu}{dt}\right\} + \frac{1}{\varepsilon}\left\{2S_t^+\left(\varepsilon_s + \varepsilon\varepsilon_p\right) + \varepsilon_t + H_s + (\varepsilon H)_p\right\} \tag{4.8.49}$$

As another example, assume a quiescent state in front of the wave defined by

$$\begin{aligned} v &= 0 , \\ S &= S(z) , \\ p &= \text{constant} . \end{aligned} \tag{4.8.50}$$

These imply

$$\begin{aligned} u &= w = c , \\ S_t^+ &= v_z^+ = v_t^+ = p_z^+ = p_t^+ = 0 , \\ H &= \psi = 0 , \\ \frac{dS}{dt} &= c\,S_z^+ , \qquad \eta = 1 . \end{aligned} \tag{4.8.51}$$

The γ_α's become

$$\gamma_1 = -2 , \tag{4.8.52}$$

$$\gamma_2 = \frac{1}{c}\left\{3 + 2\delta + S\left(\varepsilon_s/\varepsilon + \varepsilon_p\right)\right\}, \tag{4.8.53}$$

$$\gamma_3^* = \omega_1 = -\left\{ \frac{c}{S}\zeta + \frac{1}{S}\frac{dS}{dt} + \frac{1}{c}\frac{dc}{dt} - \frac{N}{S} \right\} + \frac{1}{\varepsilon}\left\{ \varepsilon_\epsilon + H_s + \varepsilon H_p \right\} . \qquad (4.8.54)$$

For the flat-profile theory the δ term in (4.8.53) and the N term in (4.8.54) are absent.

With (4.8.36) - (4.8.41), an acceleration wave solution for the general theory contained in Eqs. (3.1.1) and (4.1.1) and (4.8.1) can be constructed given any set of circumstances. For most problems of practical interest numerous simplifications can be made. Various special cases have been derived in Barnard et al. [8], Seymour and Varley [18] and Seymour [20].

V. NUMERICAL SIMULATION OF THE ONE-DIMENSIONAL THEORIES

5.1 Introduction

When the second-order viscous term is omitted in the momentum balances (Eqs. (3.1.2) or (4.1.1)), the flat or no-slip profile theories result in a hyperbolic system of balance laws, cf. Eq. (3.2.1). First-order hyperbolic systems are of great interest in many physical problems and have been studied extensively in recent years in the finite difference literature (see for example Richtmyer and Morton [60] and Kreiss and Oliger [61]). Despite this, the practical problem of computing a solution is not a closed issue by any means. In the present chapter, some numerical aspects particularly relevant to the one-dimensional theory of blood flow are considered.

5.2 Lax-Wendroff and Abarbanel-Goldberg Algorithms

The Lax-Wendroff (LW) and Abarbanel-Goldberg (AG) algorithms will be described since they have been employed for the analyses herein. The model equation is Eq. (3.2.1).

The LW two-step scheme (see Richtmyer-Morton [60]) is contained in the following formulas:

$$U_{j+1/2}^{n+1/2} = \frac{1}{2}(U_j^n + U_{j+1}^n) - \frac{\lambda}{2}(F_{j+1}^n - F_j^n) - \frac{k}{4}(G_j^n + G_{j+1}^n) \quad , \quad \lambda = \frac{k}{h} \, , \tag{5.2.1}$$

$$\begin{cases} U_j^{n+1} = U_j^n + CU_j^n , \\ CU_j^n = -\lambda \left(F_{j+1/2}^{n+1/2} - F_{j-1/2}^{n+1/2} \right) \\ \qquad\qquad - \frac{k}{2} \left(G_{j+1/2}^{n+1/2} + G_{j-1/2}^{n+1/2} \right) \end{cases} \tag{5.2.2}$$

where the typical finite difference notation is adopted, viz., U_j^n is the value of U at the spatial mesh point j and temporal mesh point n (see Fig. 5.1);

$F_{j+1/2}^{n+1/2} = F\left(U_{j+1/2}^{n+1/2}\right)$, etc.; and the equations are to be interpreted in terms of each component of Eq. (3.2.1). The predictor, Eq. (5.2.1), is spatially centered at point p (see Fig. 5.1), and the central differences and means result in second-order accuracy in h ; the forward difference formula for the time derivative results in only first-order accuracy in k . The corrector, Eq. (5.2.2), is centered in space and time and uses only central differences and mean values, hence is of second-order accuracy in both h and k . When Eqs. (3.2.1) are linear and $\underset{\sim}{G} = \underset{\sim}{0}$, the scheme reduces to the Lax-Wendroff one-step scheme (see [60]) which is of full second-order accuracy. For the Cauchy problem the stability limit of the scheme is given by the Courant-Friedrichs-Levy (CFL) criterion

$$\lambda \leq 1/a , \tag{5.2.3}$$

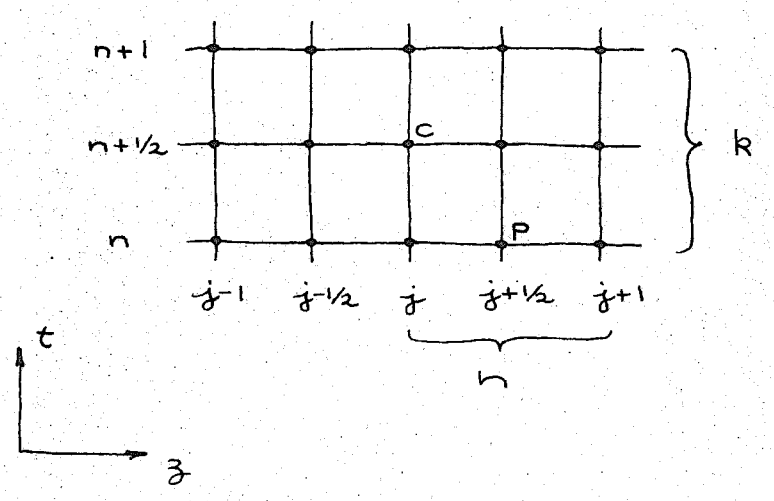

Figure 5.1

where $\mu = \max_{i=1,2}(|\mu_i|)$ and μ_i are the eigenvalues of A, taken over all spatial mesh points. For the initial-boundary value problem the same stability limit is achieved if the boundary data are treated in appropriate fashion (see Kreiss and Oliger [61]). An example of such a technique is given as follows:

Consider the mesh at the left boundary (see Fig. 5.2). Initial data will be given along $t=0$, $x \in [0,L]$, i.e., at mesh points 2,3,...; and one boundary datum will be given at points A,B,... . To compute the remaining variable at A, using Eqs. (5.2.1) and (5.2.2), one needs both data at point 1. They can be computed by passing an n^{th} degree interpolatory polynomial through points $2,3,\ldots,n+2$, and computing the extrapolated values at 1. The accuracy of the resulting approximation is of order h^{n+1}. Thus the second-order spatial accuracy of the scheme is maintained if a polynomial of degree ≥ 1 is employed.

The Abarbanel-Goldberg algorithm [62] was conceived to improve upon the Lax-Wendroff algorithm for shock-like phenomena. It changes the fundamental error term (see [60], p.332) of the LW scheme from a dispersive term, which manifests itself in the form of high-frequency oscillations about discontinuities, to a dissipative term, which results in smoothed shock profiles. The scheme is an iterative one which uses the LW one-step scheme for its first iteration. In the

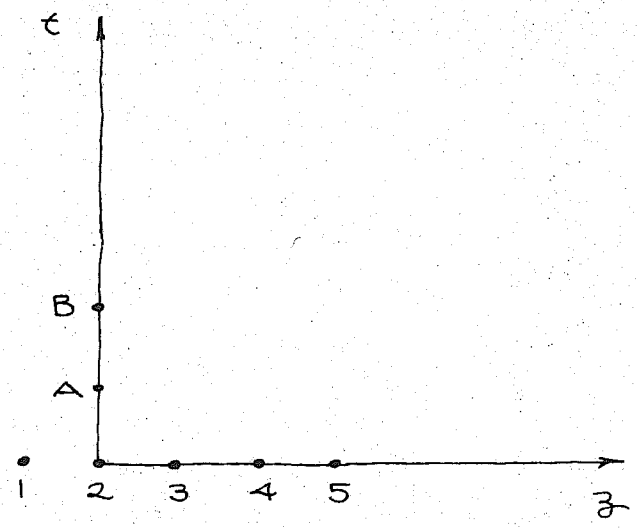

Figure 5.2

present work this approach has been modified to use the LW two-step scheme for the first iteration. Strictly speaking, this results in a reduction in accuracy of the method to $O(k) + O(h^2)$, however, the saving in storage, increased computational efficiency, and the fact that the procedure is still $O(k^2) + O(h^2)$ for the linear problem, is felt to outweigh the loss in accuracy. Abarbanel and Goldberg have recommended only one iteration be used beyond the basic LW solution. Following this recommendation, the scheme, as employed here can be written

$$U_j^{n+1,2} = U_j^{n+1} + \Theta\left[CU_j^{n+1,1} - CU_j^n\right], \qquad (5.2.4)$$

where U_j^{n+1} and CU_j^n are given by Eqs. (5.2.2), and $CU_j^{n+1,1}$ is given by Eq. $(5.2.2)_2$ evaluated using Eq. (5.2.1) with U_j^{n+1} instead of U_j^n. Θ is a real number which affects the amount of dissipation and the stability limit of the algorithm. Goldberg [63] has established the stability criterion

$$\lambda \leq 1/(a\sqrt{2\Theta}) \quad \text{for} \quad \Theta \in [1/6, 1/2]. \qquad (5.2.5)$$

Thus for this range of Θ, a larger time step can be employed than that indicated by the CFL criterion. Abarbanel and Goldberg have recommended the value $\Theta = .2$, for which time steps may be taken 1.58 times as large

as specified by (5.2.3). Unless otherwise indicated this has been done here.

5.3 Consistency with Weak Forms and Shock Stability

For purposes of shock analysis, it is important that one knows under what circumstances a numerical algorithm is faithful to a particular weak form of the equations. One of the reasons for selecting the LW algorithm is that it often is faithful to the weak form in which the governing equations are written. This is just a rule of thumb since exceptions have been noted (e.g., [64]). The following examples suggest that, for the equations of blood flow, the LW scheme is consistent.

The equations to be analyzed are:

$$\frac{\partial S}{\partial t} + \frac{\partial Sv}{\partial z} = 0 \quad ,$$

$$\frac{\partial v}{\partial t} + \frac{\partial}{\partial z}\left(\frac{v^2}{2} + \frac{S^2}{18}\right) = 0 \quad , \quad \text{(vel. form)} \quad , \qquad (5.3.1)$$

$$\frac{\partial Sv}{\partial t} + \frac{\partial}{\partial z}\left(Sv^2 + \frac{S^3}{27}\right) = 0 \quad , \quad \text{(mom. form)} \quad .$$

This corresponds to the constitutive equation $p = \rho S^2/18$. The Cauchy data are given by

$$S_0(z) = \begin{cases} 3 & z < 0 \\ 1 & z > 0 \end{cases}$$

$$v_0(z) = \begin{cases} 2/3 & z < 0 \\ 0 & z > 0 \end{cases} \qquad (5.3.2)$$

The exact solutions are plotted at $t=15$ in Fig. 5.3 along with the results for the LW two-step algorithm. In the numerical computation $k=1/25$ and λ was taken to be .6, which corresponds to the CFL criterion. Note that the velocity and momentum forms produce different exact solutions due to the presence of a shock wave. In the latter case the initial data does not satisfy the shock relations, thus the discontinuity splits into a shock and a simple wave. Aside from the overshoot at the shock front, the numerical results are seen to be in close agreement with the exact solutions. Thus for this example, at least, the LW algorithm is faithful to the weak forms of the equations.

The preceding examples involve a stable shock according to the notions of Sections 3.8, 3.9 and 4.5. It is of interest to see what the algorithm does when unstable initial data are employed.

To this end, consider the Cauchy problem:

$$S_0(z) = \begin{cases} 1 & z<0 \\ 3 & z>0 \end{cases} \qquad (5.3.3)$$

$$w_0(z) = \begin{cases} 0 & z<0 \\ 2/3 & z>0 \end{cases}$$

The time step k and λ are the same as for the preceding problem. The exact and numerical solutions are plotted in Fig. 5.4. This time both the velocity and momentum forms have the same exact solution (a

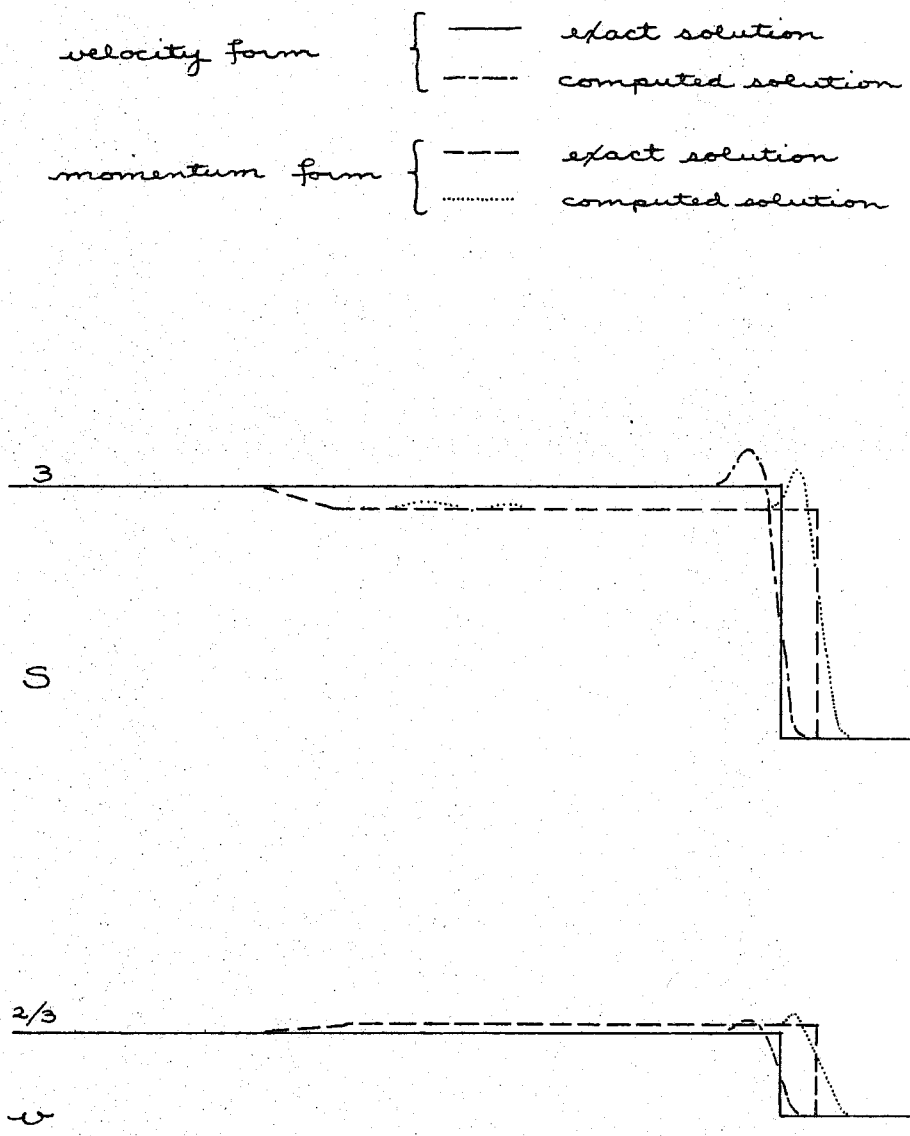
velocity form
exact solution
computed solution
momentum form
exact solution
computed solution
3
S
1
2/3
v
0

Figure 5.3

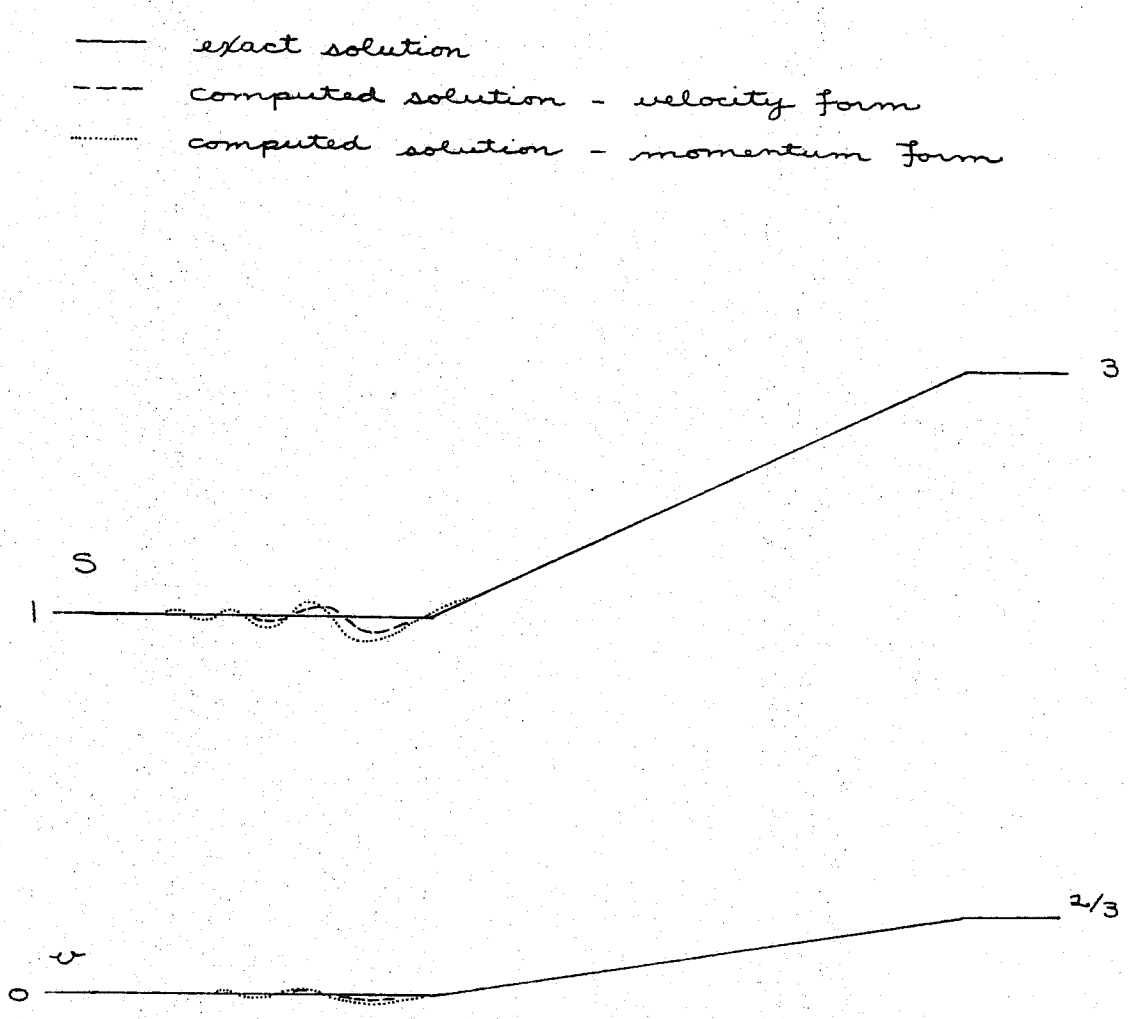
exact solution
computed solution - velocity form
computed solution - momentum form
3
S
1
2/3
v
0

Figure 5.4

simple wave) and the numerical results reflect this.

5.4 Boundary Condition Study

In the course of evaluating the algorithms, an analysis was performed which indicates the difficulties encountered when discontinuities impinge upon boundaries. It is clear that when such a situation occurs, the technique of using polynomial extrapolation for the point outside the boundary is no longer valid, due to the lack of smoothness of the solution. In fact, for problems of this class, the higher-order the polynomial used, the worse the solution gets!

The problem consists of the first-order form of the wave equation

$$\begin{aligned} \frac{\partial S}{\partial t} &= \frac{\partial v}{\partial z} \quad , \\ \frac{\partial v}{\partial t} &= \frac{\partial S}{\partial z} \quad , \end{aligned} \tag{5.4.1}$$

on $\mathcal{D} = \{(z,t) \mid z \in [0,10],\ t \geq 0\}$, with initial and boundary data given by

$$\left.\begin{aligned} S_0(z) &= 0 \\ v_0(z) &= 1 \end{aligned}\right\} \quad z \in (0,10)$$

$$\left.\begin{aligned} v(0,t) &= 0 \\ S(10,t) &= 0 \end{aligned}\right\} \quad t \geq 0 \quad . \tag{5.4.2}$$

The exact solution, up to $t=20$, consists of the three constant zones, as illustrated in Fig. 5.5. This problem has a physical interpretation, namely, a linear elastic rod, traveling at constant velocity, and impacting a rigid wall at $t=0$.

Numerical computations were made for both the LW and AG algorithms. The data for points outside the boundary were computed by polynomial extrapolation, i.e., with respect to Fig. 5.2,

$$
\begin{aligned}
&\text{(first-order)} && S_1^n = S_2^n \\
& && v_1^n = 0 \\
&\text{(second-order)} && S_1^n = 2S_2^n - S_3^n \\
& && v_1^n = -v_3^n \qquad (5.4.3) \\
&\text{(third-order)} && S_1^n = 3(S_2^n - S_3^n) + S_4^n \\
& && v_1^n = -3v_3^n + v_4^n \\
&\text{(fourth-order)} && S_1^n = 4(S_2^n + S_4^n) - 6S_3^n - S_5^n \\
& && v_1^n = 4v_4^n - 6v_3^n - v_5^n
\end{aligned}
$$

and analogously at $z=10$.

Results are presented in Fig. 5.6 for the third-order boundary extrapolation which illustrate oscillatory behavior along the left boundary $z=0$. The AG algorithm represents a considerable improvement over LW in this case, however the results along $z=0$ are still not very good. For this example the boundary

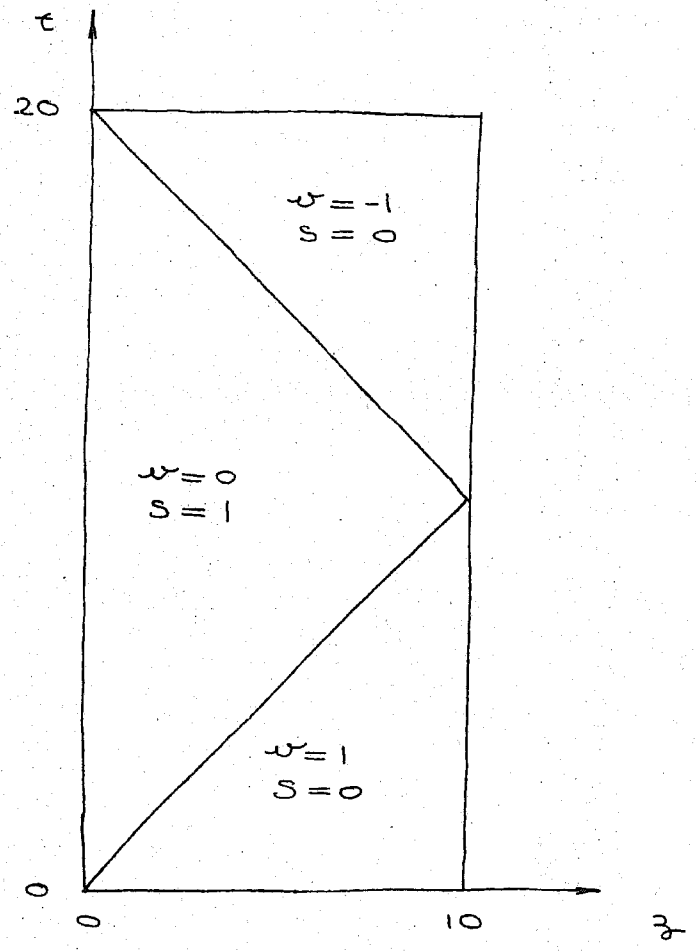

Figure 5.5

$h = .5$, $k = .25$, third-order boundary conditions

——— exact solution

– – – – LW

..... AG

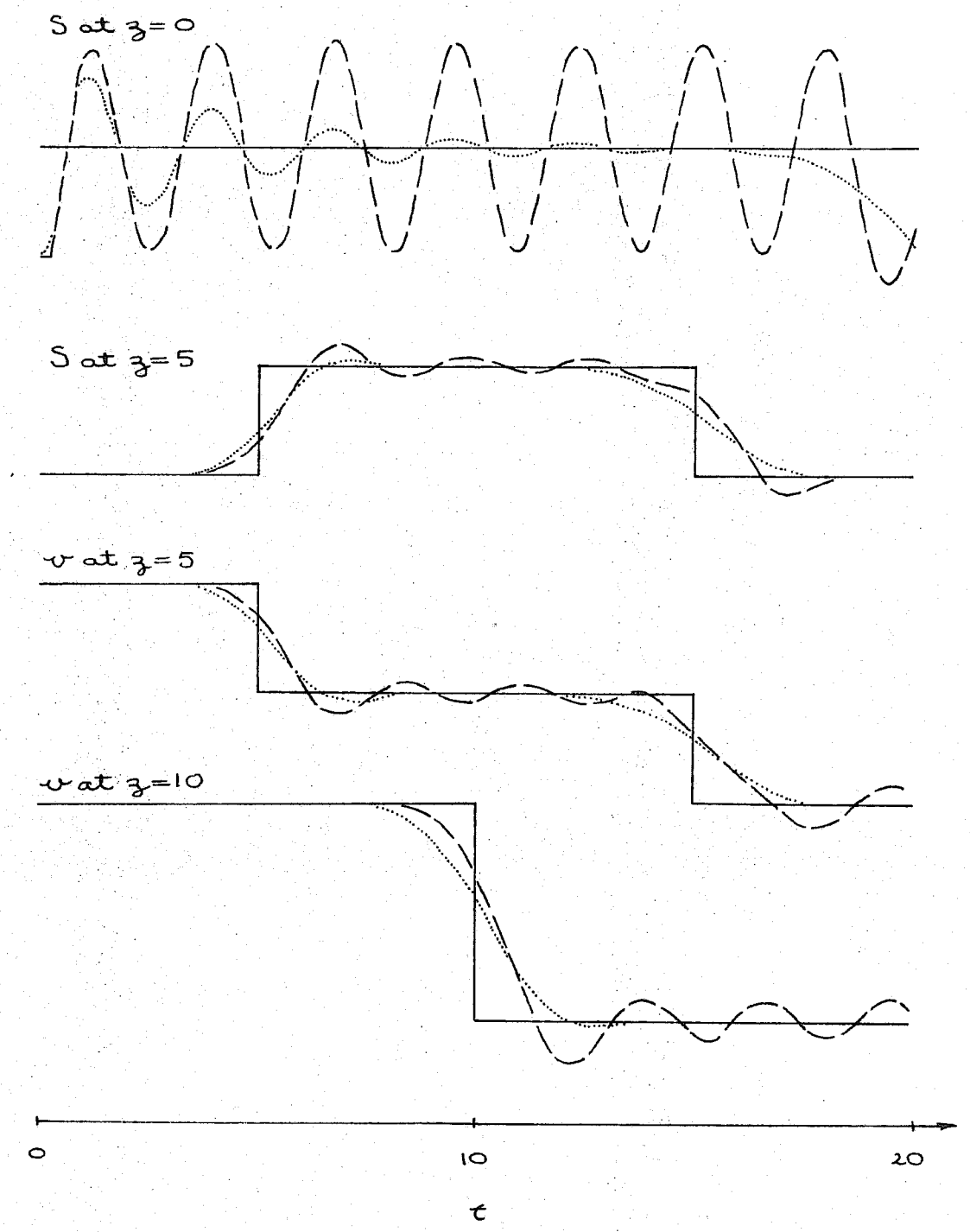

Figure 5.6

oscillations have not been detrimental to the solution in the interior.

Refining the mesh causes the LW results to blow up, Fig. 5.7, whereas the AG results are improved noticeably along the left boundary.

Lowering the order of the boundary extrapolation stabilizes the solution, Fig. 5.8. However, the location of wave fronts for all cases (LW, first and second-order; AG, first-order) in this example are slightly off.

A final example indicates that the AG algorithm gives the appropriate location for wave fronts in all cases except first-order boundary extrapolation, Fig. 5.9. The results are almost identical away from the left boundary, for second through fourth-order extrapolation. At the left boundary, the fourth-order case exhibits rapid oscillations, whereas in the first through third-order cases, the oscillations are damped out quickly.

Based upon the above examples, second-order boundary conditions seem to be the most appropriate when discontinuities impinge upon the boundaries.

5.5 Comparison of One-Step and Two-Step LW Algorithms

A calculation was performed to see if any differences could be noted between the one-step and

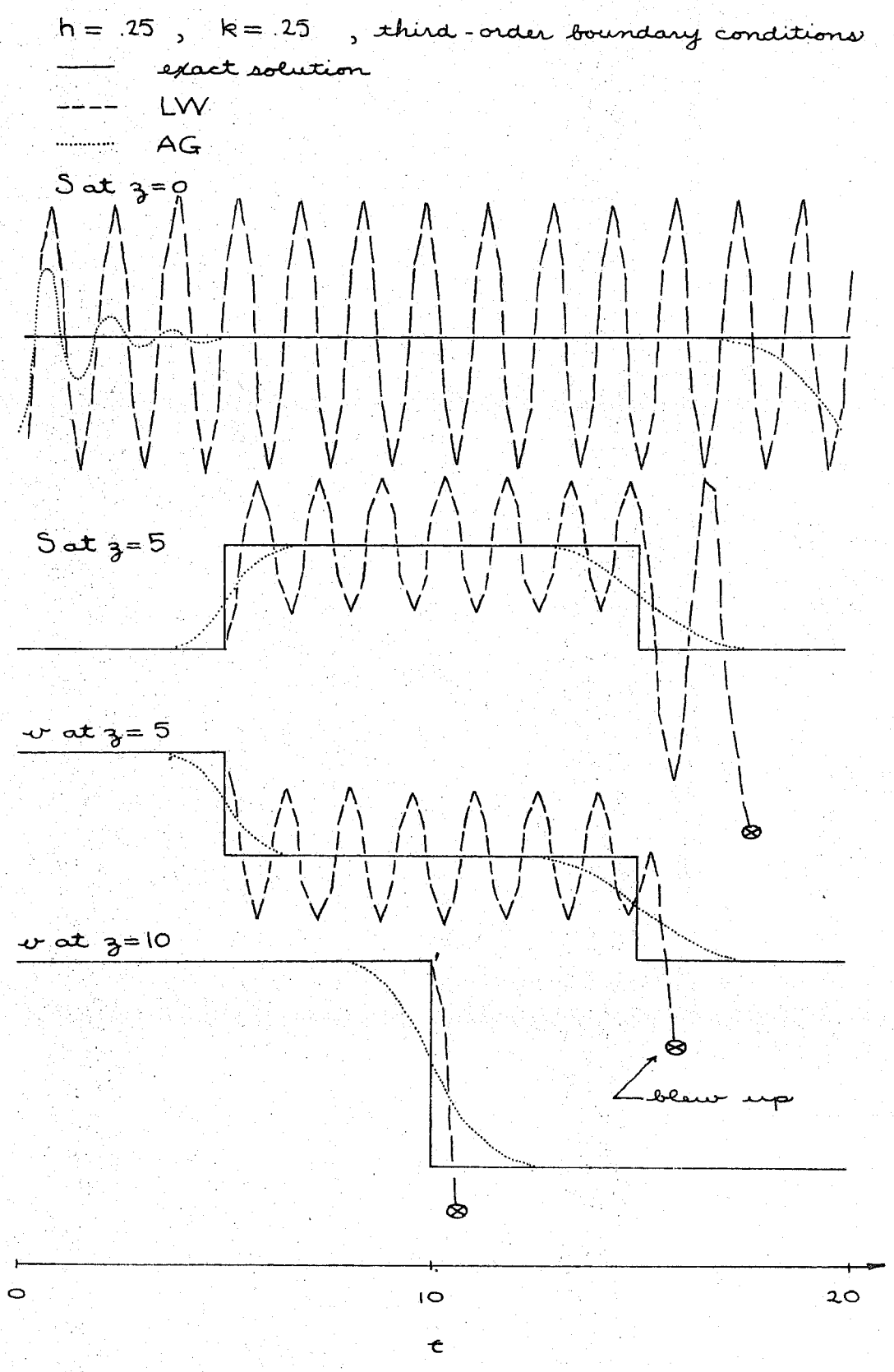
h = .25 , k = .25 , third-order boundary conditions
exact solution
LW
AG
S at z=0
S at z=5
v at z=5
v at z=10
blew up
0
10
20
t

Figure 5.7

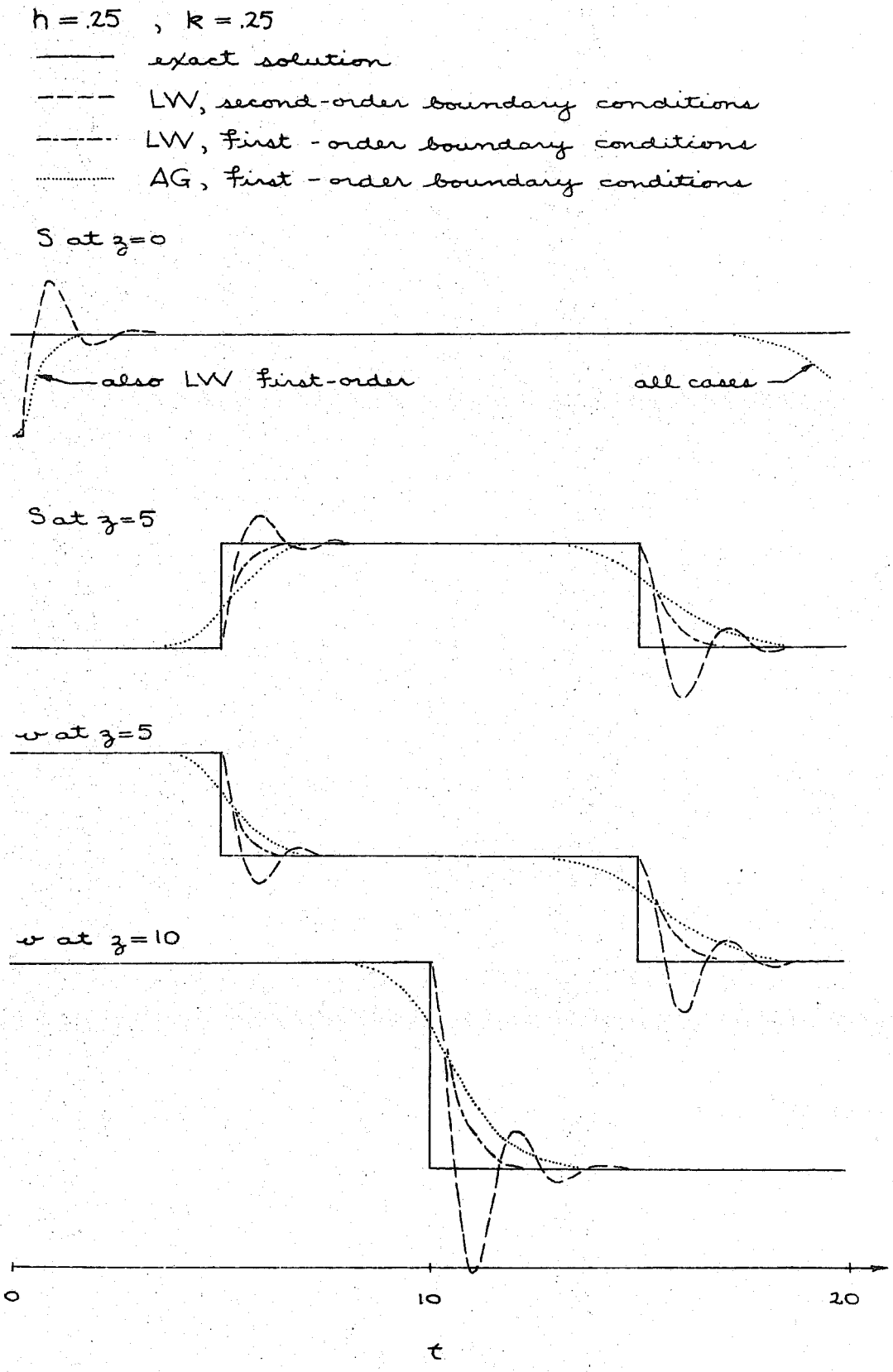
h = .25 , k = .25
exact solution
LW, second-order boundary conditions
LW, first-order boundary conditions
AG, first-order boundary conditions
S at z=0
also LW first-order
all cases
S at z=5
v at z=5
v at z=10
0
10
20
t

Figure 5.8

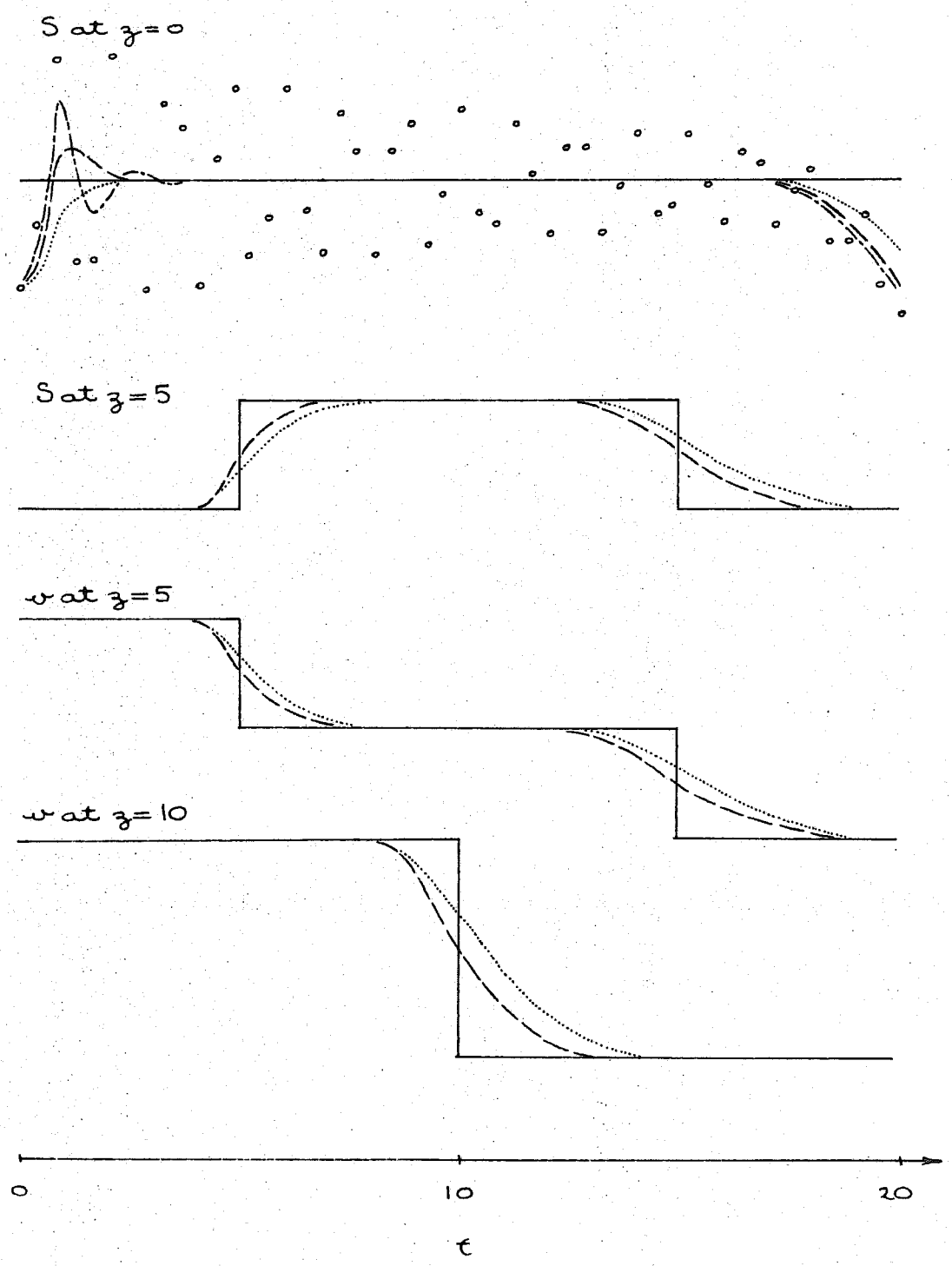
h = .25 , k = .4 , AG algorithm
exact solution
first-order boundary conditions
second-order, third-order, fourth-order
S at z = 0
S at z = 5
v at z = 5
v at z = 10
0
10
20
t

Figure 5.9

two-step LW algorithms. This amounts to differencing in non-conservation and conservation form, respectively.

The equations analyzed are:

$$\begin{aligned} &\frac{\partial S}{\partial t} + S\frac{\partial v}{\partial z} + v\frac{\partial S}{\partial z} = 0 , \\ &\frac{\partial v}{\partial t} + v\frac{\partial v}{\partial z} + \frac{\partial S}{\partial z} = 0 , \end{aligned} \tag{5.5.1}$$

(i.e., $p = \rho S$). The two "equivalent" systems of conservation laws are:

$$\begin{aligned} &\text{(I)} \quad \text{(vel. form)} \quad \frac{\partial S}{\partial t} + \frac{\partial Sv}{\partial z} = 0 , \\ &\qquad\qquad \frac{\partial v}{\partial t} + \frac{\partial}{\partial z}\left(\frac{v^2}{2} + S\right) = 0 , \\ &\text{(II)} \quad \text{(mom. form)} \quad \frac{\partial S}{\partial t} + \frac{\partial Sv}{\partial z} = 0 , \\ &\qquad\qquad \frac{\partial Sv}{\partial t} + \frac{\partial}{\partial z}\left(Sv^2 + \frac{S^2}{2}\right) = 0 \end{aligned} \tag{5.5.2}$$

Systems (I) and (II) were analyzed, using the one and two-step LW algorithms, for the initial data given in Fig. 5.10. To capture the phenomena at $t = 2$, the problem was solved in the interval $-1/2 \le z \le 3\frac{1}{2}$. The mesh units were selected as $k = 1/20$ and $h = 1/10$. This corresponds to the maximum allowable time step under the CFL criterion, based on the initial data. The results are plotted in Fig. 5.11. The use of the one-step or two-step formulas proved negligibly different here. However, the results of the two systems (I) and (II), are considerably different, as is to be expected, since an elementary characteristics analysis indicates that

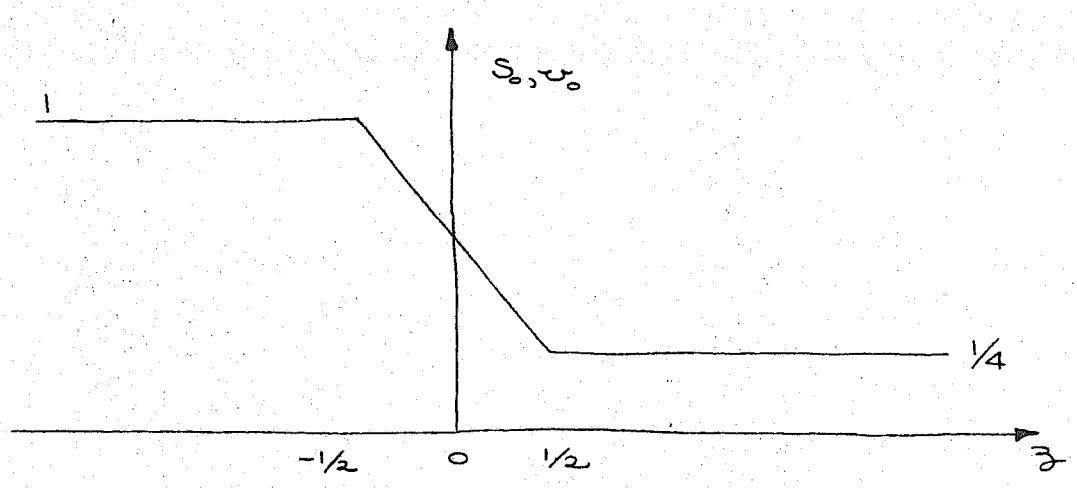

Figure 5.10

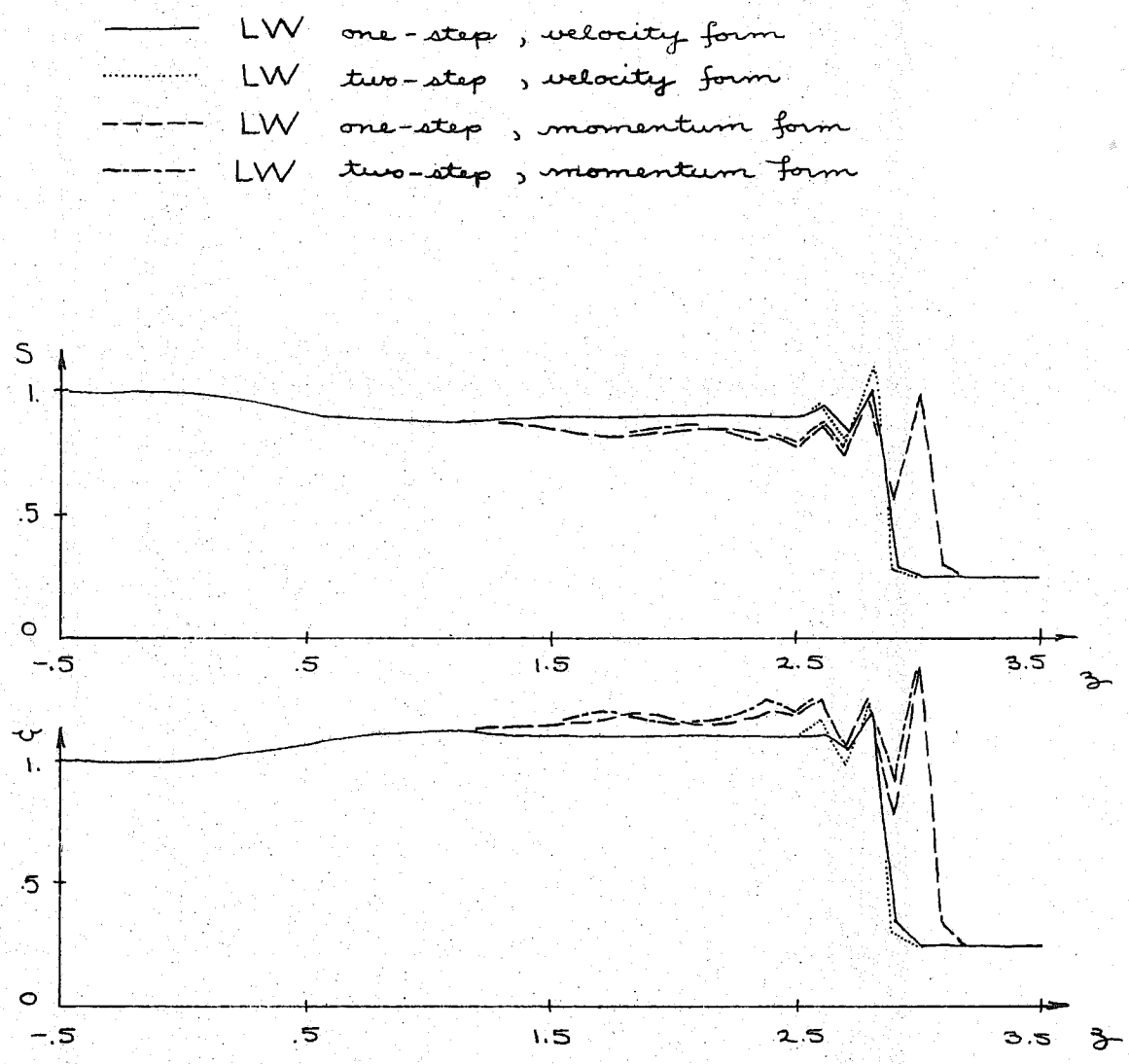
LW one-step, velocity form
LW two-step, velocity form
LW one-step, momentum form
LW two-step, momentum form
S
1.
.5
0
-.5
.5
1.5
2.5
3.5
x
v
1.
.5
0
-.5
.5
1.5
2.5
3.5
x

Figure 5.11

a shock forms at $(z,t) = (1.1,.8)$. For $t > .8$ the shock relations are different for the velocity and momentum forms, and the solutions evolve differently (cf. Section 5.3).

5.6 Rockwell's Model of the Canine Aorta

Rockwell's "standard case" [17] consists of the following:

$$\frac{\partial S}{\partial t} + \frac{\partial Sv}{\partial z} + \psi = 0 ,$$

$$\frac{\partial v}{\partial t} + \frac{\partial}{\partial z}\left(\frac{v^2}{2} + \frac{p}{\rho}\right) = \frac{Nv}{S} , \qquad (5.6.1)$$

where

$$S(z,t) = \tilde{S}(p(z,t), z)$$

$$= \begin{cases} 4.63\ e^{-.045z + \frac{p-p_1}{\rho c(p,z)c(p_1,z)}} & z \le 54 \\ .41\ e^{-.089(z-54) + \frac{p-p_1}{\rho c(p,z)c(p_1,z)}} & z \ge 54 \end{cases}$$

$$c(p,z) = \left(97 + \frac{2.03}{1330.}\,p\right)(1 + .02z) \quad cm/sec$$

$$\psi(p,z) = \begin{cases} \alpha(p-p_e)(1.1 + \cos\frac{5\pi}{2}\frac{z}{z^*}) & z \le z^* \\ \alpha(p-p_e)(1.1)\,e^{-.08(z-z^*)} & z \ge z^* \end{cases} \qquad (5.6.2)$$

$$N = -8\pi\frac{\mu}{\rho}$$

$$\mu = .049 \text{ poise}$$

$$\rho = 1.06 \text{ gm/cm}^3$$

$$p_1 = 133000 \text{ dynes/cm}^2 \quad (= 100 \text{ mm Hg})$$

$$z^* = 70 \text{ cm}$$

$$\alpha = \left(9.29 \times 10^{-3} \frac{cm^3}{sec - mm\,Hg}\right) \Big/ \left(1330. \frac{dynes}{cm^2 - mm\,Hg}\right)$$

$$p_c = 33250 \text{ dynes}/cm^2 \quad (= 25 \text{ mm Hg})$$

The domain $\mathcal{O} = \{(z,t) \mid z \in [0,150],\ t \geq 0\}$; boundary data, which are periodic, consists of that given in Table 5.1 for $z=0$, and $p = 33250$ dynes/cm^2 at $z = 150$ cm . Initial data were set approximately to the expected steady state values as given in Fig. 9, p. 33 of [17]; namely, the values of Table 5.2 were linearly interpolated.

In the present analyses $\tilde{S}$ was inverted, yielding

$$\rho \tilde{p}(S,z) = a\{(1/b) - 1\} ,$$

$$a = (97.)(1330.)/2.03 ,$$

$$b = \left\{1/(1+2.03p_1/97.) - \rho\frac{(2.03)(97.)}{1330.}(1+.02z)^2 \ln\left(\frac{S}{s}\right)\right\} , \quad (5.6.3)$$

$$s(z) = \tilde{S}(p_1,z).$$

and then substituted in Eq. $(5.6.1)_2$.

The momentum form of Rockwell's standard case consists of replacing Eqs. (5.6.1) by

$$\frac{\partial S}{\partial t} + \frac{\partial Q}{\partial z} + \psi = 0,$$

$$\frac{\partial Q}{\partial t} + \frac{\partial}{\partial z}\left\{(1+\delta)\frac{Q^2}{S} + \frac{1}{\rho}\int_0^p \tilde{S}(p',z)\,dp'\right\} \quad (5.6.4)$$

$$-\frac{1}{\rho}\int_0^p D_2\tilde{S}(p',z)\,dp' = \frac{Q}{S}(N-\psi) .$$

Table 5.1, [65]

t (sec)	Q (cm /sec)
.0	0
.01	8
.03	380
.04	386
.05	372
.09	210
.13	109
.155	-55
.165	6
.18	-6
.19	0
.5	0

Table 5.2 Initial Data for the Standard Case

(cm)	(cm/sec)	(mmHg)
0	0	80
20	10	80
40	30	80
60	40	77
80	30	74
100	20	55
150	0	25

The integrals were computed using two-point Gaussian quadrature. Since n-point rules are exact for polynomials of order $2n-1$ and $\tilde{S}$ is well behaved (see Fig. 3.28), this approximation seemed adequate.

Unless otherwise specified, numerical results for this model were computed using the AG algorithm with $\Theta=.2$, $h=2cm$, and k computed on the basis of the AG criterion (5.2.5). Pressure boundary data were converted to area data via the constitutive equation, Eq. $(5.6.2)_1$. For the velocity form of the equations, the flow boundary data were converted to velocity by dividing by S.

It was found that in the distal portion of the model the right hand side terms of Eqs. $(5.6.1)_2$ and $(5.6.4)_2$ were causing instabilities and resulting in the numerical solution "blowing up." This was rectified by setting these terms to zero for $z \geq 112.5$. Otherwise the initial-boundary value problem was exactly Rockwell's standard case.

This model was used to study the effect of varying δ and also properly including (excluding, resp.) the outflow term in Eq. $(5.6.1)_2$ (Eq. $(5.6.4)_2$) according to the no-slip forms of the momentum equation (Eqs. (4.1.1) and (4.1.2)). These results are discussed in Section 4.1.

In the course of performing these analyses, it was found that first-order boundary conditions

produced results in general agreement with Rockwell's, whereas second-order boundary conditions produced considerably different results (see Fig. 5.12). Second-order boundary conditions were also found to be unstable for the momentum form of the equations. The results depicted in Figs. 4.1 and 4.2 were all computed using first-order boundary conditions. The results for the momentum form of the equations, Fig. 4.2, were computed with the outflow term in Eq. $(5.6.4)_2$ omitted, which is consistent with Eq. (4.1.1).

Based upon the analysis of Section 5.4, the fact that the only results which look good were computed using first-order boundary conditions indicates that they may in fact be seriously in error. The magnitude of the error is indicated in Fig. 5.12.

5.7 Aortic Phenomena and Shock Waves

In this section it is argued that realistic data (including the natural pulse) is shock-like within the context of the one-dimensional theory.* Several cases are considered emanating from Rockwell's work [17]. The first, a semi-infinite tube problem, is analyzed in detail since the model used for this problem is simple and amenable to definitive interpretation. Consideration is then given to the standard case and the case of aortic insufficiency.

---

* Rudinger [19] first called attention to this possibility.

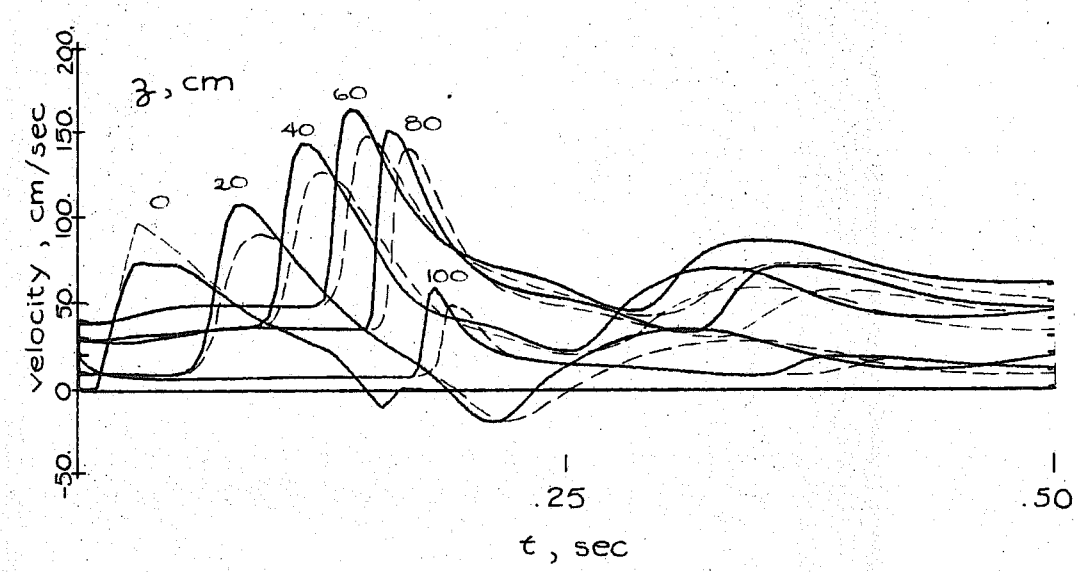

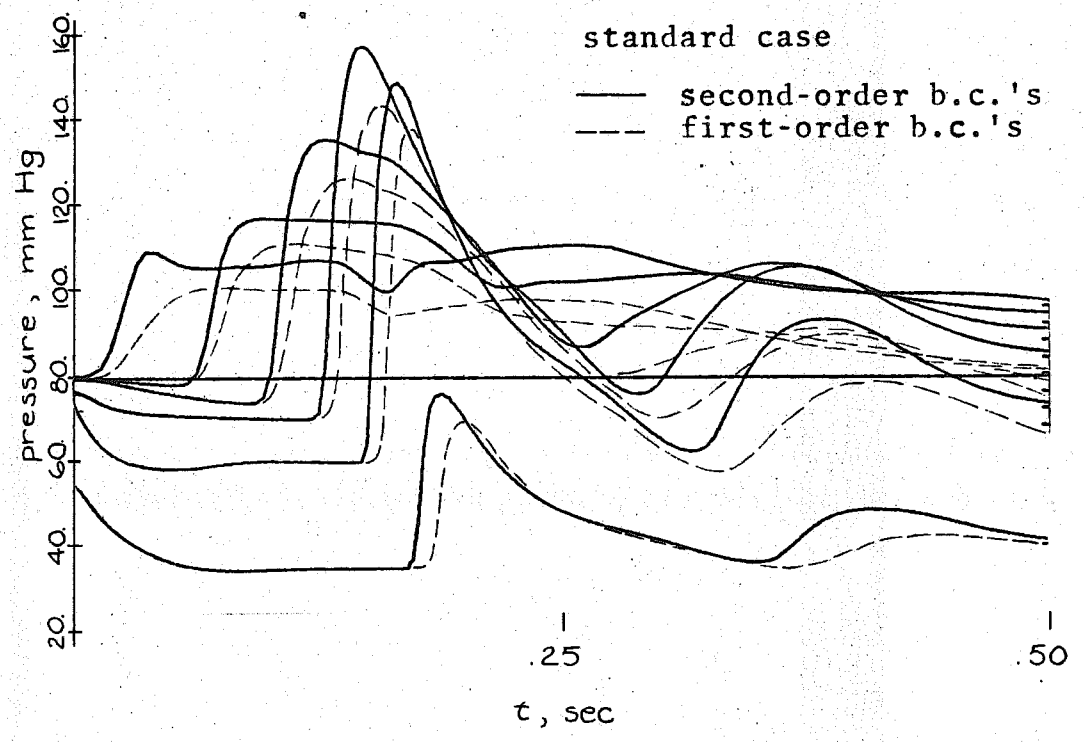

Figure 5.12 Effect of boundary conditions on the standard case

Consider the following example (Rockwell [17], case 4, p.53):

$$\begin{cases} \dfrac{\partial S}{\partial t} + \dfrac{\partial Sv}{\partial z} = 0 , \\ \dfrac{\partial v}{\partial t} + \dfrac{\partial}{\partial z}\left(\dfrac{v^2}{2} + \tilde{p}\right) = N\dfrac{v}{S} , \\ \tilde{p} = \dfrac{p_1}{\rho} + c^2 \ln \dfrac{S}{s} , \\ \text{where} \\ N = -8\pi\mu/\rho \\ \mu = .049 \text{ poise} \\ \rho = 1.06 \text{ gm/cm}^3 \\ c = 300. \text{ cm/sec} \\ s = 4.63 \text{ cm}^2 \\ p_1 = 133{,}000 \text{ dynes/cm}^2 \quad (= 100 \text{ mm Hg}) \end{cases} \tag{5.7.1}$$

The initial data are $v_0(z) = 0$, $S_0(z) = s$; and the boundary data at $z=0$ correspond to the data in Table 5.2 amplified by a factor of 2. The domain for this problem is $\mathcal{O} = \{(z,t) \mid z \geq 0, t \geq 0\}$ and the characteristic velocities are

$$\sigma^{\pm} = v \pm c .$$

Computed v at $z=0$ are less than 140 cm / sec, thus the problem is well posed (cf. Section 3.3). Computations were performed using the AG algorithm for the velocity form of the equation; $h = 2\text{cm}$, k computed according to the AG criterion (5.2.5) and second-order boundary conditions were employed. The results are given in Fig. 5.13, and are in fair agreement with Rockwell's computations. Despite the

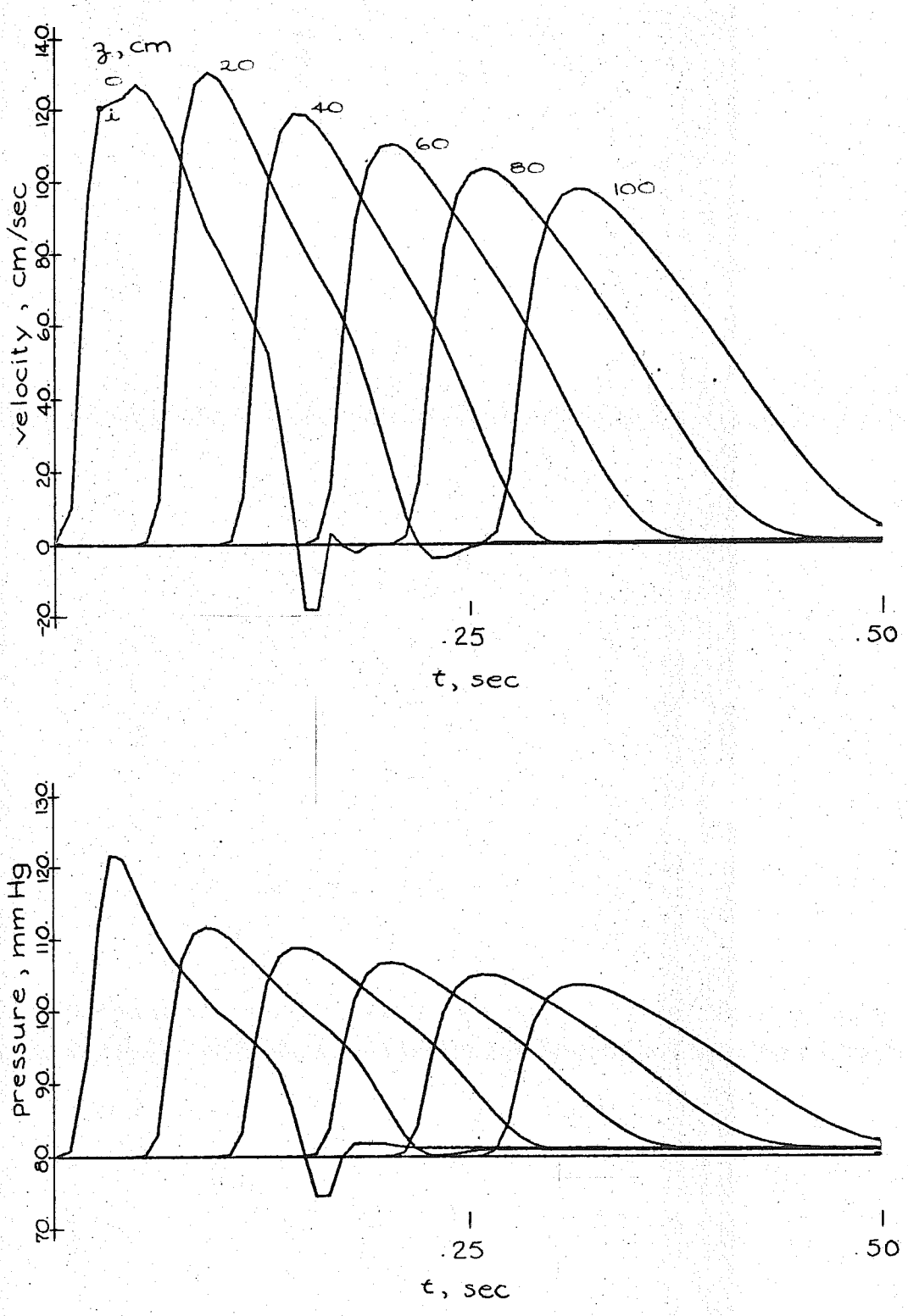

Figure 5.13 Semi-infinite tube problem

fact that the computed data reveals a smooth front, the wave is a shock. The evidence for this consists of three analyses based upon

(A) acceleration-wave theory

(B) characteristics

(C) numerical data

These analyses will now be given:

(A) The asymptotic formula, Eq. (4.8.35), can be used to estimate shock formation distance, z_∞. Since c is constant, $\partial c/\partial p = 0$; thus only $a(0)$ need be evaluated to estimate z_∞. From the $z=0$ plot of pressure, Fig. 5.13, and employing Eqs. (4.8.7), one has

$$a(0) \approx (\partial p/\partial t)^{-}/\rho c \approx \left(\frac{\Delta p}{\Delta t}\right)/\rho c \quad ,$$

$$\Delta p = (42.)(1330.) \text{ dynes/cm}^2 \quad ,$$

$$\Delta t = .03 \text{ sec} \quad ,$$

$$z_\infty \approx \rho c^3 \frac{\Delta t}{\Delta p} = 15.4 \text{ cm} \quad .$$

(B) Since c = constant and $u_0 = 0$ the wave front initially propagates at constant velocity, namely c. A shock will form if characteristic wavelets behind the front travel fast enough to catch the front. The characteristic velocity of the wavelet located at the point i of the velocity pulse at $z=0$ (Fig. 5.13) is 420. cm/sec. It emanates from $z=0$ at $t=.03$ sec.

An estimate can be given as to where this wavelet will catch the front by drawing the linearized characteristic and seeing where it intersects the front (Fig. 5.14). According to this, point i catches the front at approximately $z = 33$ cm. Since the velocity peak decays slowly, the approximation by a straight characteristic through $(0, .03)$ is seen to be appropriate.

(C) The numerical data also supports the hypothesis that the front becomes a shock. To set a proper context for this, recall the analysis in Section 5.4. The results of this analysis indicate that even though the exact solution is discontinuous, the numerical solution will be just a smoothed out approximation (e.g., Fig. 5.9). However, the AG algorithm does capture the correct propagation shock velocity for the midpoint of the front when second-order boundary conditions are employed, i.e., with reference to Fig. 5.15, the point j should travel at the shock velocity if the true solution of the equations is a shock. A plot of the mid-point path for the front of the velocity pulse in Fig. 5.13 reveals an approximately constant velocity of 354 cm/sec, 18% greater than c.

There should be little doubt left that the exact solution of this problem involves a shock front. Consideration will now be given to the cardiac pulse

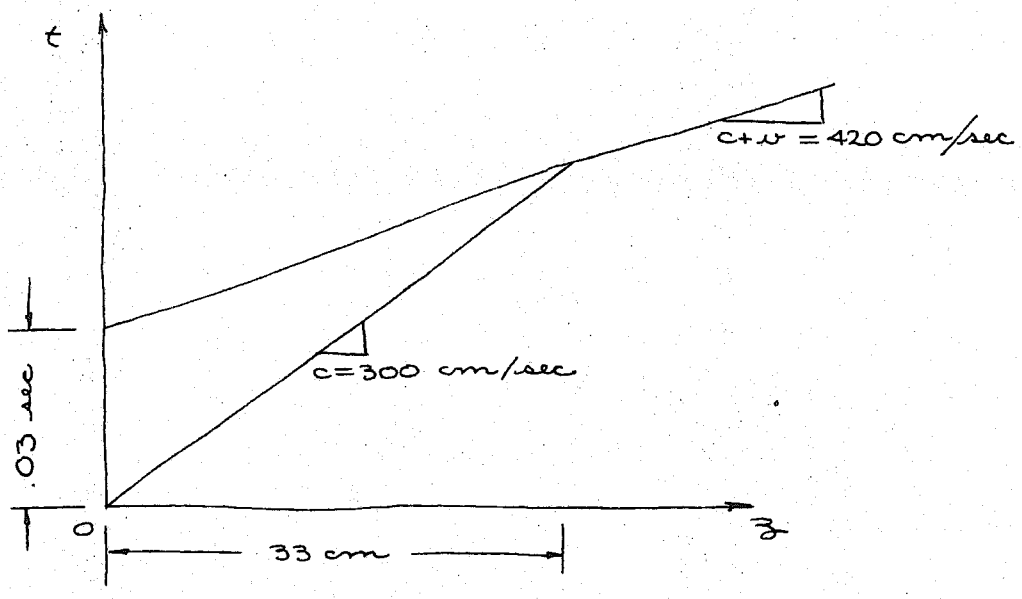

Figure 5.14

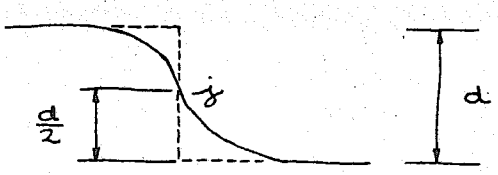

Figure 5.15

and aortic insufficiency.

For the standard case ([17], pp. 32-35) the wave speed is given by Eq. $(5.6.2)_2$. Diastolic pressure at $z=0$ is 80 mm Hg. Thus for the purposes of evaluating Eq. (4.8.35),

$$c(0) = c(106,400,0) \approx 260.$$

$$\rho c(0) \frac{\partial c}{\partial p}(0) \approx 1.06\,(260.)\frac{(2.03)}{1330.} = .42$$

An estimate for $a(0)$ can be made from Fig. 9, [17]:

$$a(0) = \frac{\partial v}{\partial t}(0) \approx 3480.$$

With these, Eq. (4.8.35) gives

$$z_\infty = 13.7 \text{ cm}.$$

To make sure this was a valid estimate, Eq. (4.8.19) was evaluated using Gaussian quadrature, where μ and β were computed from the properties of the model and the data in front of the wave taken from [17], Fig. 9, p.33. The limits of integration in Eq. (4.8.19) were converted from t to z via $t = \gamma^{-1}(z)$ and two-point Gaussian quadrature was used over each 10 cm sub-interval in [0,100]. The denominator in Eq. (4.8.19) was computed to go to zero between $z=10$ and 20 cm, thus corroborating the above estimate.

For conditions such as those indicated in

Fig. 48 of [17], (schematically reproduced here in Fig. 4.8) for an incompetent aortic value, the shock formation distance is reduced further, i.e., $x_{sh} \approx 4$ cm. Attempts were made to solve this problem using the AG algorithm, but the results always blew up after a short time ($\approx .1$ sec).

Attempts were made to assess the effects of including the second-order viscous term in the finite difference equations. The standard case and semi-infinite tube problem (second-order boundary conditions and velocity form) were run with the term

$$\nu \frac{k}{h^2} (w_{j+1} - 2w_j + w_{j-1}) \tag{5.7.2}$$

added to the velocities at the end of each time step. This is a first-order correction approximating the effects of the second-order viscous term. In each case no differences, from the case where (5.7.2) was neglected, were discernable. These analyses indicate that the second-order viscous term is indeed insignificant compared with the amount of dissipation inherent in the algorithm.

The question arises, what is responsible for the front of the cardiac pulse steepening into a shock so quickly, whereas experimental data indicates the contrary, [46]? It seems it is not the fault of the data used to construct the aortic model, since the

asymptotic formula (4.8.35) is independent of them, i.e., all one needs for an estimate of this type is the signal speed at $\zeta=0$ and the approximate slope of a cardiac ejection plot (e.g., Fig. 4.8). The term $\partial c/\partial p$, even if set to zero, could only increase the estimates of ζ_∞ by about 40%. Thus it does not seem to be this. Also, wall dissipative effects would not affect the asymptotic formula. At present the answer to this question cannot be given. However, omissions in the model may be responsible, e.g., the curvature of the aortic arch or $\partial S/\partial \zeta$ terms in the constitutive equation.

REFERENCES

1. Lambert, J.W., "Fluid Flow in a Nonrigid Tube." Ph.D. Thesis, Purdue University (1956).

2. Lambert, J.W., "On the Nonlinearities of Fluid Flow in Nonrigid Tubes." J. Franklin Inst., 266, 83-102 (1958).

3. Fox, E.A. and E. Saibel, "Attempts in the Mathematical Analysis of Blood Flow." Trans. Soc. Rheology, 7, 25-31 (1963).

4. Streeter, V.L., W.F. Keitzer and D.F. Bohr, "Pulsatile Pressure and Flow Through Distensible Vessels." Circ. Res., 13, 3-21 (1963).

5. Streeter, V.L., W.F. Keitzer and D.F. Bohr, "Energy Dissipation in Pulsatile Flow Through Distensible Vessels." In Pulsatile Blood Flow. E.O. Attinger, editor. McGraw-Hill, New York, 149-177 (1964).

6. Bird, G.A. and W.E. Bodley, "Finite Wave Propagation in Deformable Tubes," J. Appl. Mech., 32, 207-208 (1965).

7. Barnard, A.C.L., W.A. Hunt, W.P. Timlake and E. Varley, "A Theory of Fluid Flow in Compliant Tubes." Biophys. J., 6, 717-724 (1966).

8. Barnard, A.C.L., W.A. Hunt, W.P. Timlake and E. Varley, "Peaking of the Pressure Pulse in Fluid-Filled Tubes of Spatially Varying Compliance." Biophys. J., 6, 735-746 (1966).

9. Rudinger, G., "Review of Current Mathematical Methods for the Analysis of Blood Flow." In Biomedical Fluid Mechanics Symposium, ASME, New York, 1-33 (1966).

10. Skalak, R., "Wave Propagation in Blood Flow." In Biomechanics. Y.C. Fung, editor. ASME, New York, 20-40 (1966).

11. Wylie, E.B., "Flow Through Tapered Tubes With Nonlinear Wall Properties." In Biomechanics. Y.C. Fung, editor. ASME, New York, 82-95 (1966).

12. Olsen, J.H. and A.H. Shapiro, "Large-Amplitude Unsteady Flow in Liquid Filled Tubes." J. Fluid Mech., 29, 513-538 (1967).

13. Beam, R.M., "Finite Amplitude Waves in Fluid-Filled Elastic Tubes: Wave Distortion, Shock Waves and Korotkoff Sounds." NASA TN D-4802 (1968).

14. Schoenberg, M., "Pulse Wave Propagation in Elastic Tubes Having Longitudinal Changes in Area and Stiffness." Biophys. J., 990-1009 (1968).

15. Seymour, B.R. and E. Varley, "High Frequency, Pulsatile Flow in a Tapering, Viscoelastic Tube of Varying Stiffness." In Hemorheology. Pergamon Press, New York, 131-142 (1968).

16. Campbell, J.L. and T. Yang, "Pulsatile Flow Behavior in Elastic Systems Containing Wave Reflection Sites." J. Basic Eng., 91, 95-102 (1969).

17. Rockwell, R.L., "Nonlinear Analysis of Pressure and Shock Waves in Blood Vessels." Ph.D. Thesis, Stanford University (1969).

18. Seymour, B.R. and E. Varley, "Pulsatile Flow in Flexible Tubes." Report No. CAM-120-1, Lehigh University (1969).

19. Rudinger, G., "Shock Waves in Mathematical Models of the Aorta." J. Appl. Mech., 37, 34-37 (1970).

20. Seymour, B.R., "Discussion of 'Shock Waves in Mathematical Models of the Aorta' by G. Rudinger, J. Appl. Mech., 37, 34-37 (1970)." J. Appl. Mech., 37, 1202-1204 (1970).

21. Bergel, D.H. and D.L. Schulz, "Arterial Elasticity and Fluid Dynamics." In Progress in Biophysics and Molecular Biology, 22. J.A.V. Butler and D. Noble, editors. Pergamon Press, New York, 1-36 (1971).

22. Bodley, W.E., "The Nonlinearities of Arterial Blood Flow." Phys. Med. Biol., 16, 663-672 (1971).

23. Anliker, M., R.L. Rockwell and E. Ogden, "Nonlinear Analysis of Flow Pulses and Shock Waves in Arteries." ZAMP, 22, 217-246 (1971).

24. Anliker, M., R.L. Rockwell and E. Ogden, "Nonlinear Analysis of Flow Pulses and Shock Waves in Arteries." ZAMP, 22, 563-581 (1971).

25. Anliker, M., "Toward a Nontraumatic Study of the Circulatory System." In Biomechanics, Its Foundations and Objectives. Y.C. Fung, N. Perrone and M. Anliker, editors. Prentice-Hall, Englewood Cliffs, New Jersey, 337-379 (1972).

26. Kenner, T. "Flow and Pressure in the Arteries." In Biomechanics, Its Foundations and Objectives. Y.C. Fung, N. Perrone and M. Anliker, editors. Prentice-Hall, Englewood Cliffs, New Jersey, 381-434 (1972).

27. Hughes, T.J.R. and J. Lubliner, "On the One-Dimensional Theory of Blood Flow in the Larger Vessels." Mathematical Biosciences 18, 161-170 (1973).

28. Burton, A.C., Physiology and Biophysics of the Circulation. Year Book Medical Publishers, Chicago (1965).

29. Falsetti, H.L., K.M. Kiser, G.P. Francis and E.R. Bellmore, "Sequential Velocity Development in the Ascending and Descending Aorta of the Dog." Circ. Res., 31, No.3, 328-338 (1972).

30. Courant, R. and K.O. Friedrichs, Supersonic Flow and Shock Waves. Interscience, New York (1948).

31. Stanyukovich, K.P., Unsteady Motion of Continuous Media. Pergamon, London (1960).

32. Coleman, B.D., M.E. Gurtin, I. Herrera R., and C. Truesdell, Wave Propagation in Dissipative Materials. Springer, New York (1965).

33. Dieudonné, J., Foundations of Modern Analysis. Academic Press, New York (1960).

34. Gelfand, I.M., "Some Problems in the Theory of Quasi-Linear Equations." Amer. Math. Soc. Trans., Ser. 2, 29, 295-381 (1963).

35. Rozdestvenskii, B.L., "Systems of Quasi-Linear Equations." Amer. Math. Soc. Trans., Ser. 2., 42, 13-18 (1964).

36. Truesdell, C. and R.A. Toupin, "The Classical Field Theories." In Encyclopedia of Physics, III/1. S. Flugge, editor. Springer, Berlin (1960).

37. Goudreau, G.L. and R.L. Taylor, "Evaluation of Numerical Integration Methods in Elastodynamics." Computer Methods in Appl. Mech. and Engng., 2, No.1, 67-97 (1972).

38. Stakgold, I., Boundary Value Problems in Mathematical Physics, 2. MacMillan, New York (1968).

39. Lax, P.D., "Weak Solutions of Nonlinear Hyperbolic Equations and Their Numerical Computation." Communications on Pure and Applied Mathematics, 7, 159-193 (1954).

40. Lax, P.D., "Nonlinear Hyperbolic Systems of Conservation Laws." In Nonlinear Problems. R. Langer, editor. University of Wisconsin Press, Madison, 1-12 (1963).

41. Lax, P.D., "Shock Waves and Entropy." In Contributions to Nonlinear Functional Analysis. E.H. Zarantonello, editor. Academic Press, New York, 603-634 (1971).

42. Dafermos, C.M., "The Entropy Rate Admissibility Criterion for Solutions of Hyperbolic Conservation Laws." J. Differential Equations, 14, 202-212 (1973).

43. Bland, D.R., Nonlinear Dynamic Elasticity. Blaisdell, Waltham, Massachusetts (1969).

44. Aris, R. and N.R. Amundson, "First-Order Partial Differential Equations." Mathematical Methods in Chemical Engineering, 2. Prentice-Hall, Englewood Cliffs, New Jersey (1973).

45. Hurewicz, W., Lectures on Ordinary Differential Equations. MIT Press, Cambridge, Massachusetts (1970).

46. McDonald, D.A., Blood Flow in Arteries. Edward Arnold, London (1960).

47. Lax, P.D., "Hyperbolic Systems of Conservation Laws II." Communications on Pure and Applied Mathematics, 10, 537-566 (1957).

48. Chen, P.J., "One-Dimensional Shock Waves in Elastic Nonconductors." Arch. Rational Mech. Anal., 43, 350-362 (1972).

49. Chen, P.J. and M.E. Gurtin, "On the Growth of One-Dimensional Shock Waves in Materials With Memory." Arch. Rational Mech. Anal., 36, 33-46 (1970).

50. Nunziato, J.W. and E.K. Walsh, "Propagation and Growth of Shock Waves in Inhomogeneous Fluids." Phys. Fluids, 15, 1397-1402 (1972).

51. Landowne, M., "A Method Using Induced Waves to Study Pressure Propagation in Human Arteries." Circ. Res. 5, 594-601 (1957).

52. Landowne, M., "Characteristics of Impact and Pulse Wave Propagation in Brachial and Radial Arteries." J. Appl. Physiol., 12, 91-97 (1958).

53. Schuler, K.W. and E.K. Walsh, "Critical-Induced Acceleration for Shock Propagation in Polymethyl Methacrylate." J. Appl. Mech., 38, 641-645 (1971).

54. Zwas, G. and J. Roseman, "The Effect of Nonlinear Transformations on the Computation of Weak Solutions." J. Computational Physics, 12, 179-186 (1973).

55. Coleman, B.D., J.M. Greenberg and M.E. Gurtin, "Waves in Materials with Memory. V. On the Amplitude of Acceleration Waves and Mild Discontinuities." Arch. Rational Mech. Anal., 22, 333-354 (1966).

56. Lubliner, J., "On the Calculation of Acceleration Waves in Viscoelastic Materials." J. Mécanique, 6, 243-250 (1967).

57. Bailey, P.B. and P.J. Chen, "On the Local and Global Behavior of Acceleration Waves." Arch. Rational Mech. Anal., 41, 121-131 (1971).

58. Bailey, P.B. and P.J. Chen, "On the Local and Global Behavior of Acceleration Waves: Addendum, Asymptotic Behavior." Arch. Rational Mech. Anal., 44, 212-216 (1972).

59. Steen, E.B. and A. Montagu, Anatomy and Physiology, 1. Barnes and Noble, New York (1959).

60. Richtmyer, R.D. and K.W. Morton, Difference Methods for Initial-Value Problems. Interscience, New York (1967).

61. Kreiss, H. and J. Oliger, "Methods for the Approximate Solution of Time Dependent Problems." Global Atmospheric Research Program Publication Series, No.10 (1973).

62. Abarbanel, S. and M. Goldberg, "Numerical Solution of Quasi-Conservative Hyperbolic Systems - The Cylindrical Shock Problem." J. Computational Physics, 10, 1-21 (1972).

63. Goldberg, M., "A Note on the Stability of an Iterative Finite-Difference Method for Hyperbolic Systems." Mathematics of Computation, 27, No.121, 41-44 (1973).

64. Chorin, A., "Numerical Study of Thermal Convection in a Fluid Layer Heated from Below." Ph.D. Thesis, Courant Institute, N.Y.U. (1967).

65. Rockwell, R.L., Personal communication. (1972).